INSIGHTS INTO CD8 T CELL-MEDIATED PATHOLOGY DURING EXPERIMENTAL CEREBRAL MALARIA

POH CHEK MENG

(B. Sc (2nd Upper) in Biological Sciences, Nanyang Technological University)

A THESIS SUBMITTED FOR THE DEGREE OF DOCTOR OF PHILOSOPHY IN MICROBIOLOGY

DEPARTMENT OF MICROBIOLOGY, YONG LOO LIN SCHOOL OF MEDICINE

NATIONAL UNIVERSITY OF SINGAPORE

2015

DECLARATION

I hereby declare that this thesis is my original work and it has been written by me in its entirety. I have duly acknowledged all the sources of information which have been used in the thesis.

This thesis has also not been submitted for any degree in any university previously.

Poh Chek Meng

31 July 2015

Acknowledgment

I want to extend my thanks to current and former members of Laurent Rénia's lab, especially Alice Ong Soh Meoy and Chang Zi Wei, for their help and guidance during my stay in the lab. I also wish to thank Asst. Prof. Bruce Russell, an ex-member currently in NUS, for graciously accepting me as his student and helping me to complete my PhD candidature. I wish them all the best for their future endeavours.

I would like to extend my gratitude to Dr Gijsbert Grotenbreg, my former supervisor in NUS during my initial PhD years. I learnt the MHC tetramer technology from him, which was instrumental in the completion of this thesis. He asked tough, stimulating questions on my data, training me to interpret, critique and analyze my results. I also wish to thank the former lab members in his lab, particularly Stephanie Lim and Tan Zhen Wei, on their guidance in making and utilizing MHC monomers for experiments.

Most importantly, I'm saving my deepest gratitude for the last two people. I wish to thank my supervisor, Prof. Laurent Rénia, for his immense guidance rendered to me during the course of this thesis. He is a knowledgable and patient mentor, often devoting time out of his very busy schedule (he is the executive director of SIgN) to explain things to me whenever I have problems. Laurent is also very kind to give me opportunities to attend various symposiums, conferences and

summer schools to broaden my knowledge. He is one who offers ample rooms for individuals under him to grow, improve and flourish.

Lastly, I want to save my utmost gratitude for my direct mentor in the lab, Dr Shanshan Wu Howland. She is a superb mentor whom I believe anyone cannot ask for more. Her teachings are very clear and effective as she has a way to articulate the concepts of any problems to anyone. She has an incredible insight to almost everything; she can see through and identify the crucial points to problems and solutions immediately, where I will take a period of time (days to weeks of constant pondering) to understand. She has a brilliant and innovative mind and I know Laurent can attest to this: the concept, design and adaptation of T reporter cells in this study to demonstrate the most vital hallmark of ECM can only be described as ingenious.

I learnt immensely under Laurent and Shanshan, and I am very fortunate to be able hone my skills under their tutelage. It is definitely not an exaggeration to say that without them, I will not be what I am today. I only have this to say for future students who get to intern under them: treasure your chance and learn what you can, for they definitely are one of the very best mentors out there.

Table of Contents

Summary

Malaria infects 200 million people and causes more than 500 000 deaths worldwide annually. Infection by *Plasmodium falciparum* can lead to development of cerebral malaria, a fulminant and often fatal complication. In the mouse model termed experimental cerebral malaria (ECM), C57BL/6J mice develop a severe neurological complication when infected with *Plasmodium berghei* strain ANKA (PbA) that shares many features with cerebral malaria in humans.

$CD8^+$ T cells are essential for development of experimental cerebral malaria (ECM), but the epitopes recognized by these $CD8^+$ T cells were unknown. To search for novel epitopes, we constructed a PbA cDNA library and expressed it in EL4 cells (C57BL/6 background) . A novel method involving phosphorothioate-linked random primers and translational coupling was developed to enrich the cDNA library for in-frame inserts. In the EL4 cells, potential PbA epitopes are processed and presented on the cell surface bound to MHC class I molecules. Concurrently, TCRs from $CD8^+$ T cells sequestered in the brains of mice with ECM were cloned and expressed in separate T reporter cell lines harbouring a LacZ cassette controlled by an NFAT promoter. Each T reporter cell line was used to screen the PbA cDNA library, to identify and clone transduced EL4 cells able to trigger TCR ligation and hence lacZ expression. Sequencing the cDNA inserts led to the identification of GAP50 and bergheilysin as two antigens that are recognized by $CD8^+$ T cells in mice during infection. The epitopes were found to be SQLLNAKYL (Pb1) and IITDFENL (Pb2) respectively, by generating and testing candidate peptide-MHC tetramers.

With the peptide-MHC tetramers for Pb1, Pb2 and F4 (an epitope reported in the literature midway through this project), we were able to characterize the antigen-specific $CD8^+$ T cell response during ECM. $CD8^+$ T cells specific for each of the three epitopes were induced in infected mice, expressing IFNγ, granzyme B, LFA-1^{high}, and CXCR3 in the spleen, with downregulation of CXCR3 in cells in the brain. These markers are associated with pathogenicity, thus their expression by $CD8^+$ T cells in mice not succumbing to ECM seems contradictory. The apparent contradiction was resolved when we discovered that only mice with ECM cross-present high levels of malaria epitopes in the brain microvasculature, showing that this is the essential feature that determines ECM susceptibility. Accordingly, $CD8^+$ T cells recognizing Pb1, Pb2 and F4 have the capacity to damage these cells and disrupt the blood-brain barrier, presumably leading to onset of ECM development during infection. Tolerizing mice towards these three peptides could not protect infected mice against ECM, suggesting that ECM is caused by multiple malaria-specific $CD8^+$ T cells.

(430 words)

List of tables in the thesis

List of figures in the thesis

List of primers used in the thesis

3StopKanR	AAATAGATGAGTATTGAACAAGATGGATTGCAC
Acc-ins1	CCGGCGATCGCAGGTTCTCCGGCCA
Acc-ins2	TATGGCCGGAGAACCTGCGATCG
AdaptorP1	ACAGCAGGTCAGTCAAGCAGTA
AdaptorP2	AGCAGTAGCAGCAGTTCGATAA
BamHI-TRAV13-4	GTAGGATCCAGCAGTAGCAGCAGTTCGATAAGCGGG
CalphaFor	CATCCAGAACCCAGAACCTGC
CbetaFor	AGAAATGTGACTCCACCCAAGG
CPI-Vbeta8	GAGGCTGCAGTCACCCAAA
GFPfor	GGACGAGCTGTACAAGTCCG
IF-PyUIS4f	AAGGAGGTTCGGGCATGGCTAATTTGCGGTATTTTTG
IF-15-X6	AATACTCATCTATTTAXXXXXXC
IF-27-X6	TCCATCTTGTTCAATACTCATCTATTTAXXXXXXC
IF15-PyUIS4r	AATACTCATCTATTTACCCATTAAATCGCTTAATTC
IF15PS-PyUIS4r	AATACTCATCTATTTACCCATTAAATCGCTTAATTC
IF21	TGTTCAATACTCATCTATTTA
IFb-15PS-X6	AATACTCATCTATTTAXXXXXC
IFLink-a	AAGGAGGTTCGGGCATG
IFLink-b3	CATGCCCGAACCTCC
MluI-T2Arev	CATGACGCGTATAGGTCCAG
mTCRa1st	CGGTGAACAGGCAGAGGGTG
mTCRb1st	CCAAGCACACGAGGGTAGCC

mTCRaNest	GCAGGTTCTGGGTTCTGGATG
mTCRbNest	CCTTGGGTGGAGTCACATTTCT
mTCRaRT	GTTTTCGGCACATTGATTTGG
mTCRbRT	CTTGCCATTCACCCACCAG
Oligo-dC-adaptor	ACAGCAGGTCAGTCAAGCAGTAGCAGCAGTTCGATAAGCGG CCGCCATGGACCCCCCCCCCCDN
pGEX-2Tr	CAGAGGTTTTCACCGTCATC
pLv-3UTRseqr	GTAAAAGGAGCAACATAGTTAAGAATAC
preGFP	CAGGCCTAAGCTTACGCG
pScrAn-IntF	CAAATATTCTGAAATGAGCTGTTGAC
SpeI-Cbeta2Rev	GATACTAGTTCAGGAATTTTTTTTCTTGACCATG
T2A-TRBV12-1	CTGGACCTATACGCGTCATGTCTAACACTGTCCTCGCTG
T2AFor	CGGAAGGAAGAGGATCTCTG
WPRErev	GTTAAGAATACCAGTCAATCTTTCAC

Legend:

D = A or G or T

N = any of the four nucleotides

Red = nucleotides joined by phosphorothioate linkage

Underline = sequences that are homologous to the reverse end of linearized pScrAn-Int

Yellow highlight = sequences that are homologous to the forward end of linearized pScrAn-Int

List of abbreviations in the thesis

β_2m	Beta-2-microglobulin
ANOVA	Analysis of variance
Anp	3-amino-3-(2-nitro)phenyl-propanoic acid
APC	Antigen presenting cell
BBB	Blood-brain barrier
BSA	Bovine serum albumin
BSL	Brain-sequestered leukocytes
BLAST	Basic Local Alignment Search Tool
CCR2	Chemokine (CC motif) receptor 2
CCR5	Chemokine (CC motif) receptor 5
cDNA	Complementary DNA
CFSE	Carboxyfluorescein succinimidyl ester
CMV	Cytomegalovirus
CXCL9	Chemokine (C-X-C motif) ligand 9
CXCL10	Chemokine (C-X-C motif) ligand 10
CXCR3	Chemokine (C-X-C motif) receptor 3
CXCR4	Chemokine (C-X-C motif) receptor 4
DAPI	4',6-diamidino-2-phenylindole
DC	Dendritic cell
DTR	Diphtheria toxin receptor
ECM	Experimental cerebral malaria

EF-1α	Elongation factor 1α
EGFP	Enhanced green fluorescent protein
ELISpot	Enzyme-linked immunospot assay
EPO	Erythropoietin
ER	Endoplasmic reticulum
GAP50	Glideosome-associated protein 50
GrB	Granzyme B
HCM	Human cerebral malaria
ICAM-1	Intracellular adhesiom molecule 1
IFNγ	Interferon gamma
IL2	Interleukin-2
i.p	Intraperitoneal injection
IPTG	isopropyl β-D-1-thiogalactopyranoside
iRBC	Infected red blood cell
i.v	Intravenous injection
Kan^R	Kanamycin resistance gene
LFA-1	Lymphocyte function-associated factor 1
LTα	Lymphotoxin alpha
MHC	Major histocompatibility complex
NFAT	Nuclear factor of activated T-cells
NK	Natural killer
NP	Influenza nucleoprotein
ORF	Open reading frame

OVA	Chicken ovalbumin
Pb1	SQLLNAKYL epitope
Pb2	IITDFENL epitope
PbA	*Plasmodium berghei* strain ANKA clone 15cy1
PbNK65	*Plasmodium berghei* NK65
pMHC	peptide-MHC
PO	Phosphodiester
PS	Phosphorothioate
PVM	Parasitophorous vacuole
Py17X	*Plasmodium yoelii yoeill* clone 17X
PyUIS4	*Plasmodium yoelii* upregulated in infectious sporozoite gene 4
RANTES	Regulated on activation, normal T-cell expressed and secreted
SD	Shine-Dalgarno
TAP	Transporter associated with antigen processing
TCR	T cell receptor
TdT	Terminal deoxynucleoside transferase
TNFα	Tumor necrosis factor alpha

List of publications

- Howland SW, **Poh CM**, Rénia L. Activated brain endothelial cells cross-present malaria antigen. PLoS Pathog. 2015 Jun 5;11(6):e1004963.

- Howland SW, Claser C, **Poh CM**, Gun SY, Renia L. Pathogenic $CD8^+$ T cells in cerebral malaria. Semin Immunopathol. 2015 May;37(3):221-31.

- **Poh CM**, Howland SW, Grotenbreg GM, Rénia L. Damage to the Blood-Brain-Barrier during Experimental Cerebral Malaria results from synergistic effects of $CD8^+$ T cells with different specificities. Infect Immun. 2014 Nov;82(11):4854-64.

- Horne-Debets JM, Faleiro R, Karunarathne DS, Liu XQ, Lineburg KE, **Poh CM**, Grotenbreg GM, Hill GR, MacDonald KP, Good MF, Renia L, Ahmed R, Sharpe AH, Wykes MN. PD-1 dependent exhaustion of CD8+ T cells drives chronic malaria. Cell Rep. 2013 Dec 12;5(5):1204-13

- Howland SW, **Poh CM**, Gun SY, Claser C, Malleret B, Shastri N, Ginhoux F, Grotenbreg GM, Rénia L. Brain microvessel cross-presentation is a hallmark of experimental cerebral malaria. EMBO Mol Med. 2013 Jul;5(7):916-31

- Howland SW, **Poh CM**, Rénia L. Directional, seamless, and restriction enzyme-free construction of random-primed complementary DNA libraries using phosphorothioate-modified primers. Anal Biochem. 2011 Sep 1;416(1):141-3.

Introduction

Malaria, an ancient disease

Malaria is a blood-borne disease caused by *Plasmodium* protozoan parasites and is transmitted by mosquitoes of the *Anopheles* genus. This disease is estimated to be more than 100,000 years ago, about the same age as the modern human race (1). It is hypothesized that these parasites originated from an ancestor protozoa that gained the ability to parasitize and replicate sexually in early aquatic invertebrates (2). As the first modern mosquitoes appeared circa 150 million years ago, some parasites mutated and gained the ability to develop an asexual life cycle in the hosts that the mosquitoes feed on, including early birds, reptiles, mammals and eventually humans. When human agriculture started more than 10,000 years ago (3), the congregation of large human populations close to sources of water presented an environmental adaption of mosquitoes from zoophilic to increasingly anthropophilic, causing the parasites to co-evolve together (4, 5). The periodic fevers and chills that characterize malaria have been documented in the ancient civilizations of ancient Egypt (6), China (7), and Rome. It was erroneously believed that the mists (**mal**a = bad, **aria** = air) from the marshes and swamplands were the cause of this disease, giving rise to the name (8).

Epidemiology of malaria

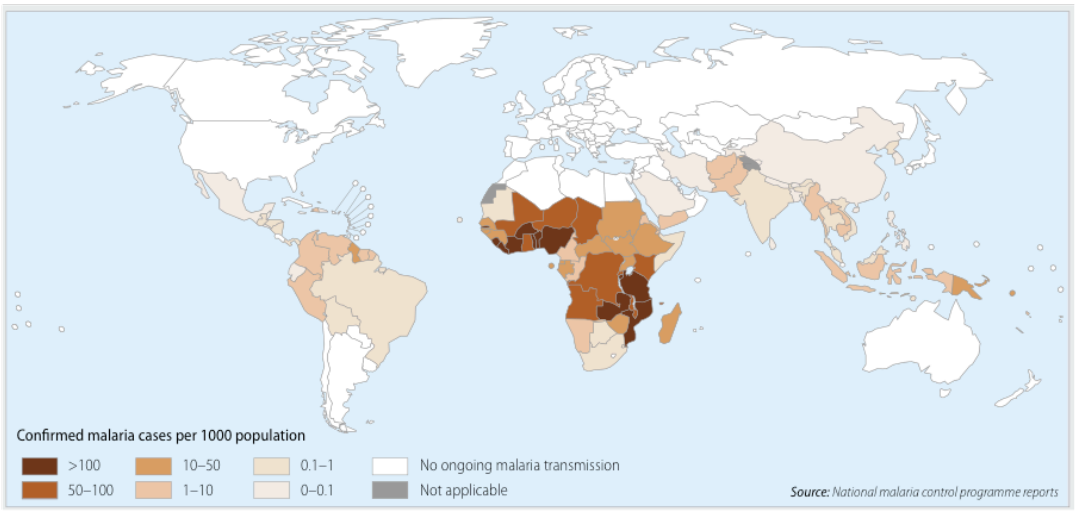

Figure 1: Transmission of malaria in the world as at 2013. Diagram reproduced from (9).

Currently, malaria causes over 200 million infections and 500,000 deaths worldwide annually, with children accounting for 70% of the fatalities (9). Five *Plasmodium* species are known to infect humans – *P. falciparum, P. vivax, P. ovale, P. malariae* and *P. knowlesi*. Of these, *P. falciparum* is considered the most dangerous as it accounts for the wide majority of deaths, and thus remains the main focus of research to develop therapeutic and elimination strategies. *P. vivax* is gaining attention due to its larger geographic distribution and its ability to develop into hypnozoites, a dormant stage in the liver capable of causing disease relapses that can remain undetected for up to 30 years.

Geographically, malaria transmission is spread broadly across the tropical parts of the world (figure 1), concentrated mainly in sub-Saharan Africa, parts of South America, India and Southeast Asia, with sub-Saharan Africa being the site of

most fatalities (9). These areas generally have high levels of precipitation and humidity, and together with the warm temperatures, make it easy for mosquitoes to breed, aiding the spread of malaria.

Life cycle of malaria

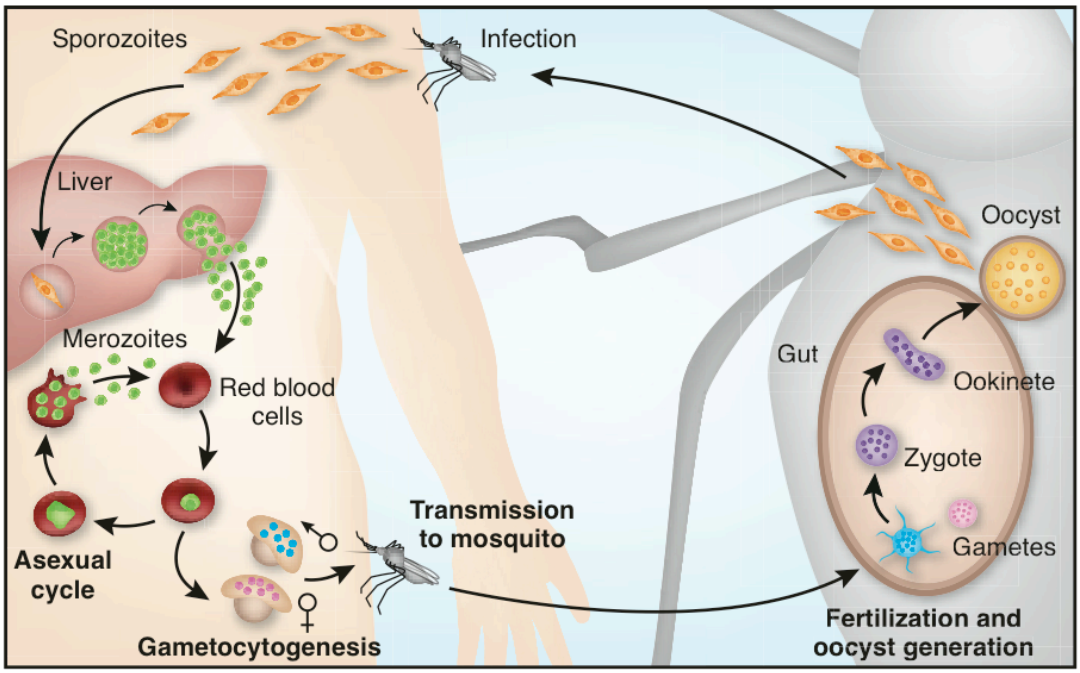

Figure 2: Life cycle of the *Plasmodium* parasite. See the main text for details. Diagram reproduced from (10).

The life cycle of malaria (figure 2) is complex, involving vertebrate and mosquito hosts and spanning three stages. The life cycle of *P. falciparum* is described below; the cycles of rodent malaria parasites are qualitatively similar but differ in terms of the time frames and cell numbers. Infection begins when infected female mosquitoes feed on the blood from the host, depositing the parasites in its motile sporozoite form in the skin. Up to 100 sporozoites are transmitted into the skin, where they can stay for as long as 4 days (11). These motile parasites burrow their way into the bloodstream and travel to the liver, where they traverse multiple

hepatocytes before finally residing and developing within one (12, 13). Each sporozoite then develops into an exo-erythrocytic form, wherein replication and differentiation of as many as 40,000 asexual forms (termed merozoites) occurs in a week's time. At this point, infected hepatocytes develop merosomes, vesicles that are filled with merozoites, and these bud off from the dying hepatocyte. The lack of phosphatidylserine expression on the surface of merosomes prevents phagocytosis by Kupffer cells, ensuring their successful release into the bloodstream (14). These merosomes travel to the lung microvasculature where they disintegrate, releasing the merozoite cargo into the blood (15). Each merozoite then proceeds to make contact with an erythrocyte, realigning itself with its apical end interacting with the erythrocyte membrane (16). Localized secretory granules (micronemes, rhoptries and dense granules) at the apical end of the merozoite then unload their contents at the site of contact, forming interactions with receptors on the erythrocyte membrane (17-19). These are then translocated across the merozoite surface, mediated by the actin-myosin motor complex in the parasite's inner membrane complex (20, 21), pulling the erythrocyte's membrane to form an envelope around the merozoite. Eventually, the membrane traverses the whole parasite and fuses together, enclosing it in a parasitophorous vacuole (PVM) within the erythrocyte, completing the invasion process. This whole process of erythrocyte invasion happens rapidly, averaging less than two minutes (22, 23). The nascent ring stage parasite then develops into a tropozoite, actively feeding on the host cell's hemoglobin, before replicating and undergoing schizogony to form up to 32 merozoites in each infected erythrocyte. Schizonts then rupture, releasing new merozoites to continue the asexual blood stage cycle. Some of the infected erythrocytes will exit this cycle

and develop into sexual gametocytes, which remain circulating in the host until taken up by a mosquito during a blood meal. Gametogenesis occurs inside the midgut, and flagellated male gametes swim and fertilize female gametes to form ookinetes, which invade the gut epithelium and develop into oocysts at the basal membrane (24). After about 15 days, oocysts mature and release sporozoites into the hemolymph, where they traverse and invade into the salivary glands (24), ready to restart the life cycle when the mosquito takes a blood meal again.

Drug treatments and resistance in malaria

Treatments for malaria existed in antiquity, with the use of chinchona bark in the West and sweet wormwood in the East for hundreds of years (25). The respective key ingredients, quinine and artemisinin, were isolated and discovered only in the 19th and 20th century. Though there are a number of antimalarial drugs available on the market, most drugs were rendered obsolete, mainly due to the parasites having acquired resistance to them. Two antimalarial drugs, chloroquine and artesunate, stand out among the others.

After its implementation in 1947 as a treatment against malaria, chloroquine became the most widely used antimalarial drug due to its affordability, effectiveness and good tolerance in humans. Its mechanism of action is through formation of complexes with ferriprotoporphyrin IX, a toxic intermediate that is produced from the digestion of hemoglobin by the parasite for energy and growth (26). This prevents further modification of the toxic product into non-toxic hemozoin, causing

the parasite to be killed by its own metabolite. Overuse of chloroquine led to the emergence and spread of resistant strains, with the first reports of chloroquine-resistant *P. falciparum* infections came from Thailand and Colombia in 1957, just 12 years after it was adopted as the drug of choice (27, 28). Chloroquine resistance then spread outwards from these two regions in Asia and South America, and taking hold in Africa within 20 years (29). This sparked development and eventual deployment of other anti-malarial drugs in order to combat drug resistance. Unfortunately, all these drugs also met the same fate, with drug-resistant strains appearing at alarming rates of 5 years or less (28). A number of reasons were put forth to explain the emergence of these resistant parasites. The earlier attempts to eradicate malaria through mass distribution of table salt mixed with anti-malarial drugs to endemic areas were often poorly controlled, leading to inconsistent and sub-therapeutic dosing (25, 29). The continued and presumptive use of drugs, especially chloroquine, in areas with resistant parasites also contributed to its spread (29). Chloroquine still remains effective in treating *P. vivax*, *P. malariae* and *P. ovale* infections. However, resistance in *P. vivax* has been observed in Southeast and South Asia and South America (30).

Artemisinins, employed in traditional Chinese medicine in treating malaria, emerged as the last line of defence against drug-resistant malaria. The fastest-acting among all antimalarial drugs, artemisinin affects both early and late stages of blood infection, reducting parasite mass by 10 000–fold in 48 hours (31, 32). Its mechanism of action is not completely understood. It has a short half-life of 40 to 60 minutes in the body (26, 33), thus necessitating the combination with other antimalarial drugs as artemisinin-based combination therapies. This extends the duration of drug cover

against parasites and minimizes the risk of parasites developing resistance. Alarmingly, artemisinin resistance has emerged recently in Southeast Asia (34-36). The inevitable spread of malaria that will occur if artemisinin loses its efficacy frames the urgent need for research into new drugs against malaria.

Malaria vaccines

Individuals living in endemic areas could acquire natural immunity from severe forms of malaria disease during childhood, though these wanes in the absence of continued exposure (37). Researchers have been working to stimulate protective immunity for decades, but thus far, no effective malaria vaccine has been licensed. Vaccine candidates can be categorized into whole organism vaccines and subunit vaccines. The approaches that have been explored under whole organism vaccines include irradiated sporozoites (38, 39), genetically-attenuated parasites (40, 41), and the use of chloroquine as a prophylaxis while inoculating with live sporozoites (42). In all three approaches, rechallenge with live infectious sporozoites did not establish blood stage infections, conferring clinical immunity to the volunteers. The protective mechanism remains incompletely understood, but it is thought that the T cell-mediated immune responses generated against liver stage parasites were similar in all three approaches (42, 43). The need for cryopreservation of live parasites and establishment of reliable cold chain management, especially in resource-poor nations where malaria is endemic, prevents adoption and deployment of whole organism vaccines in the field.

Many antigen subunits from the parasite have been tested as vaccine candidates and most of them ended in failure. The RTS,S vaccine, based on the circumsporozoite protein, is the only frontrunner to reach phase 3 clinical trials (44, 45). Immunization with RTS,S vaccine resulted in 30-50% protection in both adults and children, and this protection lasted only a few months (46-50). The correlates of protection could not be reliably pinpointed, with varying degrees of T cell and antibody responses across the protected individuals (51-53).

Symptoms of malaria infection

The clinical symptoms of malaria infection are attributed only to the erythrocytic stage, while liver stage infection is asymptomatic. In uncomplicated malaria episodes, the intermittent fevers (once every 2 days for *falciparum, vivax* and *ovale* malaria, 3 days for *malariae* malaria) coincide with the release of merozoites and metabolic wastes from ruptured schizonts. Chills, sweating, nausea, headaches and malaise also accompany uncomplicated malaria infection, which can easily be confused with other illnesses such as influenza (54). However, some patients, especially those that are naïve to malaria infections, may progress to develop severe complications, such as acute renal failure, acute respiratory distress, severe anemia and cerebral malaria (54, 55).

Cerebral malaria in humans (HCM) is defined by the exhibition of unrousable coma in patients with *falciparum* malaria, with a score of <11 on the Glasgow coma scale. Symptoms that often precede coma include ataxia, seizures or prostration (54,

55). This complication is almost always fatal if left untreated and is responsible for most of the *P. falciparum* deaths. With prompt treatment, mortality decreases to 15 – 20% (54, 56). Survivors of cerebral malaria may display neurological sequalae, such as cognitive impairments, epilepsy, language and motor disorders (56-62). Post-mortem pathological studies reveal massive sequestration of infected erythrocytes in the microvasculature of the brain, especially at the perivascular region (63-65). Such sequestration occurs only in *falciparum* malaria and extremely rarely in *vivax* malaria (66). Petechial hemorrhages are found at the sites of sequestration, with evidence of accompanying edema (64, 67, 68). In addition to infected erythrocytes, leukocytes may also be found at the occlusion sites (65, 68-70).

Mouse models for HCM

Pre-mortem studies on HCM cannot be ethically performed and post-mortem analysis does not allow the progression of HCM to be observed or firm conclusions to be drawn (71). A mouse model is attractive because the ready availability of mice of defined genetic background and the ability to conduct experiments on whole organs in a defined setting facilitates uncovering the mechanisms of this neuro-complication. In the malaria research community, the widely recognized model is the infection of C57BL/6J mice with the rodent parasite *P. berghei* ANKA (PbA). CBA/Ca and 129,B6 mice are also susceptible but they are not as widely used as the C57BL/6J mice. In this model, infected mice develop neurological signs that closely mimic symptoms in human patients suffering from HCM: ataxia, paralysis, convulsions and coma (71). This syndrome, termed experimental cerebral malaria (ECM), appears 6-

12 days post-infection and is often fatal with <10% parasitaemia in the blood. In the brains of mice with ECM, sequestration of leukocytes in the microvasculature was observed, corroborating with the findings in HCM. However, sequestration of infected red blood cells (iRBCs) occurs to a lesser extent (72), which remains a bone of contention as to whether the ECM mouse model is relevant to HCM (73). Nevertheless, with a lack of better models or methods to analyze HCM, this mouse model with many similarities to HCM (74) remains popular is studied with the hope that any findings can be extrapolated to HCM (71, 75, 76).

There are other rodent *Plasmodium* parasites that are employed as separate mouse models for non-neurological pathologies that are associated with malaria. *P. berghei* NK65 (PbNK65) parasites, when inoculated into C57BL/6J mice, causes mice to develop experimental acute respiratory distress syndrome instead of ECM (77). *P. yoelii yoelii* 17X clone 1.1 (Py17X) is an avirulent parasite that results in acute, but self-resolving, malaria in mice (78). It is often studied together with the virulent *P. yoelii yoelii* YM strain, to investigate immune mechanisms that contribute to lethality in infected mice (78).

Blood-Brain Barrier

The blood-brain barrier (BBB, figure 3A) is one of a trio of barriers that separate the brain contents from the rest of the circulation, with the other two being the blood-cerebrospinal fluid barrier at the choroid plexus (figure 3B) and the arachnoid epithelium (figure 3C) [reviewed in (79, 80)]. Of these, the BBB is widely

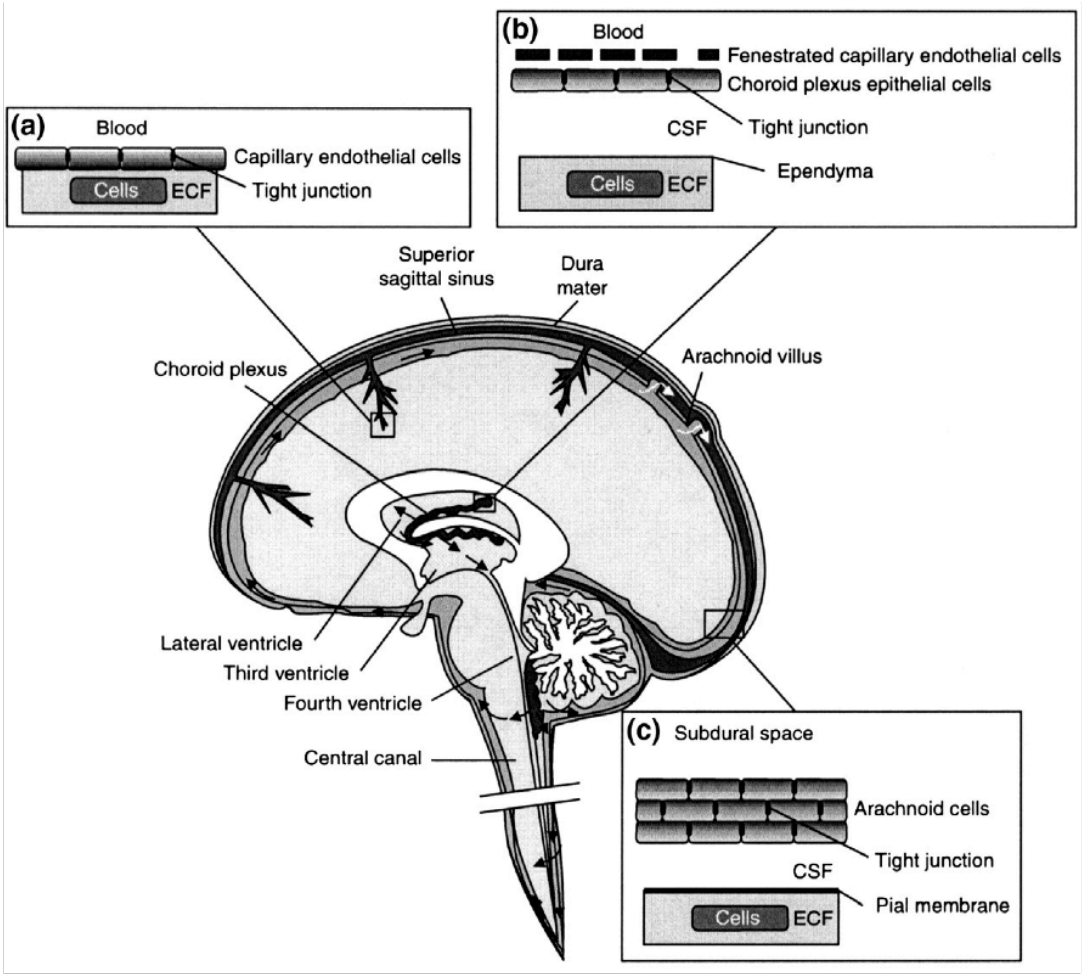

Figure 3: Diagram of the human brain, showing the 3 barriers that separate the brain and cerebrospinal fluid from the blood circulation. Diagram reproduced from (79).

regarded as the most important of the three, accounting for the largest surface area where exchange of molecules takes place (between 12 to 18 m^2) in the brain. Furthermore, the close proximity of all cells in the brain to a nearby blood vessel (about 25 µm or less) makes it an important route for nutrient acquisition and waste removal. At the cellular level, the BBB (figure 4) comprises of endothelial cells that form tight junctions in between them, surrounded partially by pericytes. This is embedded in the basal lamina, with astrocyte feets forming a complex web that encloses the whole capillary.

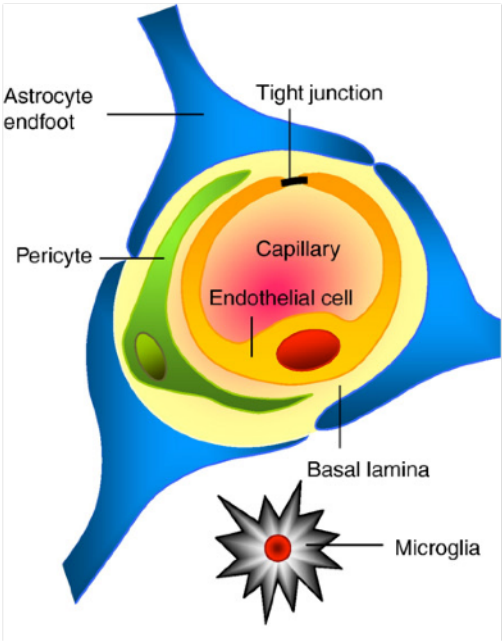

Figure 4: Structure of BBB. The endothelial cells in the brain capillaries establish tight junctions with adjacent neighbours, forming an impermeable barrier between the brain parenchyma and the blood. Pericytes surround the endothelial cells partially, and both cells are enclosed within the basal lamina. Astrocytes form networks that surround the brain capillaries with their endfoot processes, maintaining the integrity of the vessels. Microglia are found next to the vessels, ready to react to any pathogens that breach the BBB. Diagram reproduced from (79).

The BBB plays important roles in regulating the transport of ions and other small molecules into the brain parenchyma. Many of these, such as sodium, potassium ions and glutamate, must be maintained at constant levels in the brain, regardless of changes in ion levels in the blood circulation following exercise or meals (81, 82). Otherwise, neuronal damage and short circuitry of neurotransmission can occur, since glutamate is one of the neurotransmitters secreted by neurons. Other macromolecules in the blood are notably absent in the brain, where they could initiate immune activation, damage and apoptosis of the neurons if they are allowed access (83-85). Regulation of solutes across the BBB is made possible through transporters, carriers and receptors that are found on the apical surfaces of the endothelial cells.

Immune subsets involved in ECM

The observation that leukocytes are found sequestered in the brain microvasculature of both HCM and ECM prompted the dissection of immune cell types that are involved in the latter. The situation was revealed to be complex, with many different cell types involved. Macrophages are found to be present in areas where breakdown of vasculature occurs in mice (86). Their depletion at the time of inoculation but not later in infection led to protection against ECM, suggesting that they are only involved in the induction process (87, 88). Neutrophils are also observed in the brains of CBA/Ca mice during ECM and they were shown to be essential for ECM development (89). However, depletion in the 129,B6 mouse model could not protect them from ECM (87), suggesting that neutrophils have different roles to play during infection in different mice. Natural killer (NK) cells were reported to be essential for ECM development, as mice depleted of these cells with anti-asialo GM1 antibodies did not develop pathology (90). Mice devoid of B cells can still develop ECM, suggesting that these cells play minimal roles in the disease progression (91). T cells, on the other hand, are implicated heavily. Numbers of the two main types of T cells, $CD4^+$ and $CD8^+$, increased in the brain of mice during ECM (87), and mice that are deficient for T cells, either through depletion or knockout mice [such as β_2-microglobulin (β_2m)- or RAG-KO mice], do not develop ECM (91). These cells influence ECM development at different stages. $CD4^+$ T cells are shown to be important during the initial days of parasite infection, but are dispensable later in the infection when ECM is expected to develop (87, 91, 92). On the other hand, ECM prevention can be achieved with late depletion of $CD8^+$ T cells at day 6, one day

before ECM is expected to manifest, implicating these cells as the effector population (87). In the spleen, conventional dendritic cells (DC) that express $CD11c^{high}$ were reported to be essential for ECM, through depletion of these cells in CD11c-DTR (diphtheria toxin receptor) mice (93). Subsequently, the $CD8\alpha^{+}$ subset of the $CD11c^{high}$ DCs was identified as the ones most effective in cross-presenting parasite antigens to $CD8^{+}$ T cells (94), though this is restricted to days 2-3 post-infection (95). Separately, other groups used Clec9A-DTR (96) and Langerin-DTR mice (97) to target $CD8\alpha^{+}$ DC depletion and confirmed its role, as these mice were totally or partially protected when infected with PbA, respectively. In the former study, $CD4^{+}$ and $CD8^{+}$ T cell accumulation in the brains were reduced following DC depletion.

Cytotoxic ($CD8^{+}$) T cells

Cytotoxic T cells are a subset of T lymphocytes that form one half of the classical adaptive immune system. Precursors of T lymphocytes originate from hematopoietic stem cells in the bone marrow. These then exit into the blood circulation and travel to the thymus, where they undergo a complex process to differentiate into $CD4^{+}$ and $CD8^{+}$ single-positive T cells. During this process, T cells with a T cell receptor (TCR) that can interact with self-major histocompatibility complex (MHC) with intermediate avidity will survive. If the recognition is to MHC class I, the T cell will eventually become $CD8^{+}$ T cell, whereas those recognizing MHC class II become $CD4^{+}$ T cells. At the medulla, all $CD8^{+}$ T cells undergo a negative process, where they interact with MHC class I molecules presented by medullary

thymic epithelial cells. These cells present self-antigens that are normally found elsewhere in the body, through expression of the transcription factor AutoImmune Regulator. $CD8^+$ T cells that interact too strongly with these self-peptide-MHC complexes are eliminated, preventing them from mounting an immune response against host cells (central tolerance). Thus, only those that interact weakly are allowed to survive and leave the thymus as naïve $CD8^+$ T cells. These cells travel to peripheral lymphoid organs to interact with professional antigen presenting cells (APC).

The APCs in the lymphoid organs may have travelled from an infection site after capturing foreign antigens and becoming activated. Naïve $CD8^+$ T cells having the corresponding TCRs will be activated, mainly through two main interactions. The interaction between the TCR and its cognate epitope bound to MHC class I, with CD8 as a co-receptor, constitutes the first signal for activation (figure 5). If the T cell receives only this first signal, it will become anergic, rendering it unable to mount an effective immune response against target cells (98). The second signal required for activation comes from co-stimulatory molecules, which is often in the form of interaction between CD28 on the T cells, and CD80 or CD86 on the activated APCs. Other co-stimulatory molecules on the T cells that can also lead to its activation include CD134, CD137, and CD278 (Inducible T-cell COStimulator), which are expressed after T cells recognize antigen, unlike CD28 that is expressed constitutively. The third signal for $CD8^+$ T cell activation is cytokine stimulation, most often by interleukin-2 (IL2). Its binding to IL2 receptors on T cells can lead to

intracellular signaling that augments or even replaces the second signal to push T cells to activation.

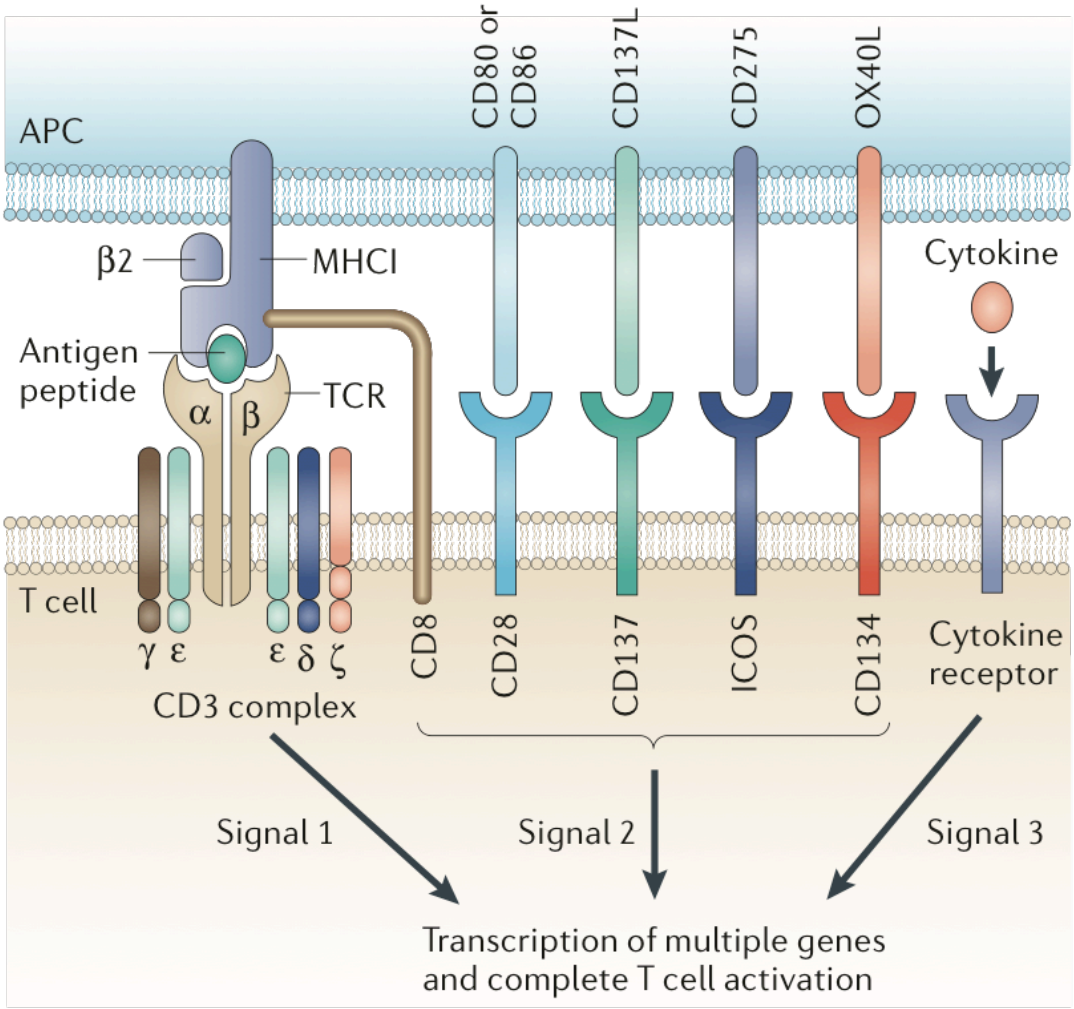

Figure 5: Different signals that drive activation of CD8$^+$ T cells. Interaction between pMHC and TCR provides the first signal for activation. Further signals come from the interactions between co-stimulatory receptors on CD8$^+$ T cells and their respective ligands, or from binding of cytokines to the corresponding receptors. Diagram reproduced from (99).

The main effector function of activated CD8$^+$ T cells is cytolysis of host cells presenting cognate peptide-MHC (pMHC) complexes. The CD8$^+$ T cells form immunological synapses with the target cells, mediated mainly by the TCR-pMHC and CD11a-ICAM-1 (intracellular adhesion molecule 1) interactions. From here, target cells can be killed in two ways. Firstly, secretory granules that contains

granzymes and perforins are released within the immunological synapse in the direction of the target cells (100). Perforin forms pores in the target cell membrane, allowing granzymes to enter the cell interior and initiate apoptosis through the caspase-dependent pathway (101). The alternative route by which $CD8^+$ T cells kill target cells is expressing Fas ligand that interacts with Fas receptors (CD95) on the target cells. This forms a death-inducing signaling complex in the cytoplasm, which then triggers a signaling cascade that ultimately leads to apoptosis through the same caspase-dependent pathway as the first approach (102). In addition to cytolysis, $CD8^+$ T cells can exert their effectors by secreting interferon γ (IFNγ) and tumor necrosis factor α (TNFα), cytokines with antiviral and antitumoral effects.

Major histocompatibility complex (MHC) class I

The MHC class I molecule comprises the α chain with a peptide-binding groove and beta-2 microglobulin (β_2m), and is expressed on the cell surfaces of all nucleated cells in vertebrates. Through interacting with TCRs on $CD8^+$ T cells, they allow the immune system to determine if the cells are healthy. During infection by intracellular pathogens or transformation into cancerous cells, epitopes from pathogen proteins or cancer antigens are presented on MHC class I molecules. $CD8^+$ T cells with TCRs that can bind these foreign pMHCs become activated by APCs and mount a cytotoxic response to eliminate these abnormal target cells. MHC class I molecules complexed with self-epitopes will not be targeted as self-reactive $CD8^+$ T cells were eliminated in the thymus prior to maturation through negative selection.

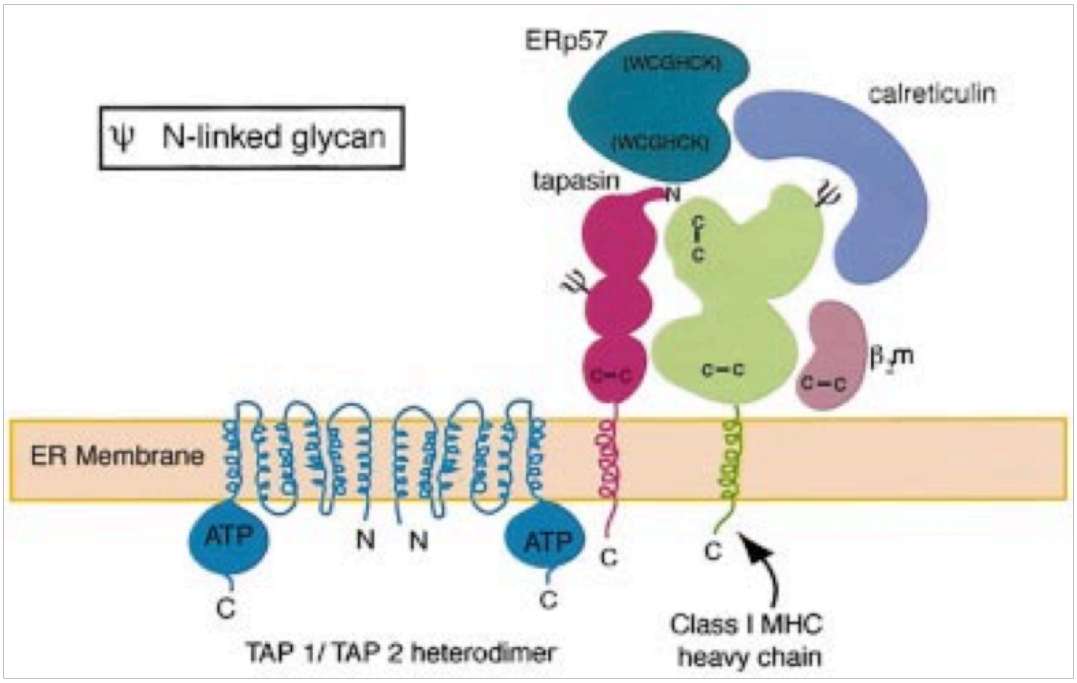

Figure 6: Stabilization of nascent MHC class I molecules. Prior to peptide loading, nascent MHC class I molecules interact with multiple chaperone proteins (tapasin, calreticulin and ERp57) in the ER. This stabilizes the complex until MHC class I epitopes get transported by TAP into the ER and load onto the MHC class I, leading to dissociation of the chaperone proteins. Diagram reproduced from (103).

Where do the peptides that bind MHC class I molecules come from? A portion of every protein that is synthesized in the cell is sent to the proteasomes to be digested into small fragments, which are transported into the endoplasmic reticulum (ER) by transporter associated with antigen processing (TAP). In the ER, nascent MHC class I molecules without peptides are first stabilized by an array of chaperone proteins (figure 6) that include tapasin, calnexin, calreticulin and ERp57 (103). Calnexin first dissociates from the complex upon binding of β_2m to the α chain, and following successful loading of a high-affinity peptide into the binding groove, the rest of the stabilizing chaperones dissociate, allowing the complete pMHC to be exported to the surface of host cells (103, 104).

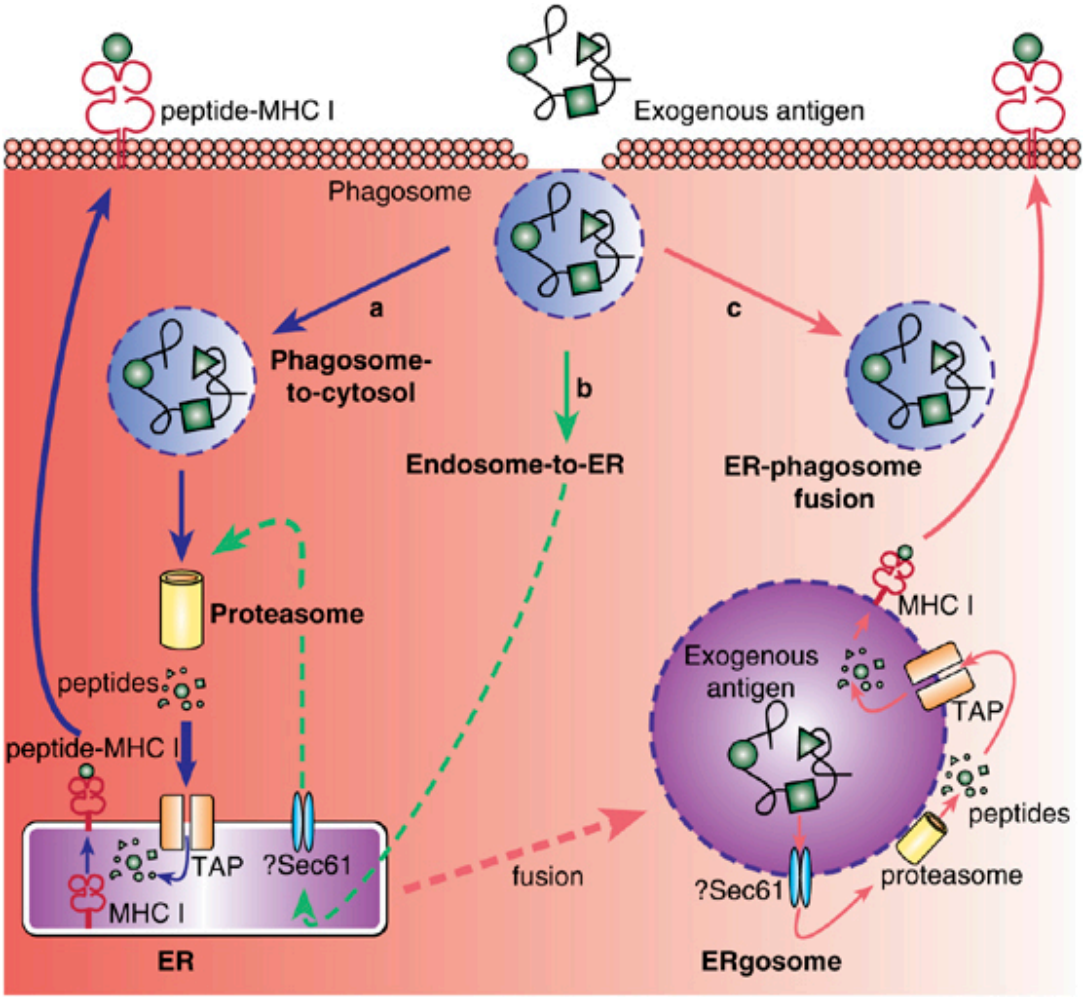

Figure 7: Proposed models of cross-presentation. Exogenous antigens are endocytosed into the cell, and from here three different models were hypothesized. The antigen is transported into the cytosol (a) and is degraded by proteasomes. The resulting peptides are translocated into the ER by TAP, loaded onto nascent MHC class I molecules and then exported to the cell surface. In (b), the antigen is transported back to the ER and gains access to the cytosol through an ER-associated protein degradation pathway, possibly by Sec61. In (c), fusion of phagosomes containing the antigen with ER occurs, providing another route for the antigen to translocate into the cytosol through Sec61 transporter. Diagram reproduced from (105).

MHC class I molecules, in general, present peptides from cytosolic sources. However, MHC class I molecules can also present epitopes from extracellular sources, a process termed cross-presentation (106). The mechanism of cross-presentation is not completely elucidated, and a number of models were proposed, shown in figure 7 (reviewed in (105)]. The canonical model (a) involves

transportation of endocytosed antigens into the cytosol, where proteasomes generate the peptides that are then exported into the ER or ER-phagosome fusion for loading onto MHC class I molecules (107, 108). An alternative model (b) proposes that transport of endocytosed antigens from the endosomes back to the ER can occur, from which the antigens access the cytosol through the ER-associated protein degradation pathway, possibly through Sec61 protein translocater (109). Antigen fragments are then transported back to ER as per the canonical model. A third model hypothesizes that phagosomes containing foreign antigens fuse directly with the ER, providing another route for antigens to access the cytosol (107, 110). However, this model was not well accepted, with others showing data to question this hypothesis (111-114). Cross-presentation is a critical process by which professional APCs induce $CD8^+$ T cell-mediated immunity against tumours and viruses that infect other cell types. These APCs have the ability to ingest dying cells, thus acquiring the foreign antigens for MHC class I presentation. In addition, they can also capture cellular antigens from intact cells, a process termed 'nibbling' (115).

MHC multimers

In a watershed work by Altman and colleagues, they created fluorescent MHC tetramers through refolding biotin-tagged MHC class I α chain with β_2m and peptides of interest, biotinylating the resulting MHC class I complex, followed by tetramerization with fluorescent streptavidin conjugates (117). The MHC multimers bind to multiple cognate TCRs on $CD8^+$ T cells at the same time, allowing them to

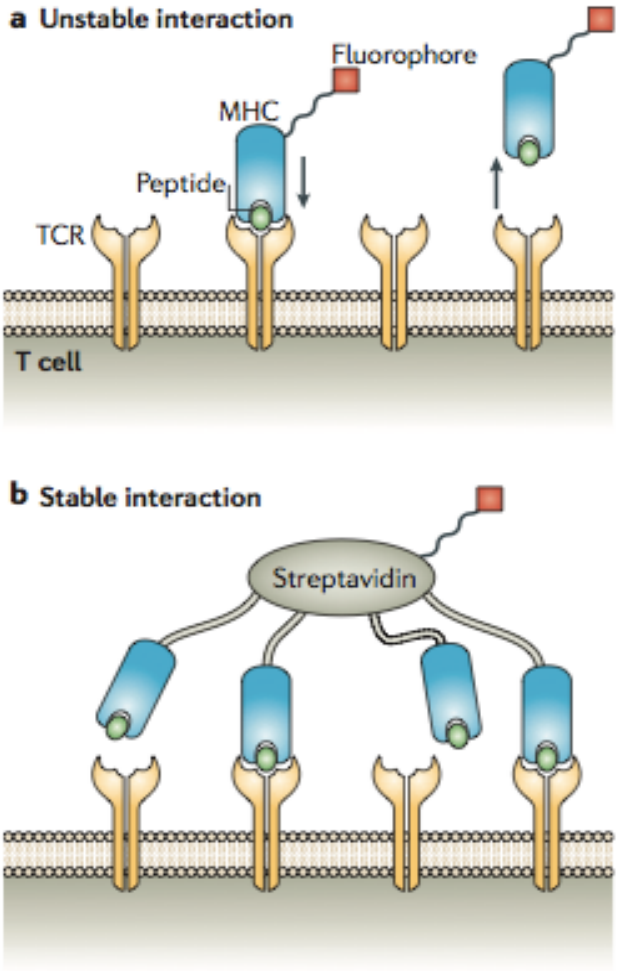

Figure 8: MHC tetramers enable the labeling of antigen-specific T cells. The interaction between TCRs and pMHC complex has a very short half-life averaging a few seconds, leading to rapid dissociation of pMHC monomers (a). However, pMHC tetramers bind to multiple TCRs on the same cell more strongly through increased avidity, allowing specific T cells to be labeled and analyzed. Diagram reproduced from (116).

stabilize this weak interaction through avidity (figure 8). This, in turn, gives researchers the ability to identify antigen-specific $CD8^+$ T cells and evaluate their functions, thereby paving the way for better understanding of the role of specific $CD8^+$ T cells in pathogenic and protective settings. Apart from tetravalency, other forms of MHC multimers exist, where more pMHC complexes available for binding to T cells facilitates the labeling of rare antigen-specific $CD8^+$ T cells or those with TCRs of a lower affinity to cognate pMHC complexes (118). One difficulty of producing pMHC multimers is the laborious need to refold the MHC chains with each peptide of interest. Other researchers improved on this technology by synthesizing unique peptides with a photo-labile (2-nitro)phenyl side chain moiety (119-121). These form complexes with MHC class I molecules during refolding. Irradiation with UV light will

induce self-cleavage of the peptide in the resulting pMHC complex. Addition of a suitable peptide of interest during irradiation causes it to replace the cleaved peptide in the peptide-binding groove of the MHC α chain. This method enables the generation of tetramers with different specificities in a rapid fashion.

CD8$^+$ T cells are involved in ECM pathogenesis

In the mouse model, a number of studies demonstrated that CD8$^+$ T cells are the effector cells that mediate ECM (87, 92, 122-125). These cells do not recognize self-antigens, as transfer of CD8$^+$ T cells from PbA-infected, ECM-susceptible mice into recipient mice only causes neurological signs only if the latter are also infected (126). When wild-type mice were adoptively transferred with chicken ovalbumin (OVA)-specific CD8$^+$ T cell and infected with transgenic parasites carrying the OVA epitope (SIINFEKL), the specific CD8$^+$ T cells were activated, proliferated, trafficked to the brain and exhibited epitope-specific cytotoxicity (94, 127). In other studies, analyzing the TCR repertoire of CD8$^+$ T cells in the brains of mice succumbing from ECM revealed that some TCRβ segments, especially Vβ8.1, were found more often, as compared to uninfected controls (87, 128). Depletion of CD8$^+$ T cells carrying these subsets resulted in a delay in ECM onset (128). All these suggest that the CD8$^+$ T cells that were found in the brains of mice during ECM were specific for parasite antigens. Characterizations of total (or OVA-specific) CD8$^+$ T cells in the ECM mouse model revealed an activated phenotype, and the types of markers they exhibit are summarized in table 1. The expression of perforin and granzyme B by CD8$^+$ T cells, but not IFNγ, was demonstrated to be vital for ECM pathogenesis (122, 123).

Table 1: Biomarkers expressed by $CD8^+$ T cells sequestered in the brains of mice during ECM. Reproduced from (129).

Markers	Expression	Reference
CD markers		
CD11a (LFA-1)	High	(128, 130, 131)
CD44	High	(123, 127, 128)
CD54 (ICAM-1)	High	(128)
CD62L	Low	(123, 127, 128)
CD69	High	(127, 128)
Cytokines		
IFNγ	Majority	(128, 131, 132)
TNFα	Subset	(128)
IL4	None	(128)
IL10	Minority	(128)
Chemokine receptors		
CCR2	Upregulated	(123, 133)
CCR5	Upregulated	(123, 131, 134)
CXCR3	Upregulated	(90, 123, 131, 135)
Cytolytic granules		
Granzyme B	Majority	(122, 127, 130-132)
Perforin	Majority	(123)

Migration of $CD8^+$ T cells to the brain

Analysis of chemokine receptor expression on brain-sequestered $CD8^+$ T cells in the ECM mouse model showed that chemokine receptors CCR2, CCR5, CXCR3 and CXCR4 were over-expressed as compared to naïve $CD8^+$ T cells, suggesting that these receptors mediate trafficking of parasite-specific $CD8^+$ T cells to the brain. However, CCR2 was eventually shown to be nonessential, as CCR2 knockout mice remain susceptible to ECM (133). CCR5 involvement varies in different laboratories. Mice lacking CCR5 were either largely protected against ECM (134), or simply had a delay in ECM occurrence (123). Those that did succumb to ECM had similar numbers of $CD8^+$ T cells in the brains as that of wild-type mice with ECM. In the case of CXCR3,

the majority of lymphocytes sequestered in the brains of mice during ECM express this receptor (90). CXCR3-deficient mice were mostly protected against ECM, concomitant with a decrease in the number of $CD8^+$ T cells found in the brains (135, 136). This protection was abolished when $CD8^+$ T cells from wild-type mice were adoptively transferred into the CXCR3-deficient mice (135, 136). A redundancy of the pathogenic roles of CCR5 and CXCR3 may exist during ECM pathogenesis, with CCR2 being excluded. The role of CXCR4 in ECM remains to be studied.

The chemokines CXCL4, CXCL9, CXCL10 and CXCL11 are the ligands for CXCR3; the former three have been investigated in ECM development. CXCL11 was omitted as C57BL/6 mice are unable to express this due to a point mutation (136). CXCL9- or CXCL10-deficient mice were partially protected from ECM in one study (136), while researchers from another lab showed almost complete protection in the latter mice, with T cells being trapped in the spleen during infection (137). The endothelial cells in the brain were pinpointed as one of the sources of CXCL9 and CXCL10 in the brain (135, 136), but other conflicting reports have implicated microglia for CXCL9, astrocytes for CXCL10 (135) and neurons for CXCL10 expression (136). CXCL4 knockout mice conferred some protection against ECM, associated with less T cell trafficking to the brain (138). The ligands for CCR5, namely CCL3, CCL4 and CCL5, were also over-expressed during infection (136, 139-142), but their involvement in ECM pathogenesis remains unclear.

Effects exerted by pro-inflammatory cytokines during ECM

Following PbA infection, sequestration of iRBC in the brain vasculature (143) lead to production of pro-inflammatory cytokines in the brain, including IFNγ (124, 144). The expression of ICAM-1 on the surfaces of these cells is also increased (145), allowing them to interact with activated T cells, which express the cognate receptor lymphocyte function –associated 1 or LFA-1, a heterodimer of CD11a and CD18. Blocking this interaction with antibodies prevented ECM (145), demonstrating that this interaction is essential for leukocytes to sequester in the brain microvasculature. TNFα production was elevated in the brains of mice after PbA infection (146, 147), but it was lymphotoxin alpha (LTα), not TNFα, that was indispensable for ECM development (148). The mechanism of LTα involvement in ECM is not clearly demonstrated, but it is thought to be similar to that of IFNγ (149).

Though expression of IFNγ by $CD8^+$ T cells is not critical for ECM, mice deficient in IFNγ or IFNγ receptor remain resistant to ECM (91, 150, 151), showing that expression of this cytokine from other cellular sources is essential for development of pathology. The diverse roles IFNγ play in causing ECM has been reviewed (152) and include the regulation of $CD8^+$ T cell trafficking to the brain (142, 151, 153) and parasite sequestration in the organs (124). Expression of chemokines CCL3, CCL4, CCL5, CXCL9 and CXCL10 in the brain was attenuated during PbA infection in IFNγ- or IFNγ receptor-knockout mice (142, 151). In NK-depleted mice, adoptive transfer of NK cells from wild-type, but not IFNγ-knockout mice, was able to restore T cell trafficking to the brain (90). In a study involving IFNγ reporter mice,

Villegas-Mendez and colleagues found that in the brain NK cells form the bulk of IFNγ-producing cells early in the infection, but $CD4^+$ and $CD8^+$ T cells eventually became the major producers over the course of infection (153). Moreover, IFNγ-knockout mice that received wild-type $CD4^+$ T cells, but not $CD8^+$ T cells, became susceptible to ECM (153). These suggest that NK and $CD4^+$ T cells form the primary producers of IFNγ in the brain, in the context of ECM pathogenesis.

Brain endothelial cells as the targets in ECM.

The pathological changes in the BBB are the hallmark of ECM [reviewed in (154)], and the cause of this breakdown is speculated to lie in the destruction of endothelial cells (87, 123, 126, 155). In certain scenarios, such as an inflammatory milieu (156), these cells acquire the ability to become APCs and become efficient in antigen presentation [reviewed in (157)]. In support of this, an increase in expression of MHC class I and II molecules, β_2m, and TAP were observed in PbA-infected C57BL/6 mice (158). Mice lacking both H-$2K^b$ and H-$2D^b$ MHC class I molecules, as well as β_2m, were resistant to ECM (128). Coupled with the requirement of granzyme B and perforin for ECM to develop (122, 123), these paint a picture that endothelial cells cross-present parasite epitopes on their MHC class I molecules during ECM, and subsequent recognition by activated parasite-specific $CD8^+$ T cells lead to endothelial cell death due to pro-apoptotic actions of granzyme B and perforin. However, no evidence of such cross-presentation had been uncovered at the outset of this work.

Much research into ECM mouse models have led to the proposed mechanism of ECM pathogenesis by Rénia *et al* in figure 9 (126, 129). In this model, infection of C57BL/6J mice with PbA leads to priming of malaria-specific $CD4^+$ and $CD8^+$ T cells in lymphoid organs by $CD8^+$ $Clec9A^+$ dendritic cells. In the brain microvasculature, sequestration of iRBC and subsequent rupture releases cell debris and inflammatory molecules, activating cells in the brain endothelium and attracting leukocytes to the brain. These form a positive feedback loop that further intensifies the proinflammatory microenvironment, eventually recruiting activated malaria-specific $CD8^+$ T cells to the brain through secretion of chemokines. Activated cells in the brain endothelium phagocytose parasite antigens, then cross-present malaria epitopes on their MHC class I molecules. These are recognized by specific $CD8^+$ T cells, leading to secretion of perforin and granzymes to destroy presenting cells, ultimately breaching the BBB. Edema and hemorrhage follow, cumulating into the neurological symptoms seen in ECM.

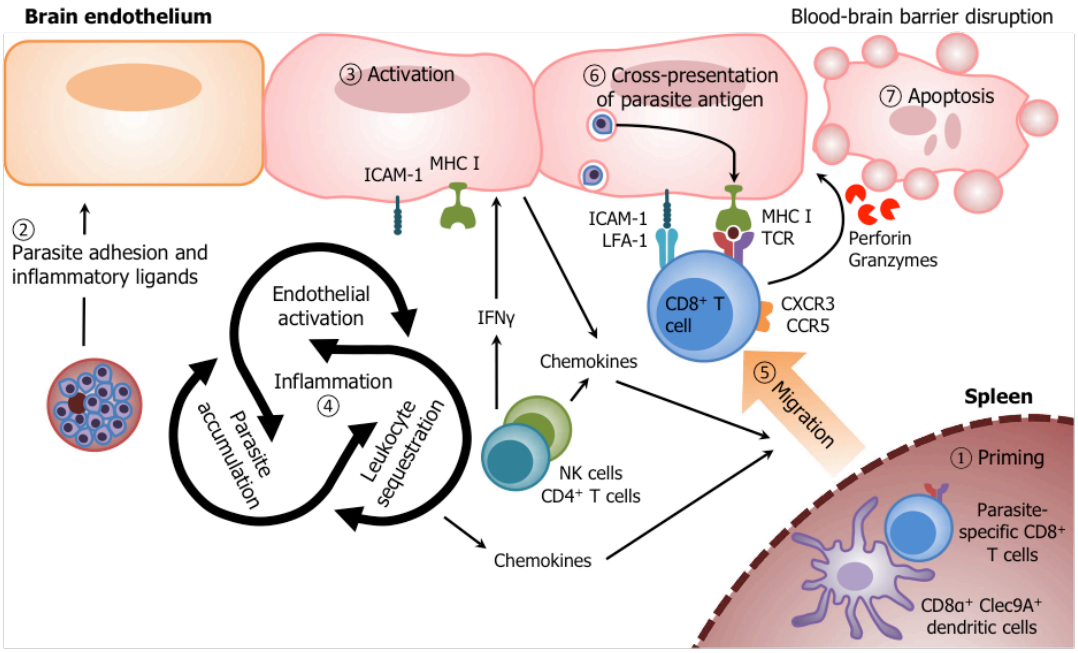

Figure 9: Proposed mechanism for ECM pathogenesis. Refer to text for details. The work in this thesis helped to refine this model. Diagram reproduced from (129).

At the beginning of this project, no epitopes that are recognized by parasite-specific $CD8^+$ T cells during ECM had been identified. The lack of known epitopes severely limited characterization of the parasite-specific $CD8^+$ T cell response and how it leads to pathogenesis. This project thus set out to address this deficiency, with the following main and sub-objectives:

1) Construct a PbA complementary DNA (cDNA) library and express it in EL4 cells (which share the same MHC haplotype as C57BL/6J mice).
2) Identify the cognate epitopes essential in ECM. This is done in two steps.
    a) Construct T reporter cell lines bearing TCRαβ chains from brain-sequestered $CD8^+$ T cells from mice with ECM, and screen the EL4 PbA cDNA library to identify cognate antigens.

b) Utilize MHC tetramer technology to identify the cognate epitope from the antigens discovered in 2a.

3) With the tetramers and T reporter cells, investigate the epitope-specific $CD8^+$ T cell responses in the PbA mouse model.
   a) Incidence and characterization of epitope-specific $CD8^+$ T cells in mice infected with PbA, Py17X and PbNK65.
   b) Incidence and extent of cross-presentation of parasite epitopes in the brain microvasculature of mice infected with PbA, Py17X and PbNK65.
   c) Demonstration of BBB damage by epitope-specific $CD8^+$ T cells in PbA mouse model
   d) Investigate the effects of tolerizing $CD8^+$ T cells of known specificites.

The research that addresses the objectives listed will be described in the following 3 chapters in this thesis.

Chapter 1: Generation of PbA cDNA library

Introduction

In general, three approaches can be adopted to search for unknown $CD8^+$ T cell epitopes. Firstly, if the pathogen genome (or even better, the pathogen proteome) is known, epitopes that can bind to MHC class I molecules can be predicted. Examples of online databases that provide such functions include SYFPEITHI (http://www.syfpeithi.de/) and IEDB (http://www.iedb.org/). A prediction program that generates a combined score from different prediction algorithms is also available (121). The output of predicted epitopes can be tested experimentally to identify those that can bind and stabilize MHC class I molecules, or those that can stimulate $CD8^+$ T cells. Secondly, APCs from the infected host can be isolated, and peptides in the binding grooves of their MHC class I molecules can be eluted and analyzed by mass spectrometry (159, 160). Thirdly, activated $CD8^+$ T cells that have experienced clonal expansion following infection can be isolated and screened against a library of pathogen epitopes presented by APCs on their MHC class I molecules. To preserve the TCR α and β chains, these $CD8^+$ T cells can be fused together with the T cell fusion partner BWZ.36 created by Professor Nilabh Shastri (UC Berkeley) (161). Engagement of TCR on the fused hybridoma leads to a signaling cascade that triggers nuclear import of the transcription factor nuclear factor of activated T-cells (NFAT), leading to activation of Shastri's NFAT-LacZ cassette, which can be visualized by X-gal staining.

To screen for the malaria $CD8^+$ T cell epitopes recognized by the generated T reporter cells, a PbA cDNA library had to be created and expressed in relevant APCs (such as EL4 cell line) that share the same haplotype as C57Bl/6J mice. In our case, we chose to work with EL4, a mouse thymoma suspension cell line, because of its ease in growing them in cultures and its histocompatibility with C57BL/6J mice. A common method of making the cDNA library is through the use of oligo-dT primers to purify mRNA and synthesize full-length cDNAs, but we reasoned that a shorter cDNA library constructed with random hexamer primers may be better in our context. With the AT-rich nature of the malaria genome, reverse transcriptase starting from the mRNA polyA tail may often fail to reach the 5' end of mRNA, leading to poorer coverage at that end. Shorter cDNAs are also less likely to be lost or expressed poorly in mammalian cell lines. However, expression of random-primed cDNA libraries was typically inefficient, with an estimated 8% of clones harbouring inserts in open reading frame (ORF) (162). Furthermore, the addition of overhangs to cDNA primed with random hexamers (in order to facilitate cloning into vectors) is difficult (163). The reason is speculated to arise from the exonuclease activity of *E. coli* DNA polymerase, which snips off unpaired DNA strands from the 5' to 3' end (162, 164). To address these shortcomings, a number of modifications were employed during the library construction in this chapter.

Materials and methods

Mice

C57BL/6J mice from 6 to 8 weeks old were used throughout the experiments, unless otherwise stated. These mice were bred under specific pathogen-free conditions in the Biological Resource Centre, Singapore. All animal experiments and procedures were approved by the Institutional Animal Care And Use Committee and complied with the guidelines of the Agri-Food and Veterinary Authority and National Advisory Committee for Laboratory Animal Research.

Parasite

PbA iRBC were passaged by intraperitoneal injection (i.p.) in C57BL/6J mice, harvested and stored in Alsever's solution in liquid nitrogen. For PbA infection, mice were injected i.p. with 0.3 to 1.0 x 10^6 iRBC, with the dose adjusted for each batch so that most mice develop neurological signs at 7 days post-infection. Parasitaemia was checked by examination of thin blood smears stained with Giemsa, or by flow cytometry (165).

Messenger RNA isolation

Mice were exsanguinated under ketamine/xylazine anesthesia through the retro-orbital route or cardiac puncture. Blood from 5 mice was collected in 10 mL

PBS with 50U/mL heparin (Sigma-Aldrich, St. Louis, MO), with frequent swirling of the mixture throughout to minimize blood clotting. The harvested blood was passed through a Plasmodipur filter (EuroProxima, Arnhem, Netherlands) twice to remove leukocytes. Erythrocytes were centrifuged at 500 g for 5 min, aspirated and re-dissolved in 15 pellet volumes of Trizol (Life Technologies, Grand Island, NY) at 37˚C for 5 min. Chloroform (Merck, Darmstadt, Germany) was added to the mixture at a ratio of 1 part to 5 parts Trizol, mixed thoroughly and spun in 30 mL Oak Ridge centrifuge tubes at 12 000 g, 4˚C for 30 min. The aqueous phase was collected and mixed with 100% molecular-biology grade isopropanol (PanReac Applichem, Darmstadt, Germany) at a ratio of 10:7, incubated at -20˚C for at least 2 hours, and passed through 0.7 µm Target glass microfiber filter (National Scientific Company, Rockwood, TN). The RNA in the filter was washed first with 70%, followed by 100% ethanol, dried and eluted with 10 mM Tris-HCl, pH 8.0. Messenger RNA was treated with DNA-free DNA removal kit (Ambion, Life Technologies), followed by isolation with PolyATtract mRNA Isolation System III kit (Promega, Madison, WA), both according to the manufacturer's instructions.

PbA cDNA synthesis

The purified mRNA (for every 1 µg) was reverse transcribed with 20 pmol IFb-17PS-X6 primer and SuperScript II reverse transcriptase (Life Technologies) according to manufacturer's instructions, with addition of 100 µg/mL bovine serum albumin (BSA, New England Biolabs, Ipswich, MA) to improve yields. For each 10 µL of the first strand synthesis product, the following reagents were added to a reaction

volume of 50 µL: 1X second strand buffer, 0.2 mM dNTP (both from Life Technologies), 0.02 U/µL RNase H, 0.4 U/µL *E. coli* DNA polymerase, 0.1 U/µL *E. coli* DNA ligase (all three enzymes from New England Biolabs) and 100 µg/mL BSA, followed by incubation at 16˚C for 2 hours, inactivation at 70˚C for 10 min. T4 DNA Polymerase (New England Biolabs) was added at 10 U/µL and incubated at 12˚C for 15 min, followed by termination of all reactions by addition of 10 mM EDTA, 70˚C for 20 min. The cDNA was purified with QIAquick MInElute spin columns (QIAgen, Hilden, Germany), following manufacturer's instructions.

Annealing of DNA adaptor

The DNA adaptors Acc-ins and IFLink-b3 were created by mixing equimolar amounts of primer pairs (Acc-ins1 and Acc-ins2; IFLink-a and IFlink-b3, respectively) in 1X T4 DNA ligase buffer (New England Biolabs) and heated at 95˚C for 5 min, followed by stepwise decrease of temperature at 1˚C per min until reaction reached 25˚C. The hybridized DNA adaptor was used without further purification.

Vector construction

To create the pScrAn-Int vector, modpGEX vector (created by Dr Shanshan Howland, derived from pGEX-2T vector) was digested with SwaI and EcoRI to clone in the kanamycin resistance gene (Kan^R). Immediately upstream of the Kan^R gene, an 11 bp DNA sequence that contains 3 stop codons in 3 different reading frames was introduced. This was transformed into OneShot TOP10 chemically competent cells

(Life Technologies), and positive transformants were identified with 3StopKanR and pGEX-2Tr primers by colony PCR.

Dr Shanshan Howland modified the pWPXL lentivector, a kind gift from Didier Trono (Addgene plasmid #12257) to pScrAn1 vector by fusing a self-cleaving T2A sequence to the distal region of enhanced green fluorescent protein (EGFP). From here, pScrAn1 was linearized with restriction enzymes XmaI and NdeI, purified with QIAquick MinElute spin columns and ligated with Acc-ins DNA adaptor with Quick T4 DNA Ligase to create pScrAn-Acc, followed by transformation into OneShot Stbl3 chemically competent cells (Life Technologies). Positive transformants were identified by colony PCR with preGFP and Acc-ins2 primers.

Amplification and cloning of PbA cDNA

The IFLink-b3 DNA adaptors at 0.18 µmol were ligated to every 1 µg PbA cDNA at the 5' end by Quick T4 DNA ligase in the presence of 100 µg/mL BSA through temperature-cycle ligation (166) as depicted in table 2. Excess DNA adaptors were removed by QIAquick MinElute spin column purification, and the PbA cDNA was amplified in 1X High-Fidelity PCR buffer with 0.5 µM IFLink-a and IF21 primers, 0.2 mM dNTP, Phusion II DNA polymerase (Life Technologies) with the conditions set out in table 3, followed by spin column purification.

Table 2: Condition for ligating IFLink-b3 DNA adaptors to PbA cDNA by temperature-cycle ligation

Step	Temperature (˚C)	Duration (sec)
1	10	30
2	30	30
3	Repeat steps 1 to 2 for a total of 480 cycles	
4	65	1200
6	20	60

Table 3: PCR cycling conditions for amplification of PbA cDNA library.

Step	Temperature (˚C)	Duration (sec)
1	98	30
2	98	10
3	38	20
4	72	60
5	Repeat steps 2 to 4 for a total of 14 cycles	
6	72	600

For In-fusion cloning into pScrAn-Int vector, the vector was cut with restriction enzymes NsiI and SwaI, run on 1% TAE gel and purified from the 182 bp fragment by gel extraction with QIAquick MinElute spin columns. This was mixed with PbA cDNA library amplicons at vector to insert ratio of 6.67:1, together with In-Fusion enzyme (Clontech, Mountain View, CA) and performed according to manufacturer's instructions. Reaction mix was purified by QIAquick MinElute spin columns, transformed into ElectroMax Stbl4 competent cells (Life Technologies), plated on LB agar plates supplemented with 50 µg/mL kanamycin (Merck) and 0.02 mM isopropyl β-D-1-thiogalactopyranoside (IPTG, Life Technologies), and incubated at 37˚C for 16 hours. Clones were harvested by adding 1 mL LB media to each plate and scraped with a spreader. Cell suspensions were pooled, pelleted at 4000 g for 5 min, and pScrAn-Int-PbA cDNA plasmids purified with Nucleospin plasmid miniprep kit (Macherey-Nagel, Düren, Germany).

To clone into lentivector pScrAn-Acc, the PbA cDNA insert in pScrAn-Int vector was excised out with EagI restriction enzyme, separated from the vector by gel electrophoresis in 1% TAE and the resulting smear purified by gel extraction. The pScrAn-Acc vector was cut with restriction enzymes BstBI and AsiSI and spin-column purified. Both the PbA cDNA insert and linearized pScrAn-Acc was incubated together with In-Fusion enzyme, electroporated into ElectroMax Stbl4 cells and plated on LB plates supplemented with 100 µg/mL ampicillin (Merck). Clones were harvested in the same fashion as described earlier and the vectors purified with Nucleospin plasmid miniprep kit.

PCR amplification

Plasmodium yoelii UIS4 (PyUIS4) gene that was cloned into a lentivector by Dr Shanshan Howland was amplified with 0.5 µM forward primer IF-PyUIS4f and 0.5 µM of either of the reverse primers IF15-PyUIS4r or IF15PS-PyUIS4r, in the presence 1X PCR buffer containing 1.5 mM or 3 mM $MgCl_2$, 0.2 mM dNTP, 0.02 U/µL AmpliTaq Gold DNA polymerase (Life Technologies). Amplicons were analyzed in 1% TAE gel, gel-purified with QIAquick MinElute kit, cloned into NsiI, SwaI-treated pScrAn-Int vector, transformed into OneShot TOP10 competent cells and grown on LB agar plates with 100 µg/mL ampicillin. In separate experiments, PCR amplicons were used as templates for a new round of amplification with 0.5 µM IFLink-a and IF21 primers in 1X High-Fidelity PCR buffer containing 1.5 mM $MgCl_2$, 0,2 mM dNTP, 0.02 U/µL Phusion II DNA polymerase. Presence of PCR product was analyzed in 1% TAE gel.

Sequencing

The PbA cDNA inserts in pScrAn-Int vector from individual clones were picked and sent to a commercial company (Suprenom, Singapore) for sequencing with pScrAn-IntF primer. Results were analyzed by BLAST against PlasmoDB database (www.plasmodb.org).

EL4 transduction with pScrAn-Acc-PbA cDNA lentivector

HEK293T cells were cultured at 37˚C, 5% CO_2 in four 100 mm tissue culture dishes to ~50% confluency in DMEM media supplemented with 10% FBS (without antibiotics). For every dish, 2.5 µg pScrAn-Acc PbA cDNA library lentivector were mixed with 0.875 µg pMD2.G envelope vector and 1.625 µg psPAX2 packaging vector (kind gifts from Didier Trono, Addgene plasmids #12259 and #12260 respectively) in 200 µL OptiMEM serum-free media (Life Technologies). This was mixed dropwise to another tube with 200 µL OptiMEM serum-free media and 15 µL EndoFectin Lenti (GeneCopoeia, Rockville, MD) while vortexing, followed by adding the whole mixture dropwise into the HEK293T cells. After overnight incubation, the DMEM media was replaced with 3 mL fresh media and cells were allowed to incubate for 2 more days. Media containing lentiviral particles were harvested, centrifuged at 500 g for 5 min to remove cell debris, aliquoted and stored at -80˚C.

EL4 cells were seeded in eighteen 6-well plates at 3 x 10^5 cells per well with RPMI complete media, followed by addition of 20 µL pScrAn-Acc PbA cDNA library

lentiviral particles in 3 μg/mL hexadimethrine bromide (Sigma-Aldrich). The plates were centrifuged at 1200 g for 1 hour at 30˚C, and then incubated at 37˚C, 5% CO_2 overnight. The media was replaced with fresh ones, and cells were allowed to culture for one more day before sorted for live $EGFP^+$ transductants. Sorted cells were grown, aliquoted and frozen in liquid nitrogen.

Results

Generation of pScrAn-Int vector

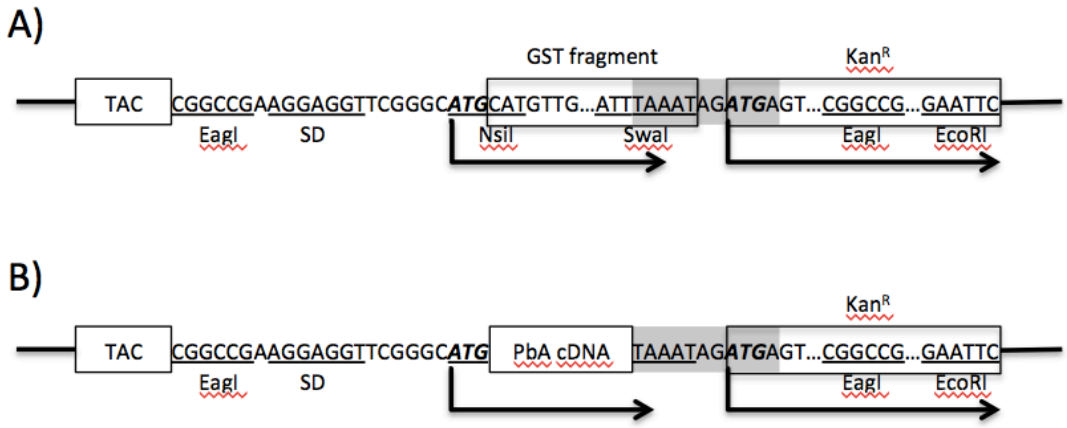

Figure 10: Creation of pScrAn-Int vector for selecting PbA cDNA clones with full ORF. The pScrAn-Int vector (A) contains a SD sequence at the proximal end and a kanamycin resistance gene (Kan^R) at the distal end. Upon excision of pScrAn-Int with NsiI and SwaI and cloning of PbA cDNA fragments to this site (B), the SD and start codon upstream of PbA cDNA enables its translation, while the unique 11 bp sequence (in gray) allows stoppage of in-frame ORF fragments at one of the 3 forward frames. Only when this occurs will translation of Kan^R be initiated through translational coupling.

We designed and constructed the pScrAn-Int vector (**Scr**een **an**tigen – **int**ermediate, figure 10A) for cloning the PbA cDNA fragments and performing ORF enrichment in bacteria. Excision of pScrAn-Int with NsiI and SwaI restriction enzymes leaves homologous ends that allow PbA cDNA fragments to be inserted by In-Fusion cloning (figure 10B). In this design, PbA cDNA in pScrAn-Int will be under the control of a tac promoter, inducible by IPTG, and translation is made possible by the Shine-Dalgarno (SD) ribosomal binding site. The 3 stop codons at the end of cDNA (highlighted in gray) will allow mRNA translation to terminate regardless of the reading frame. The Kan^R expression cassette constructed in very close proximity to the stop codons (in fact, it overlaps with the stop codon in the +3 frame). If the cDNA

is in frame with the vector's start codon and there are no intervening stop codons, the ribosome can re-initiate translation of Kan^R after it reaches the three overlapping stop codons, a process termed translational coupling (167). Thus, only clones with intact ORFs will be able to grow in the presence of kanamycin. After selecting for PbA cDNA fragments cloned in ORF, the flanking EagI sites enable them to be excised for sub-cloning into a mammalian expression vector.

Phosphorothioate (PS) bonds mildly affects PCR but severely hinders In-Fusion cloning

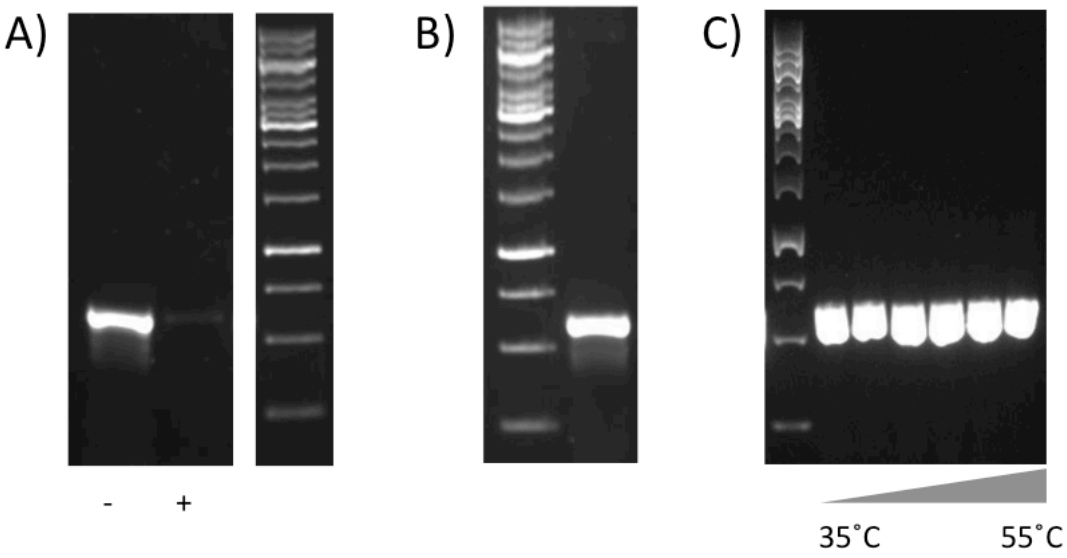

Figure 11: PCR amplification of PyUIS4 with PO- or PS- primers. (A) IF15-PyUIS4r (-) or IF15PS-PyUIS4r (+) reverse primers homologous to 3' end of PyUIS4 were used to amplify the gene and analyzed by gel electrophoresis. (B) IF15PS-PyUIS4r primer was used in amplifying PyUIS4 in 3 mM $MgCl_2$. (C) PyUIS4 PCR products from (B) were amplified with IFLink-a and IF21 primers in different annealing temperatures and the mixture analyzed by gel electrophoresis. In all figures, GeneRuler 1kb DNA ladder was used throughout, and PyUIS4 PCR products appear as bands at 582 bp region.

Efficient, directional cloning of gene fragments with undefined sequences requires the addition of exogenous sequences that are compatible with the ends of the linearized vector. In In-Fusion cloning, the vector and insert sequences are joined

through homologous sequences of at least 15 bp at their ends. No restriction digest of DNA is necessary, which is advantageous as these restriction sites could be present in some cDNAs. However, simply adding a 15 bp tail to the random hexamer primers used for cDNA synthesis will not work as the tail is vulnerable to the 5' to 3' exonuclease activity of *E. coli* DNA polymerase. This activity, however, is reported to not work on nucleotides joined by PS linkages (168, 169). We envisioned that incorporating this type of linkage into the primers would protect them from excision and allow subsequent downstream cloning. First we wanted to see how the presence of PS tails on primers would affect priming, PCR amplification and In-Fusion cloning. To test this, PyUIS4 gene was amplified with forward primer IF-PyUIS4f and either IF15-PyUIS4r or IF15PS-PyUIS4r reverse primers. In a typical PCR reaction of 1.5 mM $MgCl_2$, PyUIS4 amplification with IF15-PyUIS4r yielded more products than with IF15PS-PyUIS4r (figure 11A). By increasing the amount of $MgCl_2$ to 3 mM, IF15PS-PyUIS4r can then efficiently amplify the same gene (figure 11B). These PCR products were purified, cloned into pScrAn-Int linearized with NsiI and SwaI, transformed into competent cells and selected for positive transformants. Colonies with phosphodiester (PO)-linked 3' ends yielded about 10 times more colonies than that with PS-linked 3' ends (table 4), highlighting the incompatibility between In-Fusion cloning with PS-bonded homologous ends.

Table 4: Transformation efficiencies of pScrAn-Int-PyUIS4 synthesized by PO- or PS-linked primers through In-Fusion cloning.

	Colonies (CFU/µg)
pScrAn-Int-IF15-PyUIS4	5.2×10^3
pScrAn-Int-IF15PS-PyUIS4	5.8×10^2

As inserts with PS-linked tails were shown to be incompatible with In-Fusion cloning, the possibility of replacing the PS tails with normal PO tails through PCR is investigated. PyUIS4 PCR products with PS-linked distal tails were used as templates for regular PCR amplification with PO-linked IFLink-a and IF21 primers. This was also performed over a range of annealing temperatures, in anticipation that hybridization between PO- and PS-linked DNA sequences might be less than optimal because of slight differences in the DNA backbone structure (170). Unexpectedly, amplification was shown to be efficient with the tested annealing temperatures, between 35˚C to 55˚C (figure 11C), indicating that the "conversion" from PS linkage to PO linkage can be achieved with ease.

The use of PS primers during library synthesis yielded more colonies

To test the usage of PS-linked primers in cDNA library synthesis, 1 µg total RNA was reverse transcribed with IFb-15PS-X6 or IF-15-X6 primers, followed by second strand synthesis and subsequent downstream steps in figure 12A. Primers with phosphorothioate (PS) linkages were used to synthesize cDNA from mRNA with reverse transcriptase, and second strand synthesis performed with the enzymes RNaseH (to degrade mRNA), *E. coli* DNA polymerase (to use mRNA fragments as primers for amplification) and *E. coli* DNA ligase (to join Okazaki fragments together to form one continuous strand). T4 DNA polymerase was used to fill up the 5' ends of cDNA fragments that were vacated by the degraded mRNA, resulting in a phosphate group at that end. DNA adaptors homologous to the 3' end of linearized pScrAn-Int would be attached to the 5' end of cDNA by T4 DNA ligase through this

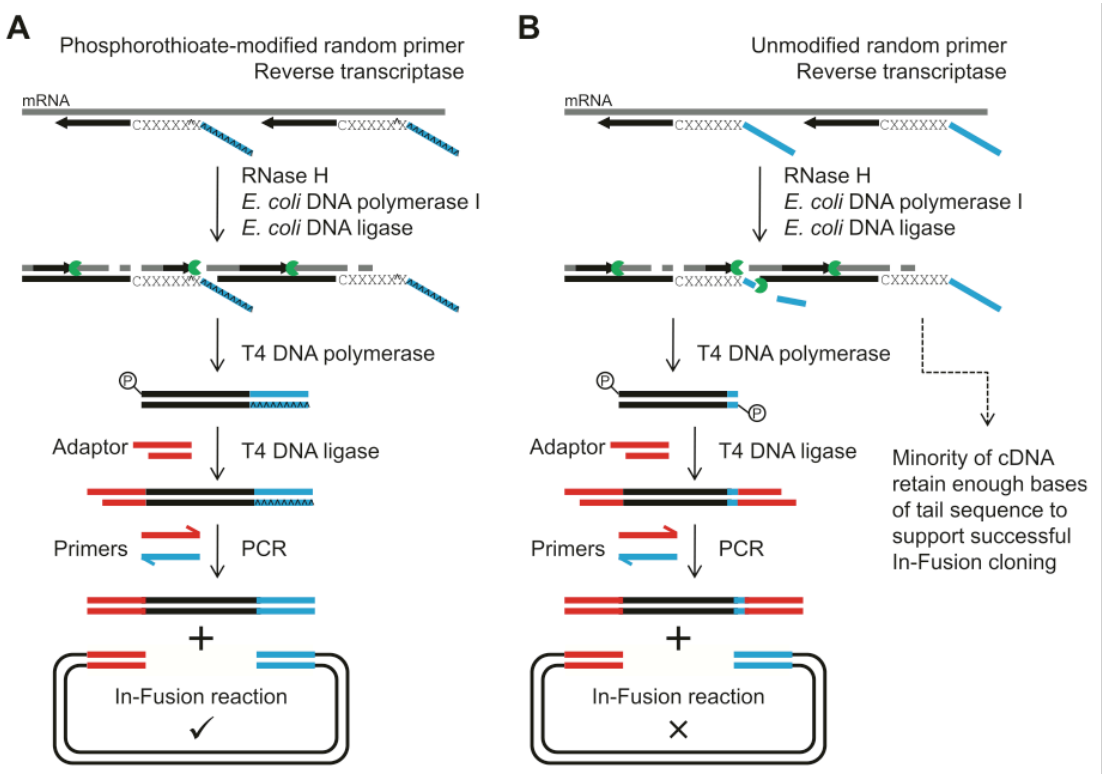

Figure 12: Schematics of generating PbA cDNA and cloning into pScrAn-Int vector. (A) Random hexamers, with a 5' PS-bonded (denoted with ^) overhang tail (in blue), were hybridized to PbA mRNA (gray), followed by 1st strand cDNA synthesis by reverse transcriptase. The mRNA was degraded by RNaseH, and *E. coli* DNA polymerase (in green) used mRNA fragments to synthesize complementary cDNA strands, with *E. coli* DNA ligase joining cDNA fragments together after synthesis. T4 DNA polymerase would fill up 5' overhangs to make cDNA fragments blunt-ended, of which the free phosphate group (yellow circle) created would allow adaptor sequences (in red) to be attached to by T4 DNA ligase. Primers (PO- or PS-based) complementary to the ends of cDNA were used for amplification, followed by cloning into NsiI-SwaI-linearized pScrAn-Int vector. (B) The use of random hexamers with PO-bonded overhang tail at 5' end would result in excision of the tail by *E. coli* DNA polymerase. The exposed phosphate group would enable ligation of adaptors to both ends, which blocks cloning into pScrAn-Int vector. Diagram reproduced from (171).

phosphate group. The cDNA would be expanded by PCR amplification with PO or PS primers, cloned into pScrAn-Int vectors through In-Fusion cloning, transformed into ElectroMax competent cells and selected by IPTG induction and kanamycin resistance.

The PCR products were cloned into linearized pScrAn-Int vector and transformed into competent bacteria. As shown in table 5, cDNA inserts synthesized with IFb-15PS-X6 primers resulted in more colonies obtained after In-Fusion cloning and transformation, more than 7 times than that with IF-15-X6 primers. Cloning the cDNA product directly into the vector gave very few colonies, demonstrating that amplification of cDNA was necessary as part of the strategy to construct PbA cDNA library. Figure 12B depicts a model explaining the low numbers of colonies obtained with the unmodified primer. The 5' overhangs in PO-linked primers were targeted by the 3' to 5' exonuclease activity of *E. coli* DNA polymerase, leaving behind a phosphate group at the 5' end of the partial downstream homologous sequence, to which a DNA adaptor can be subsequently ligated. Only a minority of inserts retaining sufficiently long portions of the downstream homologous sequence were successfully cloned into pScrAn-Int vector.

Table 5: Transformation efficiency of cDNA inserts obtained with PO- or PS-linked primers.

Reverse transcription primer	PCR performed after adaptor ligation	
	–	+
IF-15-X6	26	269
IFb-15PS-X6	19	1993
Linearized vector control	12	NA

Generation of PbA cDNA library fragments

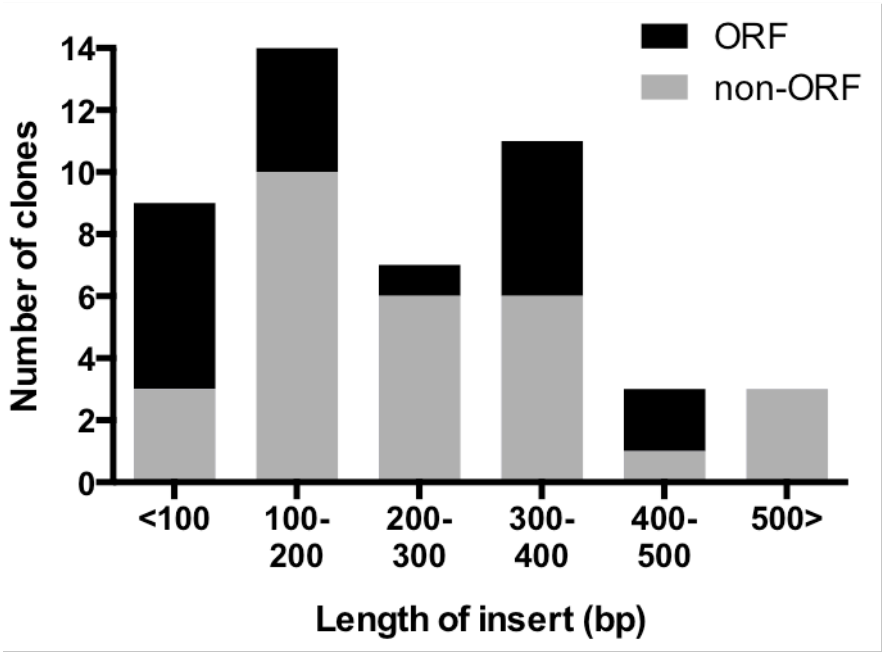

Figure 13: Breadth of PbA cDNA insert sizes and the frequency of those with full-length ORFs in pScrAn-Int library. A sample of 47 clones from pScrAn-Int-PbA cDNA library were sequenced and the length of PbA cDNA inserts were tabulated. The frequency of clones with full-length ORFs amounted to 38.3%.

Encouraged by the tests, the actual library synthesis work was performed to convert PbA mRNA to cDNA with IFb-15PS-X6 primers. The cDNA was cloned into pScrAn-Int vector in a series of steps as described earlier and the transformed bacteria clones selected for resistance to kanamycin. An estimated total of 1.2×10^5 pScrAn-Int clones were obtained from the compilation of 3 rounds of library generation. A handful of clones were picked and sequenced to assess the quality of PbA cDNA inserts. As shown in figure 13, a range of cDNA lengths was obtained in the library, with the majority at less than 400 bp. More importantly, only 1 out of 48 clones had an insert not originating from PbA, and 18 (38.3%) of these clones carried

the PbA inserts in ORF. The high percentage of clones with PbA inserts in frame validated the strategy of cDNA library synthesis outlined here.

Cloning PbA cDNA inserts into lentivector pScrAn-Acc

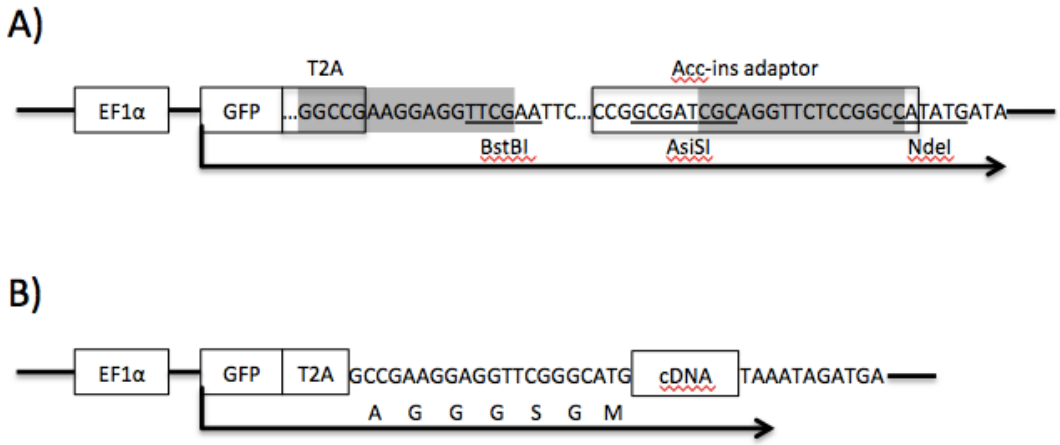

Figure 14: Creation of pScrAn-Acc lentivector for accepting PbA cDNA clones with full ORF from pScrAn-Int. The pScrAn-Acc lentivector (A) contains an EGFP tag fused with self-cleaving T2A peptide. Upon cutting with BstBI and AsiSI, PbA cDNA excised from pScrAn-Int with EagI can be cloned into pScrAn-Acc by In-Fusion cloning (required overlapping regions in gray), giving rise to pScrAn-Acc-PbA cDNA (B).

The pScrAn-Int vector was created as a means to select for PbA cDNA inserts that could be expressed in ORF. To express these cDNA inserts within EL4 cell line, they need to be excised out of pScrAn-Int and cloned into a lentivector, packaged into lentiviral particles and introduced to EL4 cells. A lentivector plasmid was thus designed to **acc**ept the **scr**eened PbA **an**tigenic inserts, hence the name pScrAn-Acc (figure 14A). When linearized with BstBI and AsiSI, the ends of pScrAn-Acc are compatible for In-Fusion cloning with cDNA excised from pScrAn-Int with EagI. The cDNA is then positioned downstream of EGFP, a T2A self-cleaving peptide and a glycine-rich linker (figure 14B). When transduced into mammalian cells, T2A peptide

ensures that EGFP and PbA cDNA fragment are produced separately even when under the control of a single elongation factor 1α (EF-1α) promoter. EGFP allows transduced mammalian cells to be identified and isolated from non-transduced cells through flow sorting. The pScrAn-Acc-PbA cDNA formed by In-Fusion cloning (figure 14B) was then transformed into Stbl4 competent cells and positive transformants selected by ampicillin resistance, followed by pooling all the clones together to harvest the plasmids.

Generation of EL4 PbA cDNA library

The pScrAn-Acc-PbA cDNA lentiviral particles were produced in HEK 293T packaging cells and titrated against EL4 cells in a small-scale transduction experiment. From a range of 1-100 µL lentivector per 1 x 10^5 cells (figure 15), we chose the dose where we obtained between 20-30% transduction, as the risk of generating cells with more than one insert becomes significant at higher transduction efficiencies. Using this dose, a larger scale transduction was performed to generate the EL4 PbA cDNA library, ensuring that at least 1.2 x 10^6 EL4 cells were transduced to maintain library diversity. Transduced cells were sorted based on EGFP expression, expanded and finally cryopreserved in aliquots. A summary of statistics of our PbA cDNA library is detailed in table 6.

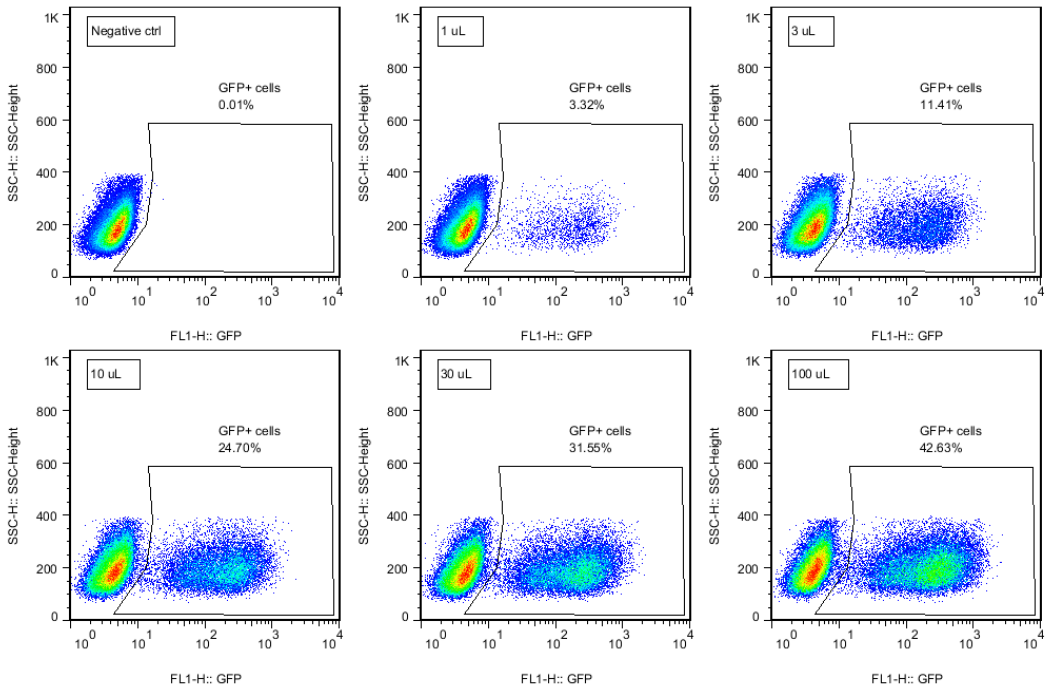

Figure 15: Titration of PbA cDNA lentiviral particles in EL4 cell line. PbA cDNA lentiviral particles were incubated with 1 x 10^5 EL4 cell line at different amounts and the frequency of live cells expressing EGFP was quantified by flow cytometry.

Table 6: Summary of statistics of the PbA cDNA library created in this study

Number of clones	1.2 x 10^5
Average insert length	441 bp
Size of PbA cDNA library	5.21 x 10^7 bp
Size of PbA transcriptome	6.64 x 10^6 bp (172)
Coverage	7.9x
Percentages of clones in ORF	38.3%

Discussion

The dearth of malaria $CD8^+$ T cell epitopes, despite that $CD8^+$ T cells were shown to be responsible for ECM pathology much earlier (87, 91, 92), was the motivation to conduct this study. In this chapter, PbA mRNA was isolated, converted into cDNA and cloned into EL4 cells. Within these cells, the cDNA fragments will be translated into proteins and degraded by proteasomes into peptides. A portion of these peptides will be loaded onto the MHC class I molecules and presented on the EL4 cell surface. These malarial pMHC complexes can be screened against malaria-specific TCRs of unknown specificities. The EL4 clone that elicits a positive response from such a screen can be analyzed to identify the transduced PbA cDNA fragment and thus the antigens.

Many decisions had to be made when planning the library construction, starting with 3 main ones: the parasite genetic material, the choice of host cells for the library and the method to introduce the former into the latter. As described earlier, blood-stage parasites are the ones responsible for the pathology associated with patients suffering from malaria, including ECM. To maximize the chance of identifying epitopes that are essential for ECM pathogenesis, mRNA of blood-stage parasites were isolated to create the library. This approach excluded the introns and non-coding regions that accompany the choice of using gDNA as the starting material. The cell line that was chosen to be the host for the cDNA library, EL4, originated from a lymphoma in a C57BL/6N mouse. It was chosen as a host for expression of PbA cDNA library due to its fast and robust proliferation, suitability as

a transfection host, and most importantly, having the same H-2^b MHC background as C57BL/6J mice. Being a suspension cell line, cell transfer during high throughput screening is easier than with adherent cells. To ensure stable expression of PbA cDNA, lentiviral transduction was selected as it allows integration of exogenous genetic material within the host chromosomes. In contrast, plasmid transfection and non-integrating viral transduction methods run a much higher risk of insert loss after multiple rounds of cell division, even if selection pressure is applied.

In the PbA cDNA library synthesis, choosing between random priming and oligo-dT priming to synthesize the cDNA was the biggest decision we faced. After much thought, we rejected the latter as the AT-rich PbA genome would result in a library that is heavily biased against long genes, genes with more AT content, and the 5' ends of genes. However, a major disadvantage of random priming is that cDNA libraries made without knowledge of correct frame or orientation are estimated to have only 8% of the clones in the correct frame (162). To circumvent this, Davis and colleagues designed the pKE-1 vector such that only those transformants with gene fragments in ORF that stopped right before a Kan^R gene can translate the latter and become resistant to kanamycin selection. Similarly, a Japanese group introduced a unique sequence that allows for full-length ORFs in all three frames to be selected for (167). The latter strategy was adopted in this study, resulting in 38.3% of the clones in the pScrAn-Int library having PbA cDNA fragments in ORF, more than four times compared to if no selection was used.

The conventional method of cloning random-primed cDNA is blunt-end ligation with the vector, which does not permit directional cloning. We also sought to avoid the problem of inserts being cloned in the reverse orientation by adding a tail to the random primers. This tail would also facilitate In-Fusion cloning by being homologous to one end of the pScrAn-Int vector, fixing the insert orientation and improving cloning efficiency. However, simply extending the random primer was virtually unreported in the literature, and we suspect that excision of this tail by *E. coli* DNA polymerase during cDNA synthesis was detrimental to cloning. We hypothesized the PS linkages throughout the length of the overhang tail would offer protection against 5' to 3' exonuclease cleavage. However, cDNA incorporating the PS primer inhibited In-Fusion cloning, as shown by the low number of clones obtained in table 4. The In-Fusion enzyme is thought to remove DNA bases from each strand in the 3' to 5' direction to generate 5' overhangs, and it is possible that the PS bonds prevent this. Fortunately, we were able to solve this by amplifying the PS-containing cDNA with unmodified primers before In-Fusion cloning. Incorporating both PS linkages in the primer tail and a PCR amplification step to "revert" to unmodified DNA allowed random-primed cDNA to be inserted by In-Fusion cloning into the vector in the correct orientation. This strategy may prove useful to other researchers interested in constructing random-primed cDNA libraries and has been published (171).

The PbA cDNA gene fragments in the pScrAn-Acc lentivector were expressed under the control of the constitutive EF-1α promoter. Although this is weaker than cytomegalovirus (CMV) promoter, high expression levels may be detrimental as

many of the cDNA inserts may be toxic to EL4 cells, which may inadvertently shrink the diversity of the library. In addition, CMV promoter can be silenced by DNA methylation over time (173, 174). Silencing of EF-1α promoter is rare, thus making it more suitable for long-term expression in mammalian cells. Due to the relatively large size of pScrAn-Acc lentivector (over 10 kilo base pairs), the length of PbA cDNA gene fragments that was cloned in could not be too large, as this would impede efficient transfection into HEK293T packaging cell line and viral packaging (175). This was part of the reason cDNA was synthesized with random hexamers, because it gives smaller fragments in contrast to full-length cDNA. The EGFP in the lentivector, occupying the EF-1α promoter, was necessary for isolating positive transformants. Cloning a separate promoter to express PbA cDNA inserts would greatly increase the size of the vector. To circumvent this, the EGFP and PbA cDNA fragments were fused together, separated by the short self-cleaving T2A peptide sequence. This eliminated the need for either another promoter to drive the expression of the cDNA gene fragment or an internal ribosomal entry site.

The size of the PbA cDNA library created here amounted to 5.21×10^7 bp (table 6), which is about 7.9 times the size of the PbA transcriptome. Note that genes have different levels of expression even in a single cell, with some of them expressed at extremely low levels. Assuming all mRNAs were successfully captured and converted into cDNA, more abundant genes would be over-represented in the library, and vice versa, making detection of rare mRNAs in the library difficult. To overcome this, some researchers have developed methods to create normalized cDNA libraries (164, 176, 177). However, it is unclear whether normalizing our cDNA

library will be beneficial for $CD8^+$ T cell epitope discovery, as generally speaking, rare antigens are less likely to be immunogenic. To minimize losses of clones in the subsequent conversion of the cDNA library from bacteria to EL4 cells, we ensured that the number of lentiviral particles and the number of transduced and sorted EL4 cells were at least ten times the library diversity (i.e. more than 1.2×10^6). In the next chapter, the screening of this EL4 library with T reporter cells carrying TCRs found in brains of mice during ECM will be described.

Chapter 2: Library screening and validation of $CD8^+$ T cell epitopes

Introduction

With the construction of the PbA cDNA library described in the first chapter, a method to screen the library for epitopes recognized by $CD8^+$ T cells during ECM is needed. As described in chapter 1, Professor Nilabh Shastri created the fusion partner cell BWZ.36 that expresses an NFAT-LacZ cassette and can fuse with murine T cells. The resulting hybridoma then expressed LacZ when its TCR binds to cognate pMHC. Dr Howland in the lab experienced a low success rate of hybridoma formation with $CD8^+$ T cells from PbA-infected mouse brains and thus developed an alternative approach. She sorted brain-sequestered $CD8^+$ T cells from mice succumbing to ECM and performed single cell sequencing of the TCRαβ chains so as to identify pairs that appeared multiple times (131, 132), indicating that they were from parasite-specific $CD8^+$ T cells that experienced clonal expansion (table 7). A BWX.36 hybridoma that had lost TCR expression (termed LR-null T reporter cells) was selected as the host for transducing these TCRs in preparation for screening with the EL4 PbA cDNA library described in chapter 1.

Table 7: TCRαβ pairs from brain-sequestered $CD8^+$ T cells in mice with ECM were isolated, sequenced and analyzed with IMGT/V-QUEST. Pairs shown in this table were found to be over-represented were selected for transduction into LR-null T reporter cells. Adapted with permission from Dr Shanshan Howland.

Clone	TRAV	TRAJ	TCRα Junction	TRBV	TRBD	TRBJ	TCRβ Junction
6.2	16D	57	CAMSPQGGSAKLIF	13-3	2-5	2	CASSDWGNQDTQYF
8.4	4D-4	52	CAAEANTGANTGKLTF	13-3	2-1	2	CASSDWGAGAEQFF
10C6	4-2	16	CAVDPTSSGQKLVF	13-3	2-5	1	CASSPGQGTDTQYF
10C11	6-7	50	CALSDRSSSFSKLVF	16	1-1	1	CASSSGTGNTEVFF
13.6	9N-2	44	CVLSRVGSGGKLTL	12-2	1-1	1	CASSLRGRDTEVFF
13.10	7-5 or 7D-5	23	CAVSGYNQGKLIF	26	2-1	2	CASSLGGRAEQFF
13.24	12D-3 or 12N-3	43	CALRNNNNAPRF	12-1	2-3	1	CASSLPGGLETLYF
13.44	7-3	40	CAVIFTGNYKYVF	3	2-5	1	CASSLGDTQYF

The principle behind the epitope discovery screen is to divide the EL4 PbA cDNA library into many pools containing a limited number of clones, and each pool is amplified and incubated overnight with a T reporter cell line in a 96-well plate. An EL4 clone containing a PbA cDNA fragment encoding the T reporter cell line's cognate epitope will present this peptide on its MHC class I molecules. This triggers TCR ligation on nearby T reporter cells, leading to NFAT signaling and transcription and translation of LacZ. These reporter cells are detected as blue spots when X-gal staining is performed. Allowing the pool or pools containing the target clone to be identified. From this, the positive pool can be cloned for a second round of screening, to isolate the incriminating EL4 clone. The PbA cDNA fragment in the EL4 clone can be sequenced and identified by comparison with the published PbA genome.

To further narrow down the corresponding epitope that is recognized by the cognate TCR, the PbA cDNA fragment can be analyzed with an epitope prediction tool (121) to select candidate peptides for synthesizing pMHC tetramers. The

traditional method of pMHC tetramer synthesis requires refolding of recombinant MHC monomers in the presence of each peptide, a slow and laborious process that cannot be multiplexed. Here, we take advantage of a UV-mediated peptide exchange strategy to quickly prepare multiple pMHC tetramers (121, 178). Biotinylated MHC class I heavy and light chains are first refolded with a photolabile peptide containing a 3-amino-3-(2-nitro)phenyl-propanoic acid (Anp) residue. Small aliquots can then be tetramerized with fluorescent streptavidin and UV-irradiated in the presence of the desired peptide. The Anp-containing photolabile peptide cleaves and dissociates from the MHC molecule to be replaced by the desired peptide. The candidate pMHC tetramers are then screened for the ability to label the T reporter cell line.

Materials and methods

Peptides

All peptides were synthesized and purchased from Genscript (Piscataway, NJ), and were redissolved in 100% dimethyl sulfoxide (Sigma-Aldrich) at 10 or 100 mg/mL. Peptides were diluted in RPMI complete media or PBS, whichever applicable, to the desired concentrations prior to use in subsequent experiments.

PbA cDNA library screening and identification of positive clones

EL4 cells containing transduced PbA cDNA inserts were cultured in 96-well tissue-culture plates in RPMI complete media at 37˚C, 5% CO_2 at initial density of 250 cells per well. In separate 96-well filter plates (Pall 8029, Pall Corportation, Port Washington, NY), 3 x 10^4 of these cells per well were incubated together with equal numbers of T reporter cell lines, LR-BSL8.4a or LR-BSL13.6b. Plates were drained the next day by centrifugation and stained for LacZ activity with β-gal staining kit (Life Technologies). Blue spots were counted and analyzed on CTL Immunospot Analyzer. The pools from which the positive wells were derived were sorted by FACS into single cells in fresh 96-well tissue culture plates, grown up and re-screened against the T reporter cell lines again to identify positive clones.

Identification of positive PbA cDNA inserts

Positive EL4 clones were processed with DNeasy blood and Tissue kit (QIAgen) to obtain purified genomic DNA. PbA cDNA inserts were amplified with the primers T2AFor and WPRErev by PCR with Phusion II DNA polymerase and analyzed on 1% TAE gel. Where necessary, bands were excised from gels and purified with QIAquick MinElute Gel Extraction kit (QIAgen), cloned into pCR®4-TOPO® vector (Life Technologies) and transformed into OneShot®TOP10 competent cells (Life Technologies). Sequencing of PbA cDNA inserts were outsourced to a commercial company (AITBiotech, Singapore), with the primers M13F and T2AFor used for inserts in TOPO vectors and EL4 genomic DNA, respectively. Amino acid sequences were analyzed and identified by performing an alignment search (BLAST – Basic Local Alignment Search Tool) with the PlasmoDB database (http://plasmodb.org/plasmo/).

Peptide-MHC tetramer generation

The production of recombinant caged MHC class I molecules were detailed elsewhere (119, 121, 179). In brief, H-2K^b or D^b heavy chains with a biotinylation tag at the C terminus (180) were refolded with β_2m light chains and a photocleavable peptide FAPGNY-J-AL, where J is 3-amiino-3-(2-nitro)phenyl-propanoic acid. Refolded monomers were biotinylated, purified by size exclusion chromatography and mixed with streptavidin R-Phycoerythin conjugate (Molecular Probes, Life Technologies) or streptavidin Brilliant Violet 421 (Biolegend, San Diego, CA) at 4:1 molar ratio respectively. For peptide exchange, desired epitopes were added to the tetramers in

vast excess and irradiated with 365 nm UV (UVP, Upland, CA) on ice for 15 min. Tetramers were then used for staining without further treatment.

Epitope identification

To identify the cognate epitopes, the peptide sequences obtained from sequencing positive EL4 clones were analyzed *in silico* for potential H-2K^b and H-2D^b epitopes (121), and the top 3 or 5 candidates for each category were synthesized. PE tetramers were generated as described earlier. T reporter cell lines were stained with LIVE/DEAD® Fixable Far Red stain (Life Technologies) at 1:1000 dilution in PBS for 30 min at room temperature, followed by staining with PE tetramer of different epitopes in separate tubes in FACs buffer, on ice for 45 min. Cells were washed with FACs buffer, fixed with 1% formaldehyde and analyzed by flow cytometry.

Validation of malaria epitopes reported by others – Tetramer staining

Five malaria epitopes reported by Lau *et al* (130) were synthesized and used to generate PE tetramers as described above. 5 x 10^6 naïve or PbA-infected splenocytes were stained with LIVE/DEAD® Fixable Aqua stain (Life Technologies), followed by desired PE tetramers as described above for 15 min on ice in the dark. Anti-mouse CD8a PerCP-Cy5.5 (clone 53-6.7, Biolegend) and anti-mouse CD16/32 APC-Cy7 (clone 93, Biolegend) were used to stain cells for an additional 30 min on ice, away from light. Cells were washed, fixed as described before, and analyzed by flow cytometry.

Validation of malaria epitopes reported by others – IFNγ-Enzyme-linked Immunospot (ELISpot) assay

Anti-mouse IFNγ (clone AN18; Mabtech, Nacka Strand, Sweden) were used to coat 96-well MultiScreen HTS plates (MSIPS4510; Millipore, Billerica, MA) at 750 ng/well, overnight at 4˚C. Wells were washed thoroughly with H_2O and blocked with RPMI complete medium for at least 2 hours at 37˚C, 5% CO_2 until ready to use. Splenocytes from infected mice were processed with CD8a T cell isolation kit II and AutoMACS Pro Separator (both from Miltenyi Biotec, Auburn, CA). The isolated $CD8^+$ T cells were left standing at room temperature for 2 hours to minimize background staining. For each well, 2.5 x 10^5 naïve splenocytes and 5 x 10^4 isolated $CD8^+$ T cells were incubated together with 12 U recombinant interleukin-2 (eBioscience, San Diego, CA) and 4 µg peptides at 37˚C, 5% CO_2 overnight, after which cells were discarded the following day. Wells were washed thoroughly with wash buffer (PBS + 0.05% Tween 20 [Sigma-Aldrich]) incubated with 20 ng/well biotinylated anti-mouse IFNγ (clone R4-6A2, Mabtech) at 37˚C for 2 hours, washed again, and incubated with 300 ng/well ExtrAvidin-alkaline phosphatase (Sigma-Aldrich) at room temperature for 45 min. After discarding the solution, wells were washed and developed with 5-bromo-4-chloro-3-indolyl phosphate-nitroblue tetrazolium chloride (BCIP/NBT) substrate (Sigma-Aldrich). Spots were quantified with CTL ImmunoSpot analyzer.

RMA/S stabilization assay

RMA/S cells were grown in RPMI complete medium at 37˚C, 5% CO_2, and shifted to 26˚C overnight one day prior to experiment. Cells (1×10^5) were seeded in 96-well tissue-culture plates and pulsed with varying concentrations of peptides tested at 26˚C for 1 hour, then moved back to 37˚C for the same duration. Excess peptides were washed and anti-mouse H-$2K^b$ (clone AF6-88.5, Biolegend) or anti-mouse H-$2D^b$ (clone KH95, Biolegend) were used for staining, depending on MHC restrictions of the peptides. Cells were washed, fixed in 1% formaldehyde and analyzed by flow cytometry.

Results

Identification of EL4 library clones recognized by T reporter cell lines

One important consideration for the screening was the number of initial EL4 library cell clones in each pool. Smaller pools make the assay more sensitive but increase the number of plates that have to be screened to have a reasonable chance of not omitting a potentially positive clone. Dr Howland's prior work diluting OVA-transduced EL4 cells with untransduced EL4 cells demonstrated that OVA-specific T reporter cells could reliably detect the former at a ratio of 1:243 but only weakly at 1:729. Thus, the pool size was set at 250 clones. The workflow for the screening is illustrated in figure 16, where 250 EL4 library cells were seeded in 92 wells of a 96-well tissue culture plate and allowed to grow. From these master plates, 3×10^4 cells per well were seeded in 96-well filter plates and incubated overnight with an equal number of T reporter cells to be screened. Filter plates facilitate downstream X-gal staining by allowing the cells to be washed without losses and by providing a white background for visualizing the blue spots. As stated in the earlier chapter, the library construction yielded 1.2×10^5 clones at the initial stage. Assuming that there was a clone that carried a cognate epitope, the probability of it being absent in the screen would be $(1 - [1/1.2 \times 10^5])^n$, where n is the number of cells to be screened. A starting point of eleven 96-well plates (with the four corners omitted for negative and positive controls for X-gal staining), amounting to 2.53×10^4 EL4 library cells was chosen to be screened, corresponding to an 11.8% probability that a particular clone

would be missing. Eleven to sixteen plates of EL4 library clones were screened for each T reporter cell line.

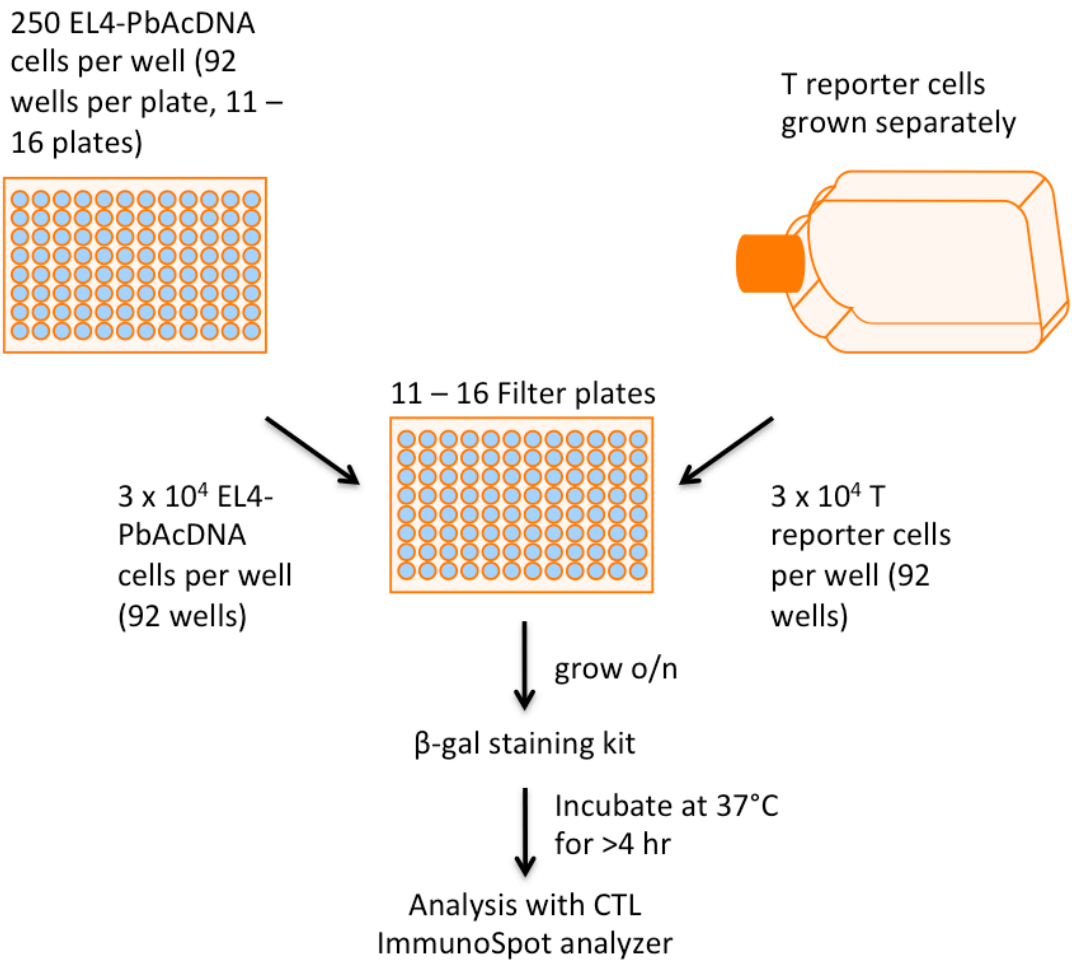

Figure 16. Schematic of X-gal screening of T reporter cell lines against EL4 PbA cDNA library cells. For internal positive and negative controls, equal numbers (3 x 10^4) of T reporter cells and EL4 cells were mixed in the remaining 4 wells per plate, with 3 x 10^4 Dynabeads T-activator CD3/CD28 added to 2 of the wells per plate.

A histogram of the number of blue spots per well for screening the LR-BSL8.4a T reporter cell line against eleven 96-well plates of EL4 PbA cDNA library cells is shown in figure 17. The vast majority (95%) of the wells contained between 0 to 6 blue spots, which probably was due to the background expression of LacZ in the absence of TCR activation. The well with the highest number of blue spots had 22 spots, well above this

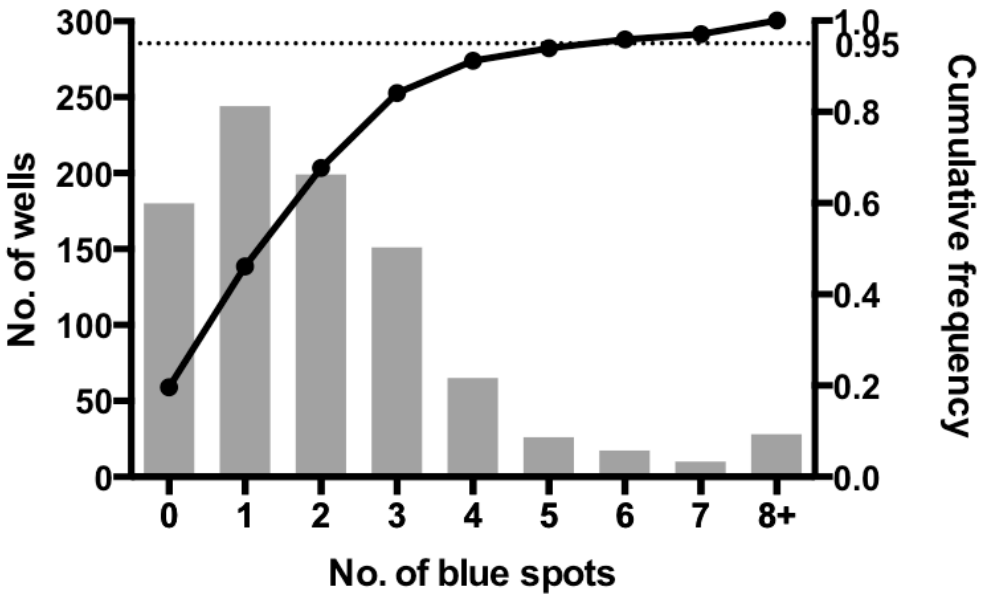

Figure 17. Graph of number of blue spots per well against frequency of wells during screening of LR-BSL8.4a T reporter cells against EL4 PbA cDNA library. The number of blue spots and the frequency of wells with the corresponding number of blue spots from 1012 wells were plotted (left Y-axis) together with the cumulative frequency on the right Y-axis. The dotted line indicates the cutoff where the top 5% of wells with the most number of blue spots.

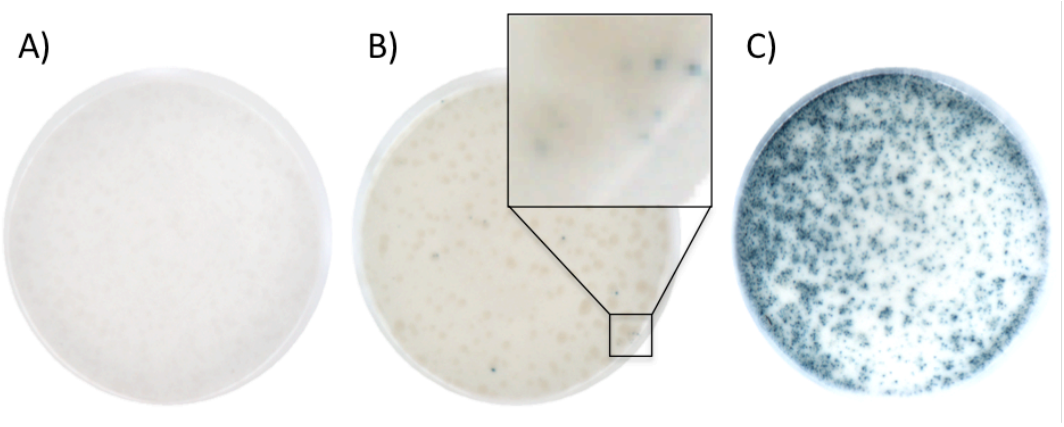

Figure 18. Identification of first antigen recognized by brain-sequestered CD8$^+$ T cells - PbGAP50. The T reporter cell line LR-BSL8.4a was incubated in 1:1 ratio with EL4 PbAcDNA library cells overnight. β-gal staining was performed on the cells the following day. (A) An image of a representative negative well. (B) The image of the well with a sub-library that contains GAP50 fragment. The inset shows blue spots that result from LacZ activation by LR-BSL8.4a. (C) An image of a well where single clones from (B) were sorted, grown and re-incubated with LR-BSL8.4a.

background. Wells of EL4 PbA cDNA library cells corresponding to the top 5% of blue spots were subjected to repeat screenings. If the results remained consistently positive, corresponding pools in the master plate would be expanded, sorted by FACS in single cells into each well of a new 96-well tissue culture plate, expanded and rescreened.

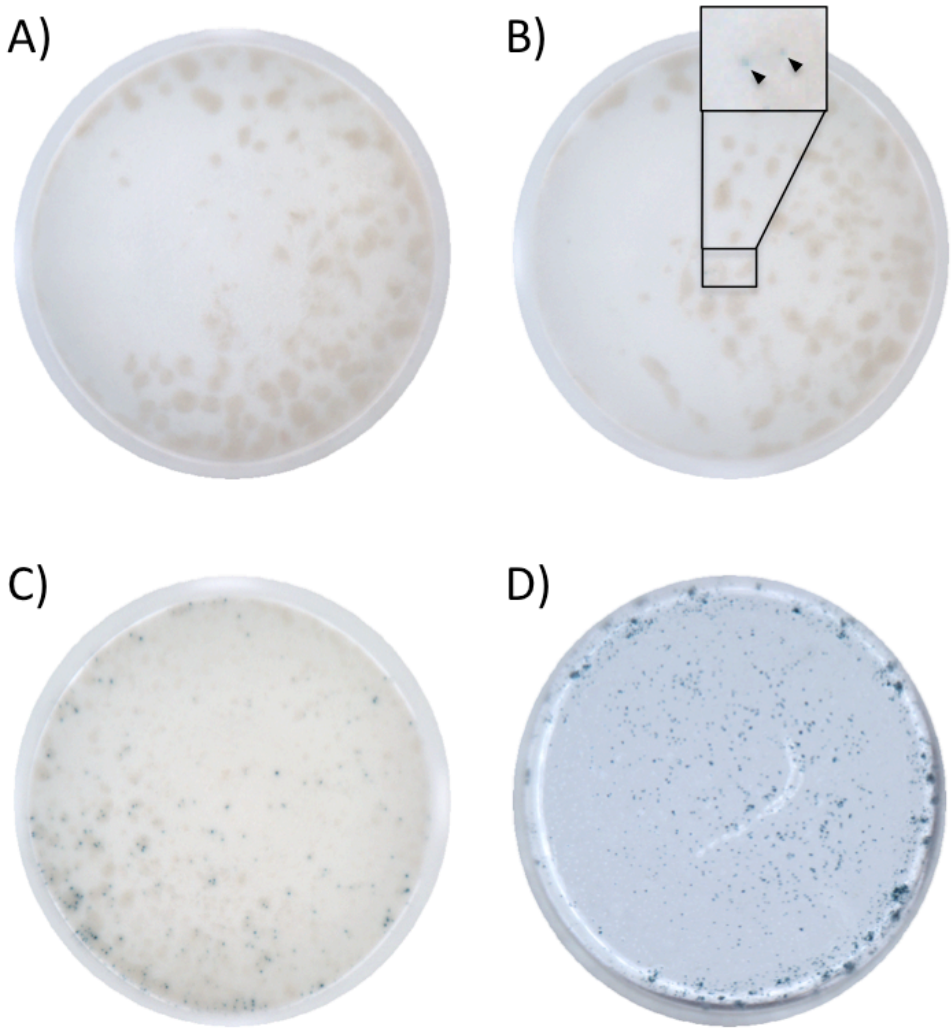

Figure 19. Identification of second antigen recognized by brain-sequestered CD8$^+$ T cells – bergheilysin. The T reporter cell line LR-BSL13.6b was treated as described in Figure 18. (A) A representative negative well. (B) A well with a sub-library that express bergheilysin gene fragment. Arrowheads in inset point to faint positive blue spots. (C) A well where single clones from (B) were sorted, grown and re-screened with LR-BSL13.6b. (D) The PbA cDNA gene fragment from (C), which was found to be expressed out-of-frame, was corrected, transduced into EL4 cells and re-screened with LR-BSL13.6b cells.

Out of eight T reporter cell lines, only two T reporter cell lines, LR-BSL8.4a (figure 18) and LR-BSL13.6b (figure 19), elicited a consistently positive well during the initial screens (figure 18B and 19B). These positive EL4 library pools were cloned and screened, leading to the identification of the positive clones shown in figures 18C and 19C. The clone recognized by LR-BSL8.4a gave a very convincing result with deep, intense blue spots throughout the well. The clone recognized by LR-BSL13.6b showed fewer blue spots, but was clearly reproducible and far higher than the background.

Identification of positive PbA antigens and epitopes

The EL4 library clones that responded to T reporter cell lines LR-BSL8.4a and LR-BSL13.6b were processed to harvest their gDNA. The region that contained the transduced parasite genetic material was amplified by PCR with flanking primers and analyzed by gel electrophoresis. In the EL4 clone that triggered LR-BSL8.4a, 4 amplicons of different sizes were observed (figure 20A), suggesting multiple transduction events. The clone that elicited response in LR-BSL13.6b only had one amplicon (figure 20B). Each amplicon was then gel-extracted, cloned into pCR®TOPO® vector and sequenced. Of the 4 PCR products in figure 20A, only the second band from the bottom contained a positive PbA gene fragment in frame: glideosome-associated protein 50 (GAP50, PlasmoDB gene ID: 081900). To confirm that this fragment was responsible, it was then cloned into pScrAn-Acc and transduced into EL4 cells, giving a positive response when incubated with LR-

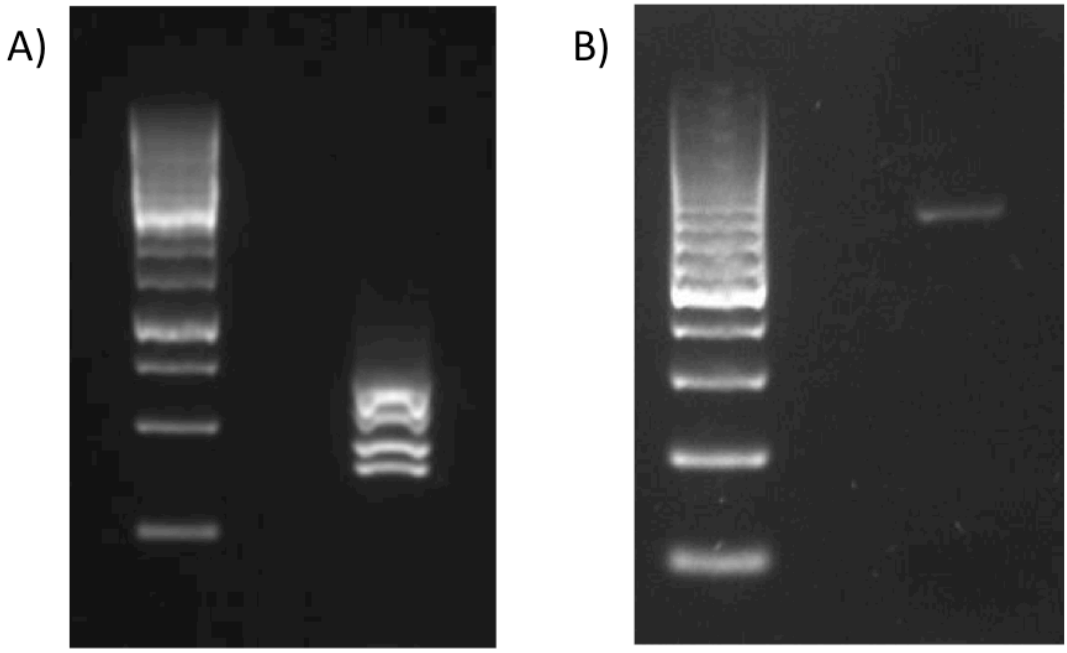

Figure 20. Identification of PbA cDNA gene fragments in EL4 clones that triggered LacZ response from T reporter cell lines. Genomic DNA from EL4 clones that elicited LacZ response in (A) LR-BSL8.4a and (B) LR-BSL13.6b T reporter cell lines were purified, the PbA cDNA inserts amplified by PCR and analyzed by gel electrophoresis. GeneRuler 1kb DNA ladder was used in both experiments.

BSL8.4a cells. Sequencing of the lone gene fragment obtained from figure 20B identified bergheilysin (PlasmoDB gene ID: PBANKA_113700), but cloned in the +2 reading frame. This could explain why relatively few blue spots were present in figure 19C, as these spots were likely to be the result of baseline translation of mRNA transcripts in the wrong frame (181, 182). This gene fragment was re-cloned back into the correct frame by a deletion of one nucleotide at the start of the gene fragment, transduced into EL4 cells and screened against LR-BSL13.6b. This yielded more blue spots (figure 19D), confirming that bergheilysin contains the cognate epitope for LR-BSL13.6b. The amino acid sequences of the GAP50 and bergheilysin fragments are shown in table 8.

Table 8: Gene fragment sequences of GAP50 and bergheilysin that was identified from figures 18 and 19.

Gene fragment	Sequence
Glideosome-associated protein 50 (GAP50)	SQLLNAKYLKQFIKSERVTFIVSPGSNFVDGVKGLNDPSWK SLYEDVYEEEKGDMYMPFFTVLGTGDWTGNYNSEVLKG Q
Bergheilysin	EKHLLNNDHRVVILLEGDENYGTEQEKLEKDMLKKRIESFT EKEKENIITDFENLTKYKNTEESPEHLDKFPIISISDLNGKTLEI PVNPFFTNLNNENNMQHYNETKNNQTLVKENMDR

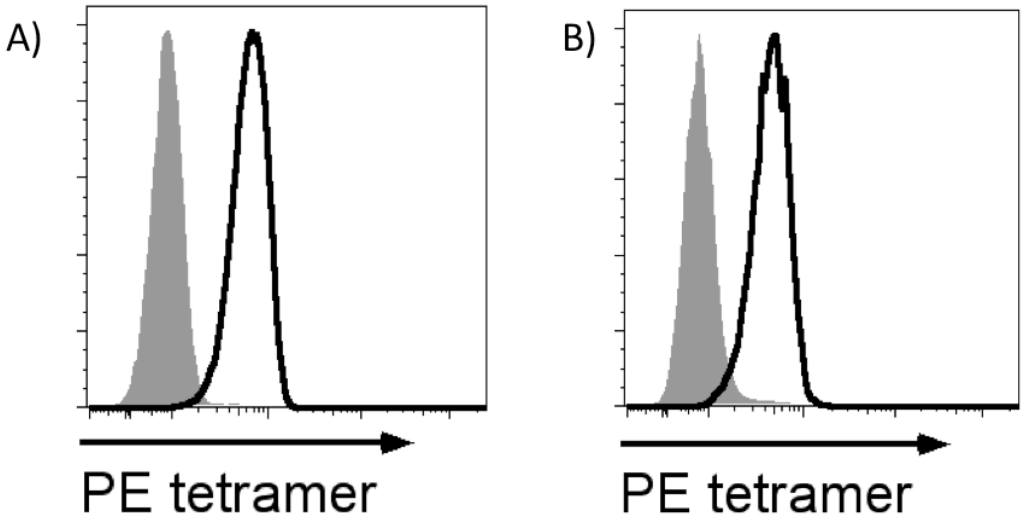

Figure 21. Identification of cognate epitopes SQLLNAKYL (Pb1) and IITDFENL (Pb2) in GAP50 and bergheilysin, respectively. Peptide-MHC PE tetramers were generated with predicted epitopes in tables 9 and 10, and used to stain corresponding T reporter cell lines. LR-BSL8.4a and LR-BSL3.6b were stained positively by (A) H-2D^b-SQLLNAKYL and (B) H-2K^b-IITDFENL, respectively (open histograms). Grey, filled histograms are representatives of negative tetramer stainings.

To go further and identify the epitopes that elicited the LacZ activity, the amino acid sequences in table 8 were analyzed with a computer algorithm (121) to predict potential H-2K^b and D^b epitopes. Four different categories were predicted: H-2K^b MHC class I molecules bound with peptides of 8 and 9 amino acids long; and H-2D^b MHC class I molecules bound with 9- and 10-mer peptides. The highest-ranked epitopes in each category were chosen (tables 9 and 10) and synthesized. Each

peptide was used to synthesize fluorescent pMHC tetramers by the photocleavable peptide exchange strategy described earlier. These were then used to stain corresponding T reporter cells to reveal the cognate epitope. For GAP50, the cognate epitope is SQLLNAKYL (figure 21A), spanning position 38 to 46 of the protein and is H-2D^{b}-restricted. For bergheilysin, it is H-2K^{b}-restrcted IITDFENL (figure 21B), from position 592 to 599 of the protein. Henceforth, these two novel epitopes will be referred to as Pb1 (SQLLNAKYL) and Pb2 (IITDFENL).

Table 9: List of top-ranked MHC class I-binding candidate epitopes predicted from GAP50 in table 8.

MHC restriction	Peptide length	Sequence
H-2K^{b}	8	YMPFFTVL MYMPFFTV QLLNAKYL FVDGVKGL GNYNSEVL
H-2K^{b}	9	MYMPFFTVL SQLLNAKYL DMYMPFFTV YMPFFTVLG LNDPSWKSL
H-2D^{b}	9	SQLLNAKYL TGNYNSEVL KSERVTFIV DMYMPFFTV NAKYLKQFI
H-2D^{b}	10	DWTGNYNSEV SPGSNFVDGV LKQFIKSERV PSWKSLYEDV FIVSPGSNFV

Table 10: List of top-ranked MHC class I-binding candidate epitopes predicted from bergheilysin in table 8.

MHC restriction	Peptide length	Sequence
H-2K^b	8	VNPFFTNL IITDFENL YGTEQEKL
H-2K^b	9	EHLDKFPII PVNPFFTNL TNLNNENNM
H-2D^b	9	ISDLNGKTL TNLNNENNM HLLNNDHRV
H-2D^b	10	HLLNNDHRVV KHLLNNDHRV TNLNNENNMQ

Analysis of other malaria CD8$^+$ T cell epitopes reported in the literature

Partway through this project, Lau and colleagues took PbA proteins expressed in the schizont stage and predicted H-2K^b-restricted peptides with SYFPEITHI, an online MHC prediction tool. Out of the 125 candidates predicted, they found 5 epitopes that were recognized by CD8$^+$ T cells in PbA-infected mice. The assays they used were intracellular IFNγ staining of peptide-stimulated splenic CD8$^+$ T cells from PbA-infected mice, and for confirmation, cytolytic activity against peptide-pulsed donor cells *in vivo* (130). The sequence of these epitopes and the antigens they came from are tabulated in table 11. The authors reported that they could not make tetramers for their epitopes to track the specific CD8$^+$ T cells *in vivo* during infection.

Table 11: List of 5 H-2K^b-restricted PbA epitopes that were reported by Lau and colleagues (130).

Epitope	Sequence	Antigen	PlasmoDB Gene ID
A6	LSGRYNDL	Hypothetical protein	PBANKA_133730
D5	WGDEFEKL	ribonucleoside-diphosphate reductase, large subunit	PBANKA_061160
F4	EIYIFTNI	replication factor A1, small fragment	PBANKA_041660
F6	LLPHFSIL	replication factor C subunit 1, putative	PBANKA_031600
G4	YYYDYDKI	Activator-protein 2 transcription factor-like protein, putative	PBANKA_052170

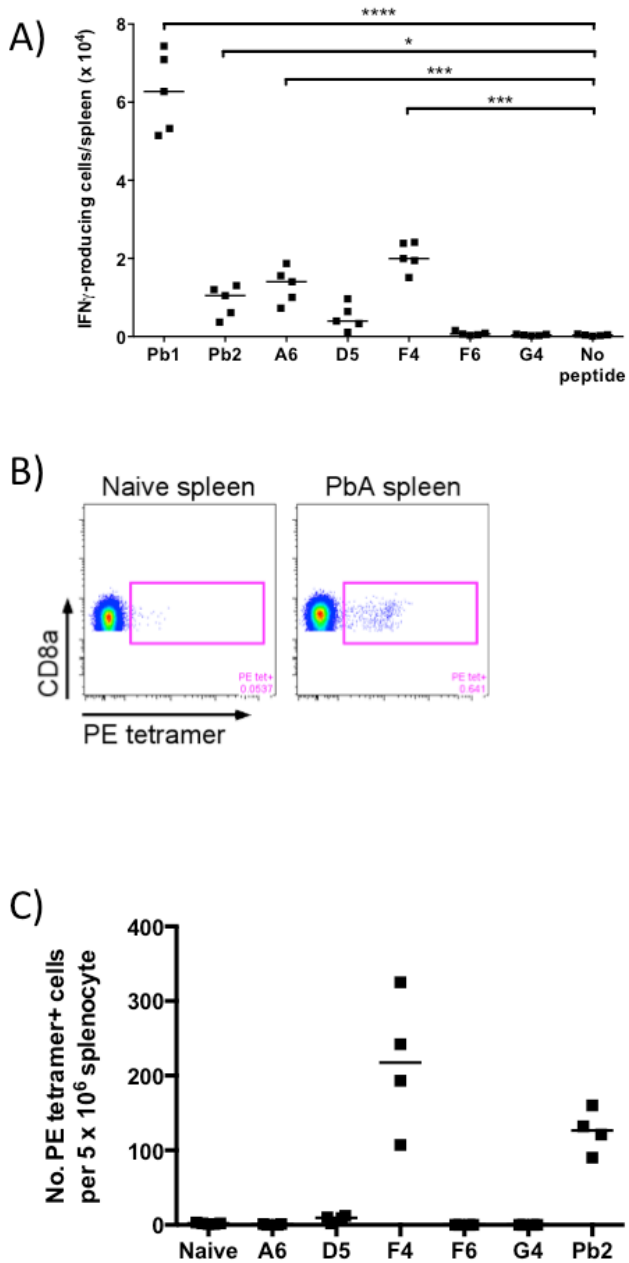

Figure 22. Validation of 5 H-2K^b-restricted PbA epitopes reported in the literature. (A) The previously reported malaria epitopes A6, D5, F4, F6 and G4 were used to stimulate CD8$^+$ T cells isolated from PbA-infected splenocytes, followed by IFNγ-ELISpot assay. They were also used to synthesize PE tetramers and stain PbA-infected splenocytes. Live CD8$^+$ CD16/32$^+$ cells were gated for tetramer-specific CD8$^+$ T cells as shown in (B). The numbers of specific CD8$^+$ T cells positive for PE tetramer staining are shown in (C). The naïve data is a representative result of naïve splenocytes stained with 6 different PE tetramers. Bars in (A) and (C) represent means and medians respectively. * $p < 0.05$, *** $p < 0.001$, **** $p < 0.0001$, One-way ANOVA with Dunnett's post-test.

To validate the findings, $CD8^+$ T cells from PbA-infected splenocytes were stimulated with donor splenocytes pulsed with Pb1, Pb2 or each of the 5 epitopes and assayed for IFNγ production by IFNγ-ELISpot (figure 22A). Pb1 epitope elicited the strongest response out of the tested epitopes, while Pb2 provoked a milder response that is still significantly higher than the background. Unexpectedly, only A6 and F4 epitopes elicited significant response after stimulation, whereas F6 and G4 were negative. D5 epitope seems to produce some IFNγ after stimulation, but this did not attain significance. Using the caged MHC tetramer technology, $H\text{-}2K^b$ MHC tetramers specific for each of the 5 epitopes were also created and used to stain PbA-infected splenocytes. The latter were also stained with antibodies against CD8a and Fc receptors CD16/32, so that $CD8^+$ T cells can be discriminated from $CD8\alpha^+$ dendritic cells that also express CD16/32. Tetramer-positive $CD8^+$ T cells were then analyzed from total $CD8^+$ T cells gated (figure 22B). Out of the 5 epitopes, only F4 tetramer showed positive staining towards its cognate $CD8^+$ T cells, while the rest were negative for staining (figure 22C). More detailed results for tetramer staining for Pb1- and Pb2-specific $CD8^+$ T cells in infected mice are presented in the next chapter.

Affinity of Pb1, Pb2 and F4 epitopes to their corresponding MHC class I molecules

The affinity of Pb1, Pb2 and F4 malaria peptides to their matching MHC class I molecules was investigated by RMA/S binding assay. These cells are deficient in TAP, a protein essential for loading MHC class I molecules with cytosolic peptides generated by proteasomes. Without peptides in the binding groove, the MHC

complex is unstable and dissociates rapidly at normal body temperature. When exposed to a lower temperature (26˚C), expression of empty MHC class I complexes on the cell surface became possible, allowing exogenous loading of peptides. By bringing the temperature back to 37˚C, MHC class I complexes bound to peptides of sufficient affinity will stay on the surface, available for detection by antibody staining. In this way, affinity of epitopes to the MHC class I molecules can be assessed. Pb1 epitope exhibits high affinity to H-2D^{b} MHC class I, as it has a similar binding curve as that with the positive control influenza peptide $NP_{366\text{-}374}$ as peptide concentration increased (figure 23A). The H-2K^{b} epitopes Pb2 and F4 share similar affinities to their cognate MHC class I molecule, but the slower rate of increase in mean fluorescence intensity for H-2K^{b} staining as peptide concentrations increase, as compared to the positive control OVA, may hint that these 2 peptides have a weaker affinity to H-2K^{b} MHC as compared to the strong-binder OVA (figure 23B).

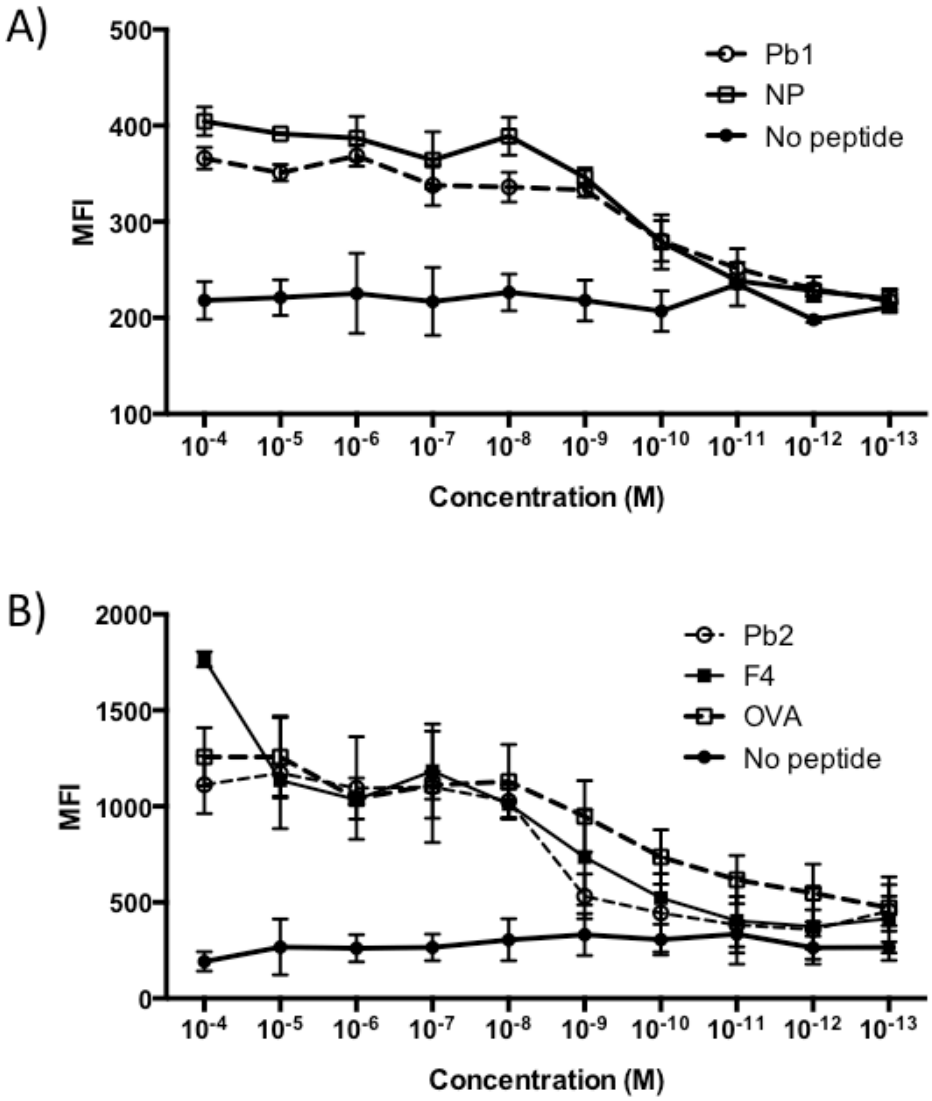

Figure 23. Pb1 and Pb2 malaria epitopes have good affinity to H-2D^b and H-2K^b MHC class I molecules respectively. RMA/S cells were pulsed with increasing concentrations of corresponding peptides at 25˚C, stained with anti-H-2D^b or H-2K^b antibodies at 37˚C and analyzed by flow cytometry. Binding curves of (A) Pb1, (B) Pb2 and F4 malaria peptides to corresponding MHC class I molecules were shown.

Discussion

The screening of the EL4 PbA cDNA library created as described in chapter 1 with the T reporter cell lines created by Dr Shanshan identified two positive leads. The EL4 library clones were isolated and PbA cDNA fragments were sequenced, leading to the identification of GAP50 and bergheilysin as the antigens that induced specific $CD8^+$ T cell response. With the sequences of antigen fragments within GAP50 and bergheilysin identified, we made use of an epitope prediction tool developed by Sette (183) and refined by Grotenbreg (121) to find putative candidates, use them to synthesize MHC tetramers and validate the epitopes. In our study, only two out of eight T reporter cell lines had TCRαβ pairs that recognize malaria epitopes in the context of MHC class I molecules. It is unknown what the other six T reporter cells recognize. Possible reasons could be that our library is not comprehensive enough, or there are subtle differences in the epitope repertoire presentation between EL4 cells and dendritic cells *in vivo*. This may be especially so, since pro-inflammatory cytokines such as IFNg that is produced during infections can induce the formation of immunoproteasomes, which breaks down and generates peptides with slightly different repertoire as compared to normal proteasomes (184, 185).

GAP50 and bergheilysin were the antigens that were discovered in this study to be able to elicit $CD8^+$ T cell response. GAP50 is part of a complex of proteins that form the glideosome, a molecular motor employed by the parasite to move and invade erythrocytes (20, 186, 187). Bergheilysin is the *P. berghei* orthologue of falcilysin, an enzyme with dual function depending on the localization. It facilitates

degradation of hemoglobin in the food vacuoles of parasites to obtain materials for growth (188-190). Elsewhere, bergheilysin is found in the apicoplast, where it is speculated to degrade transit peptides, probably participating in directing protein trafficking to other organelles. No multi-gene families exist for both genes, and given the vital functions they perform within the parasite, these two genes are potential targets for $CD8^+$-mediated immune protection against liver stage infection. In addition, the shared epitope sequences in both *P. berghei*, *P. yoelii* and *P. chabaudi* present an opportunity to examine the induction and characterization of specific $CD8^+$ T cells in non-ECM and other mouse models. This is shown in the next chapter.

It is noted that our analysis of the 5 epitopes reported by Lau *et al* did not corroborate with their results, except for F4 epitope (130). This could be due to the different parasite clones or C57BL/6 strains that were used, with subtle differences that could have affected induction of $CD8^+$ T cell repertoire. For example, in another mouse model to study protective immunity against malaria infection, infections with different strains of *P. chabaudi* led to strain-specific protective immunity that accelerated clearance of homologous parasites (191). Beside F4 epitope, we were unable to demonstrate that $CD8^+$ T cells specific for A6, D5, F6 and G4 can be stained with corresponding pMHC tetramers. For F6 and G4 that had negative ELISpot results, it is likely that no specific $CD8^+$ T cells were induced. For A6 and perhaps D5, one possible explanation is that these peptides cannot bind to and stabilize empty MHC class I complexes *in* vitro, following ablation of the caged photolabile peptide. The presence of chaperones *in vivo* during peptide loading may significantly aid in the loading of these peptides into MHC class I molecules. Another reason could be

that the affinity of the peptide-MHC interaction with cognate $CD8^+$ T cells is too low to allow stable binding with MHC tetramers alone. *In vivo*, higher avidity is generated by multiple pMHC-TCR interactions between two cell surfaces stabilized with adhesion molecules; these cannot be replicated with MHC tetramers.

Despite the revelation that $CD8^+$ T cells are essential for ECM development, studies of malaria-specific $CD8^+$ T cells have not been performed due to the lack of tools to identify these cells. Lau and colleagues, having failed to generate pMHC tetramer, can only show that the 5 malaria epitopes are recognized during infection. In this study, the ability to synthesize desired pMHC tetramers rapidly will allow us to track antigen-specific $CD8^+$ T cells during malaria infection. In addition, the T reporter cells generated in this study can be useful in quantitating the presence of malaria epitopes in the context of MHC class I molecules, potentially allowing the antigen presentation in the organs to be detected and analyzed. These will be further described in chapter 3.

Chapter 3: Characterization of $CD8^+$ T cells recognizing novel malaria epitopes in the ECM mouse model

Introduction

$CD8^+$ T cells were demonstrated to be the effector cause of ECM, as mice lacking these cells do not exhibit this pathology (87). However, how this is achieved is not fully understood because the paucity of malaria epitopes recognized by $CD8^+$ T cells hindered further studies until recently. We described in the previous chapter the discovery of two novel rodent malaria epitopes Pb1 and Pb2, their corresponding tetramers and T reporter cells. With these, we set out to track parasite-specific $CD8^+$ T cells in the spleens and brains in both ECM and non-ECM models. In other studies, many markers have been reported to be essential for ECM development. Of these, those that can be associated to $CD8^+$ T cells include activation marker LFA-1 (145, 192), pro-inflammatory cytokine IFNγ (151), granzyme B (122), and chemokine receptors CCR5 (134) and CXCR3 (136, 142). The expression of these markers by parasite-specific $CD8^+$ T cells were investigated to see if they correlate with earlier findings. Through this characterization, we seek to demonstrate that parasite-specific $CD8^+$ T cells cause damage to the BBB during ECM development, and to discover the mechanistic difference that separates PbA from non-ECM causing parasites.

To gauge the breadth of the response and the relative contribution of the known epitopes, and to investigate whether this could be a therapeutic modality, we

took the approach of suppressing induction of parasite-specific $CD8^+$ T cells through high-dose peptide tolerization, which has been used in a number of studies to study the functions of specific $CD8^+$ T cells in different settings (193-196). In this study, mice were injected with peptides to suppress specific $CD8^+$ T cells during infection to elucidate their effects on ECM development.

Materials and methods

Mice

C57BL/6J mice from 6 to 8 weeks old were used throughout the experiments, unless otherwise stated. These mice were bred under specific pathogen-free conditions in the Biological Resource Centre, Singapore. All animal experiments and procedures were approved by the Institutional Animal Care And Use Committee and complied with the guidelines of the Agri-Food and Veterinary Authority and National Advisory Committee for Laboratory Animal Research.

Parasites

The iRBC of the following species were used in the experiments: PbA, Py17X (197), and PbNK65 (198). These parasitized erythrocytes were passaged by i.p in C57BL/6J mice, harvested and stored in Alsever's solution in liquid nitrogen. For PbA infection, mice were injected i.p. with 0.3 to 1.0 x 10^6 iRBC, with the dose adjusted for each batch so that most mice develop neurological signs at 7 days post-infection. For Py17X and PbNK65 infections, 10^6 iRBC were injected by i.p. Parasitaemia was checked by examination of thin blood smears stained with Giemsa, or by flow cytometry (165).

Leukocyte isolation

Mice were anesthetized by i.p. injection with ketamine/xylazine, followed by exsanguination through retro-orbital route. Brains were mashed in 40 µm cell strainers (BD Biosciences, San Jose, CA) in 10 mL PBS with 5 mg collagenase type IV (Worthington Biochemical, Lakewood, NJ) and 100 µg DNAse I (Roche, Quebec, Canada) and mixed for 30 min at room temperature. The suspension was filtered through the strainer into a 50 mL Falcon tube and centrifuged at 500 rpm for 30 sec to pellet down cell debris. The supernatant was layered carefully on top of 10 mL 30% Percoll (Sigma-Aldrich) and spun at 1942 g for 10 min without brakes. Erythrocytes in the pellet were lysed with ACK lysis buffer (155 mM NH_4Cl, 10 mM $KHCO_3$, 0.2 mM EDTA, all chemicals from Sigma-Aldrich) for a minute and washed with RPMI complete medium supplemented with 10% fetal bovine serum, 100 U/mL pemicillin/streptomycin, 1mM sodium pyruvate, 55 µM 2-mercaptoethanol (all from Gibco, Life Technologies) and 100 µg/mL Primocin (Invivogen, San Diego, CA). Spleens were mashed through 40 µm cell strainers into 10 mL RPMI complete medium, spun down and the splenocyte pellets were treated with ACK lysis buffer as described above.

Tetramer staining

Brain-sequestered leukocytes (BSL) and splenocytes were stained with LIVE/DEAD® Fixable Aqua stain (Molecular Probes) at 1:1000 dilution for 30 min at room temperature, followed by centrifugation to remove supernatant. In separate

experiments, the cells were added with H-2D^b-Pb1 PE tetramers only, or H-2K^b-Pb2 PE and H-2K^b-F4 BV421 tetramers (refer to Materials and Methods in chapter 2 for tetramer synthesis) on ice for 15 min, away from light. The following antibodies were used for staining: anti-mouse CD8α BV605, PerCP-Cy5.5 (clone 53-6.7; Biolegend) or APC (BD Biosciences); anti-mouse CD16/32 APC-Cy7 (clone 93; Biolegend); anti-mouse CD11a FITC (clone M17/4; BD Biosciences); anti-mouse CD183 PerCP-Cy5.5 (clone CXCR3-173; eBioscience); anti-mouse CCR5 APC (clone MC-68; a kind gift from Dr Matthias Mack, University of Regensburg, Germany (199), conjugated with Lynx APC conjugation kit from AbD Serotec, Kidlington, Oxford, United Kingdom). Cells were washed, fixed with 1% formaldehyde and acquired on LSRFortessa (BD Biosciences). To protect the fluorophores against degradation for future acquisition in some cases, the formaldehyde solution was spun down, discarded and replaced with FACS buffer (PBS + 0.5 mg/mL bovine serum albumin [Sigma-Aldrich] + 2 mM EDTA).

Intracellular cytokine staining

BSL and splenocytes were incubated in RPMI complete medium with 10 µg/mL Brefeldin A (eBioscience) at 37˚C for 2 hours before proceeding with tetramer staining. After fixing the samples in 1% formaldehyde overnight at 4˚C, cells were permeabilized with 0.5% (w/v) saponin (Sigma-Aldrich) and stained with anti-mouse IFNγ FITC (clone XMG1.2; BD Biosciences) and anti-mouse granzyme B PE-Cy7 (clone NGZB; eBioscience).

In vivo cytolysis assay

Naïve splenocytes were pulsed with 10 µg/mL peptides at 37˚C for 1 hour, labeled with 0.5 µM carboxyfluorescein succinimidyl ester (CFSE, Molecular Probes) and washed thoroughly with RPMI complete medium. Separately, unpulsed splenocytes were labeled with 5 µM CFSE. Equal numbers of pulsed and unpulsed splenocytes were mixed together and transferred into infected recipient mice at 6 days post-infection intravenously (i.v.), at a total of 2 x 10^7 cells per mouse. Twenty hours later, recipient splenocytes were isolated, stained with 100 ng/µL 4',6-diamidino-2-phenylindole (DAPI, Molecular Probes) and CFSE-labeled cells were quantified by flow cytometry. The percentage of specific lytic activity is calculated as follows: $\{1 - [(CFSE^{high}/CFSE^{low})^{naïve}/(CFSE^{high}/CFSE^{low})^{infected}]\} \times 100\%$

Brain microvessel cross-presentation assay

The protocol for brain microvessel isolation was adapted from elsewhere in the literature (200, 201). Each mouse was anaesthetized, exsanguinated and the brain (excluding the brain stem and meninges) was chopped in 1 mL RPMI complete medium with a scalpel blade. The mixture was homogenized by forcing through a 23-gauge needle 5 times, then mixed with an equal volume (approximately 1.3 mL) of 30% dextran (MW ~70,000; Sigma-Aldrich) in PBS and spun at 10,000 g for 15 min at 4˚C. The pellet was resuspended in PBS, passed through 40 µm cell strainer and backflushed with 2 mL PBS into a 6-well plate to collect the trapped brain microvessels. Fetal bovine serum, collagenase type IV and DNAse I at 2%, 1 mg/mL

and 10 µg/mL respectively, were added to the microvessels and the mixture was shaken at room temperature over an orbital shaker for 90 min. Treated microvessels were topped with 5 mL RPMI complete medium, spun down at 500 g for 5 min, resuspended in 500 µL RPMI complete medium and divided into 5 wells of a 96-well filter plate (Pall 8029, Pall Corportation). T reporter cell lines (3 x 10^4 cells per well) were added to a total of 200 µL/well and the plate was incubated at 37˚C overnight. X-gal staining was performed the next day as described in Chapter 1.

Sequencing TCRαβ sequences from F4-specific $CD8^+$ T cells

PbA-infected splenocytes were stained with tetramers and antibodies as stated earlier. Single cell sorting was performed to sort live $CD8a^+$ $CD16/32^-$ PE-$tetramer^+$ cells into separate PCR tubes coated with 2 µL of lysis buffer (final concentrations: 1X Superscript III RT First Strand buffer, 10 mM DTT, 0.5 mM dNTP, 0.8 U/µL RNaseOUT [all from Life Technologies], 0.25% Nonidet P-40 [Roche], 0.1 mg/mL BSA [New England Biolabs], 0.1 µM mTCRaRT, 0.1 µM mTCRbRT) and stored at -80˚C. Tubes were thawed, reverse-transcribed at 55˚C for 1 hour with 16 U/µL Superscript III RT enzyme (Life Technologies) in 1X First Strand buffer, followed by oligo-dG tailing by terminal deoxynucleoside transferase (TdT) at 37˚C for 1 hour in a total volume of 10 µL reaction mix (final concentration: 10 mM Tris-HCl [Sigma-Aldrich], 10 mM $MgCl_2$, pH 7.5, 1 mM DTT, 2 mM dGTP, 0.75 U/µL TdT [all from Life Technologies]). Heat inactivation of the enzymes was performed at 70˚C for 10 min. Second strand synthesis was carried out in a total reaction mix of 50 µL (final concentration: 1X GC buffer, 2 U/µL Phusion II DNA polymerase [both from

Finnzymes], 0.2 mM dNTP, 0.5 µM oligo-dC-adaptor) with the PCR cycle listed in table 12. The resulting cDNA transcripts (2 µL) were used to amplify TCRα in a first round of PCR in 20 µL reaction mix (final concentration: 1X GC buffer, 0.2 mM dNTP, 0.5 µM mTCRa1st primer, 0.5 µM AdaptorP1 primer, 0.02 U/µL Phusion II DNA polymerase) with the PCR cycle listed in table 13. To amplify TCRβ, this step is repeated with mTCRb1st and Adaptor P1 primer pairs. From these, 4 µL of the reaction mix was used to do a nested PCR with primer pairs mTCRaNest, AdaptorP2 for TCRα, and mTCRbNest, AdaptorP2 for TCRβ, in the same conditions as that in the first run. Amplicons were analyzed by gel electrophoresis on 1% TAE gel, excised, purified, cloned into pCR®4-TOPO® vector and transformed into OneShot TOP10 competent cells. Positive transformants were miniprepped and sequenced.

Table 12: PCR cycling conditions for second strand synthesis of TCRαβ sequences.

Step	Temperature (˚C)	Duration (sec)
1	98	30
2	98	10
3	60	20
4	72	90
5	Repeat steps 2 to 4 for a total of 24 cycles	
6	72	300

Table 13: PCR cycling conditions for amplification of TCRαβ sequences.

Step	Temperature (˚C)	Duration (sec)
1	98	30
2	98	10
3	64	20
4	72	30
5	Repeat steps 2 to 4 for a total of 30 cycles	
6	72	300

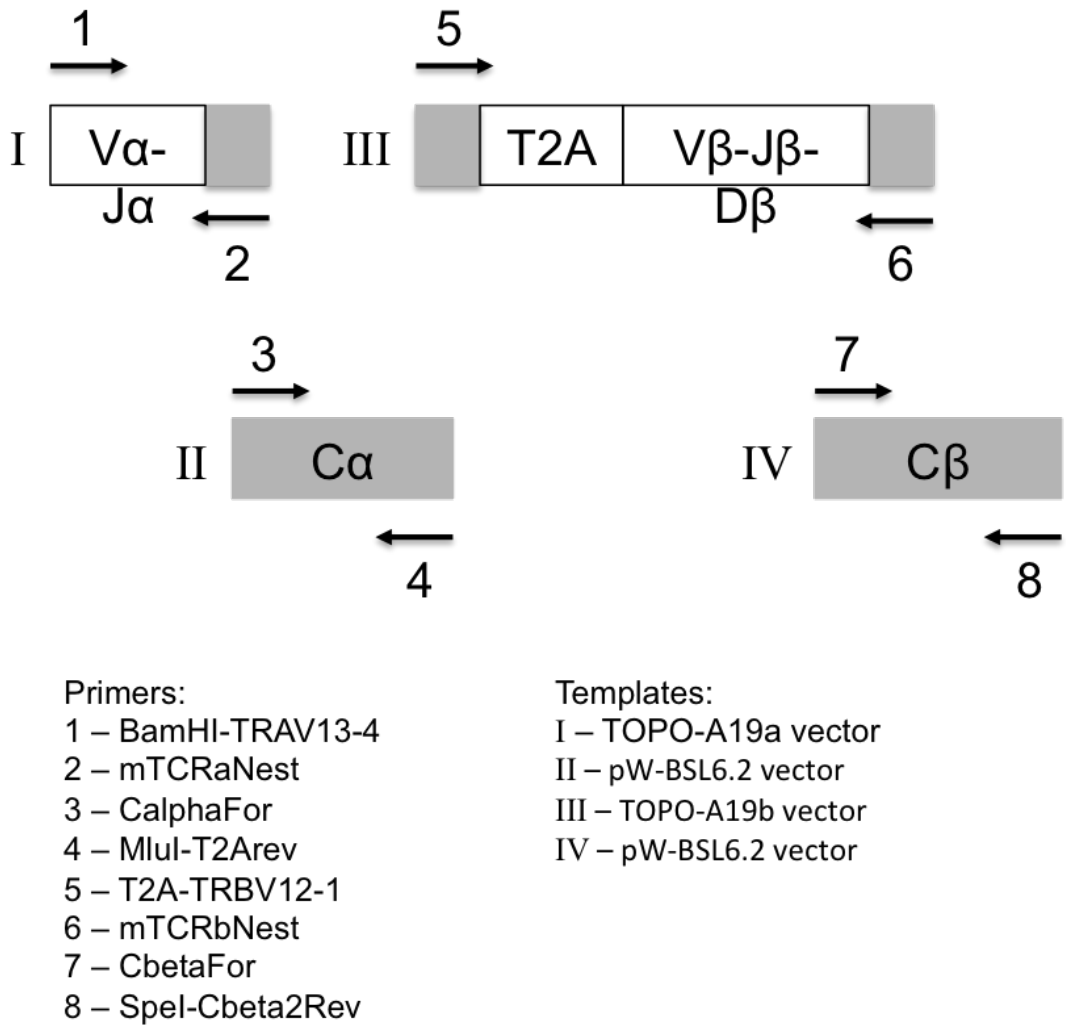

Figure 24. Schematic of assembling F4-specific TCRαβ sequences in one reading frame. The TCRαβ sequences, with corresponding constant regions, from F4-specific $CD8^+$ T cells were amplified with different primer sets, and then assembled together by PCR. A self-cleaving T2A peptide were inserted between the α and β chains to allow bicistronic expression. This was then cloned into the MCS region of pW-luc-GFP. The templates needed were generated in the lab.

Cloning of F4-specific TCRαβ sequences into lentivector

TCR variable regions were assembled with constant regions and a T2A self-cleaving peptide into a single open-reading frame with appropriate primers (depicted in figure 24) by overlap-extension PCR. Adjoining fragments were generated first, followed by combining all 3 of such fragments together in a separate

PCR with BamHI-TRAV13-4 and SpeI-Cbeta2Rev primers. Reactions were analyzed by gel electrophoresis in 1% TAE buffer, excised, purified, cloned into BamHI-, SpeI-digested pW-luc-GFP lentivector by using vector:insert molar ratio of 1:3 with Quick Ligase (New England Biolabs), followed by transformation into OneShot Stbl3 chemically-competent cells (Life Technologies). Positive clones were screened by colony PCR with CbetaFor and WPRErev primers, miniprepped and stored at -20˚C.

Generation of lentiviral particles

HEK293T cells were cultured at 37˚C, 5% CO_2 in a 60 mm tissue-culture dish to ~50% confluency in DMEM media supplemented with 10% FBS. Lentivector containing F4-specific TCRαβ construct (1 µg) were mixed with 0.35 µg pMD2.G envelope vector and 0.65 µg psPAX2 packaging vector (both from Trono lab, EPFL, Switzerland) in 80 µL OptiMEM serum-free media (Life Technologies). This was mixed dropwise to another tube with 80 µL OptiMEM serum-free media and 6 µL EndoFectin Lenti (GeneCopoeia, Rockville, MD) while vortexing, incubated at room temperature for 15 min, followed by adding the whole mixture dropwise into the HEK293T cells. After overnight incubation, the DMEM media was replaced with 3 mL fresh media and cells were allowed to incubate for 2 more days. Media containing lentiviral particles were harvested, centrifuged at 500 g for 5 min to remove cell debris, aliquoted and stored at -80˚C.

Creation of LR-WH3.4 T reporter cell line

LR-null T reporter cells (132), which express TCR δ and ζ chains and NFAT-LacZ cassette, were seeded at 10^5 cells in a 24-well tissue-culture plate with RPMI complete media, transduced with 100 µL lentiviral particles obtained earlier and incubated at 37˚C, 5% CO_2. Change of media was done the next day, and cells were incubated for 2 more days, before harvested and stained with anti-mouse TCRβ PE at 1:1000 dilution for 30 min on ice in FACs buffer. Cells were washed and resuspended in FACs buffer with 100 ng/µL DAPI (Molecular Probes), followed by sorting for $DAPI^-$ PE^+ cells into a 96-well tissue culture plate filled with 200 µL RPMI complete media per well, with one cell in each well. Cells were then cultured, and 12 wells with good cell growth were tested by incubating 3 x 10^4 Dynabead Mouse T-Activator CD3/CD28 (Life Technologies) with equal numbers of cells overnight, followed by staining for LacZ activity as described earlier.

Folic acid challenge

To reduce parasite load rapidly before onset of ECM, PbA-infected mice were treated by i.p. injection with 0.8 mg chloroquine diphosphate (dissolved in H_2O) twice on days 6 and 7, 0.1 mg artesunate (dissolved in 5% sodium bicarbonate, then added an equal amount of 0.9% sodium chloride, all chemicals from Sigma-Aldrich) twice on the morning and evening of day 6. Unless specified otherwise, 100 µg of each peptide were introduced i.v. into each mouse thrice on day 7, at 4 hours apart. The next day, folic acid at pH 7, 0.25 mg/g body weight (Sigma-Aldrich) were injected

i.v. twice at 1 hour apart, and monitored for 90 min after second injection. Mice that survived past this observation period were euthanized.

Peptide tolerization

Prior to PbA infection, mice were injected i.v. with 300 µg of each peptide at day -7, and 100 µg of each peptide on days -4 and -1 (196). Mouse survival was monitored and tetramer staining on BSL and splenocytes were performed as described earlier in separate experiments.

Statistical analysis

Flow cytometry data and all calculations were analyzed with Flowjo (TreeStar, Ashland, OR) and Prism 6 (GraphPad, La Jolla, CA) respectively. The results for staining of tetramer-specific $CD8^+$ T cells were analyzed by Mann-Whitney U test. ELISpot readings were analyzed with one-way analysis of variance (ANOVA) and Dunnett's post test with the unpulsed samples as the control group. The blue spots counted in brain microvessel cross-presentation assay were log transformed to achieve homogeneity of variance and analyzed with one-way ANOVA with Bonferroni's post test. Folic acid challenge and survival was analyzed with Fisher's exact test, while peptide tolerization and survival after PbA infection was analyzed with log rank (Mantel Cox) test.

Results

Induction of CD8$^+$ T cells specific for malaria epitopes during Plasmodium infection

With the identification of 2 novel *Plasmodium* epitopes and the description of other epitopes in the literature in the previous chapter, we first asked if we can detect the induction of these specific CD8$^+$ T cells in mice during ECM using pMHC tetramers. Brains and spleens of PbA-infected mice at day 7 post-infection were processed to isolate leukocytes and stained for live CD8$^+$ T cells, defined by CD8a$^+$ and CD16/32$^-$ expression (since T cells lack CD16 and CD32 Fc receptors). PE-labeled Pb1 tetramer was used in one experiment, while in a separate experiment, PE-labeled Pb2 tetramer and BV421-labeled F4 tetramer were used together (figure 25A). Clear populations of tetramer-specific CD8$^+$ T cells were observed in the spleens and brains of PbA-infected mice and not in naïve mice (figure 25B). This demonstrates that CD8$^+$ T cells specific for natural malaria epitopes expanded and migrated to the brains of mice during infection.

As these epitopes are conserved in the non-ECM causing parasites Py17X and PbNK65 (table 14), one possibility is that malaria-specific CD8$^+$ T cells are not induced during infections with these parasites, thereby rendering the infected mice ECM-resistant. Tetramer staining revealed that they are also found in the brains and spleens of mice infected with Py17X (figure 26) and PbNK65 (figure 27). Of note, the numbers of Pb1-specific CD8$^+$ T cells in Py17X-infected mice are 2 to 10-fold (in

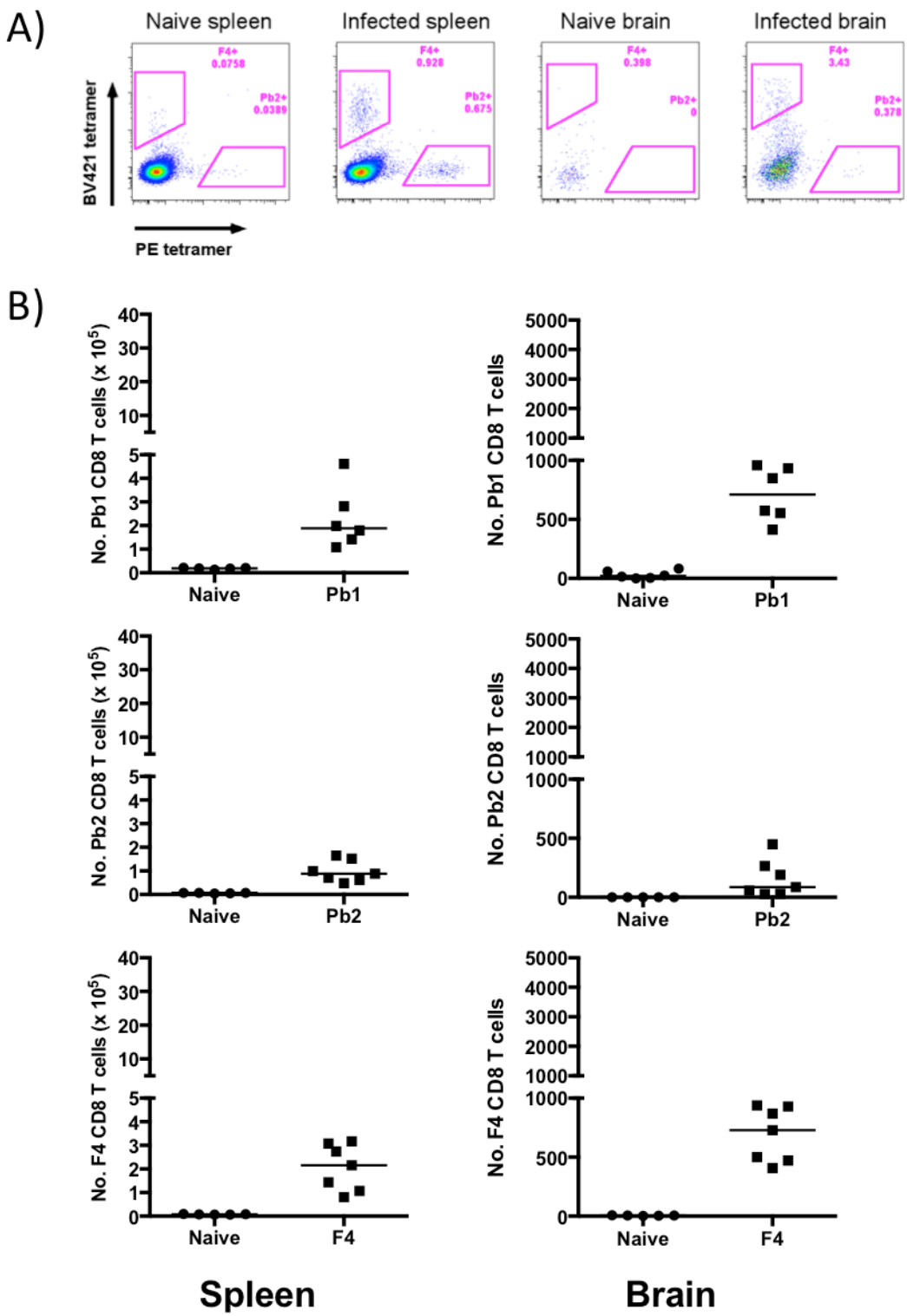

Figure 25. Induction of malaria-specific CD8$^+$ T cells during PbA infection. The gating strategy to identify tetramer-specific CD8$^+$ T cells in double tetramer staining is shown in (A). In (B), the number of CD8$^+$ T cells specific for Pb1 (top), Pb2 (middle) and F4 (bottom) in the spleens and brains of infected mice are shown. Bars represent medians. Results shown here are pooled from two independent experiments. $p < 0.01$ for all results, Mann-Whitney U test.

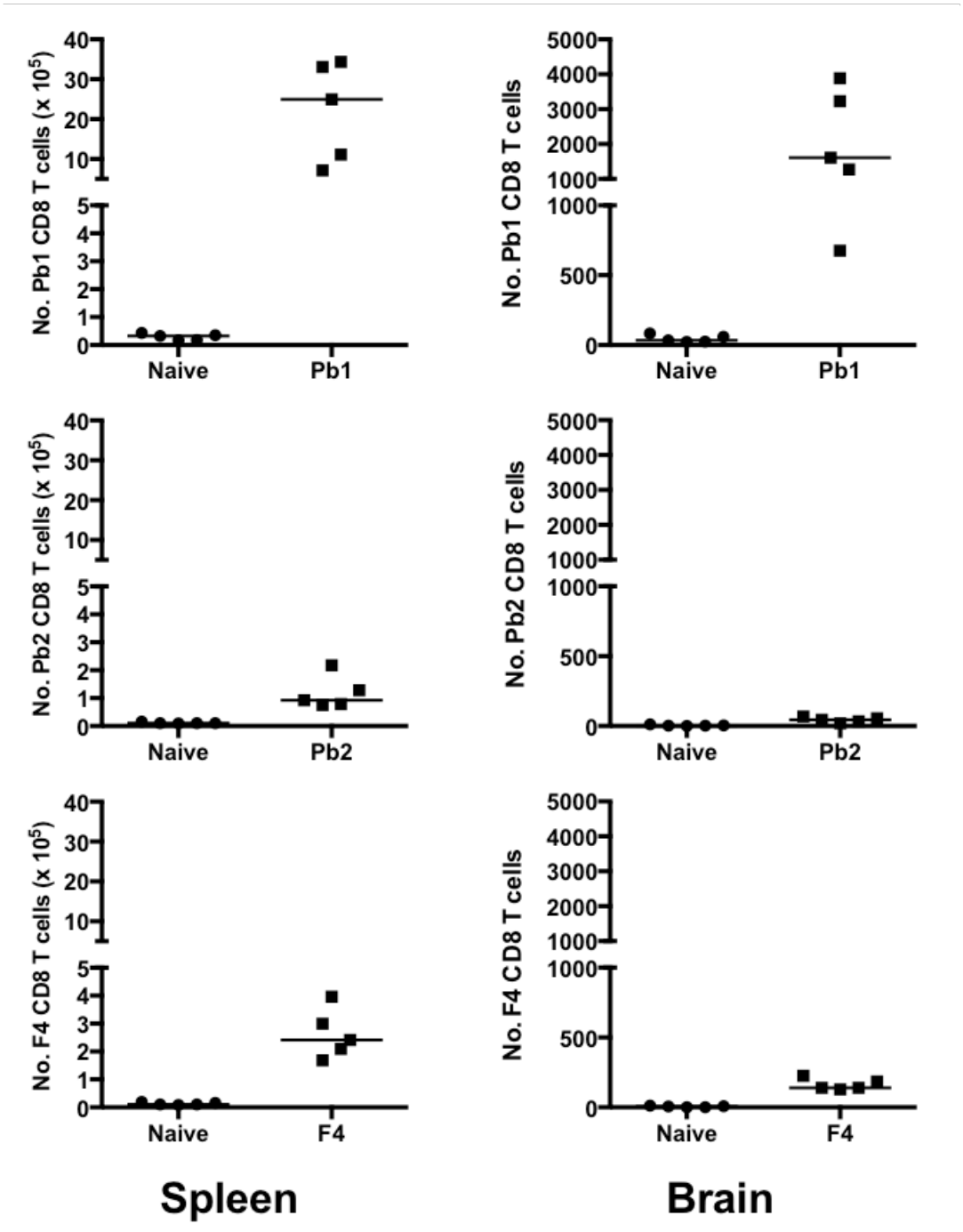

Figure 26. Induction of malaria-specific CD8$^+$ T cells during Py17X infection. See figure 25b legends for description. $p < 0.01$ for all results, Mann-Whitney U test.

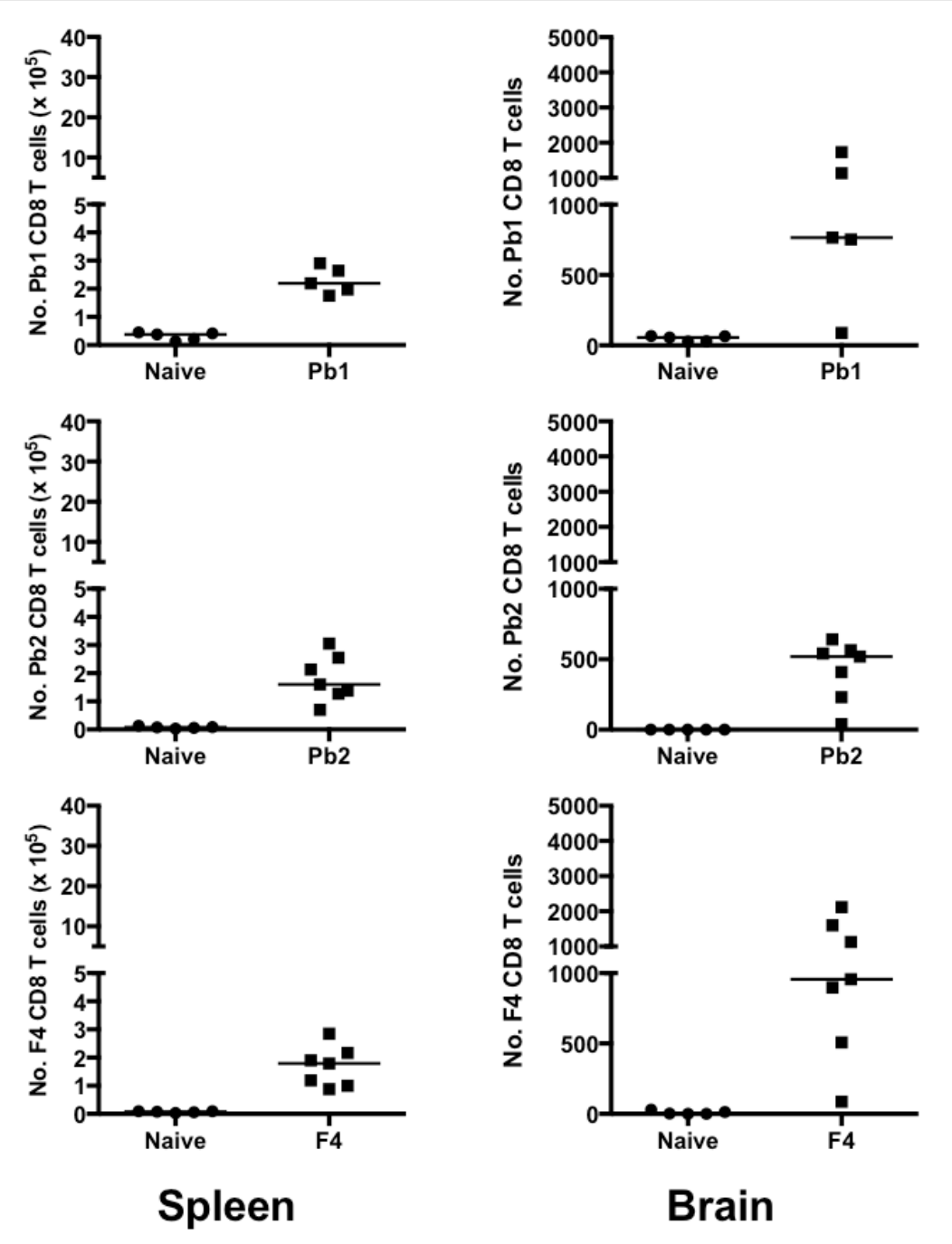

Figure 27. Induction of malaria-specific CD8$^+$ T cells during PbNK65 infection. See figure 25b legends for description. $p < 0.01$ for all results, Mann-Whitney U test.

brains and spleens respectively) larger than in *P.berghei*-infected mice. Therefore, the mere presence of these specific CD8$^+$ T cells is not sufficient to cause ECM.

Table 14: Conservation of epitope sequences in different murine *Plasmodium* parasites. The database PlasmoDB was used to search for conservation of epitopes across different murine parasites, with sequences from *P. berghei* as the reference. Sequence that differs from the reference is indicated.

MHC specificity	Epitope Name	Sequence	Sequence conservation in: *P. yoelii*	*P. chabaudi*
H-2D^b	Pb1	SQLLNAKYL	√	√
H-2K^b	Pb2	IITDFENL	√	IINDFENL
H-2K^b	F4	EIYIFTNI	√	√

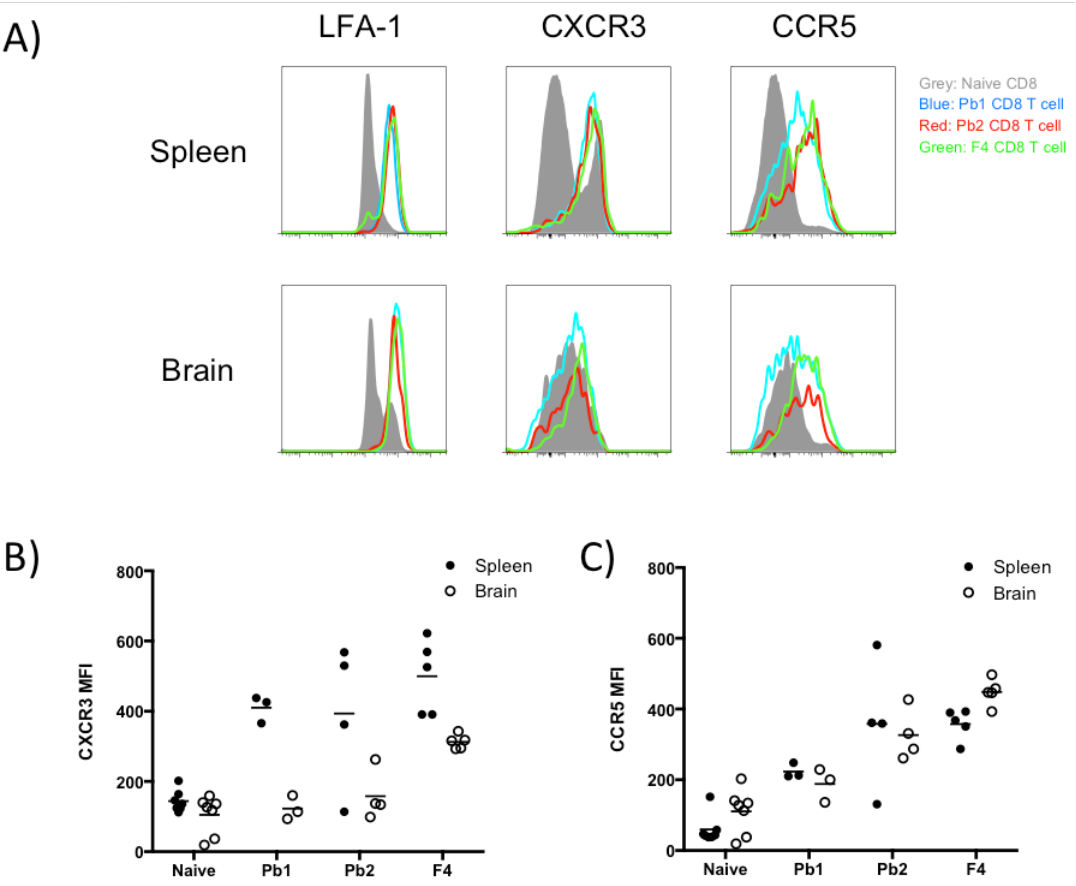

Figure 28. Flow cytometric analysis of expression of cell surface markers on malaria-specific CD8$^+$ T cells during PbA infection. Tetramer-specific CD8$^+$ T cells from BSL and splenocytes of PbA-infected mice were stained for LFA-1, CXCR3 and CCR5. The histograms are the sums of data from 3 to 7 mice that were analyzed separately (A), showing the expression of the tested markers on naïve (gray, filled) and tetramer-specific CD8$^+$ T cells (coloured lines) in the spleens and brains of mice. The comparisons of MFI of CXCR3 and CCR5 between the different CD8$^+$ T cells are depicted in (B) and (C) respectively.

Characterization of malaria-specific CD8$^+$ T cells

The CD8$^+$ T cells specific for malaria-epitopes during PbA infection were analyzed for expression of surface markers by flow cytometry (figure 28A). Tetramer-specific CD8$^+$ T cells in the spleens of infected mice were clearly positive for LFA-1, CXCR3 and CCR5 expression. In the brain, these cells still express LFA-1 but CXCR3 expression was downregulated (figure 28B), while no obvious difference was seen for CCR5 expression (figure 28C).

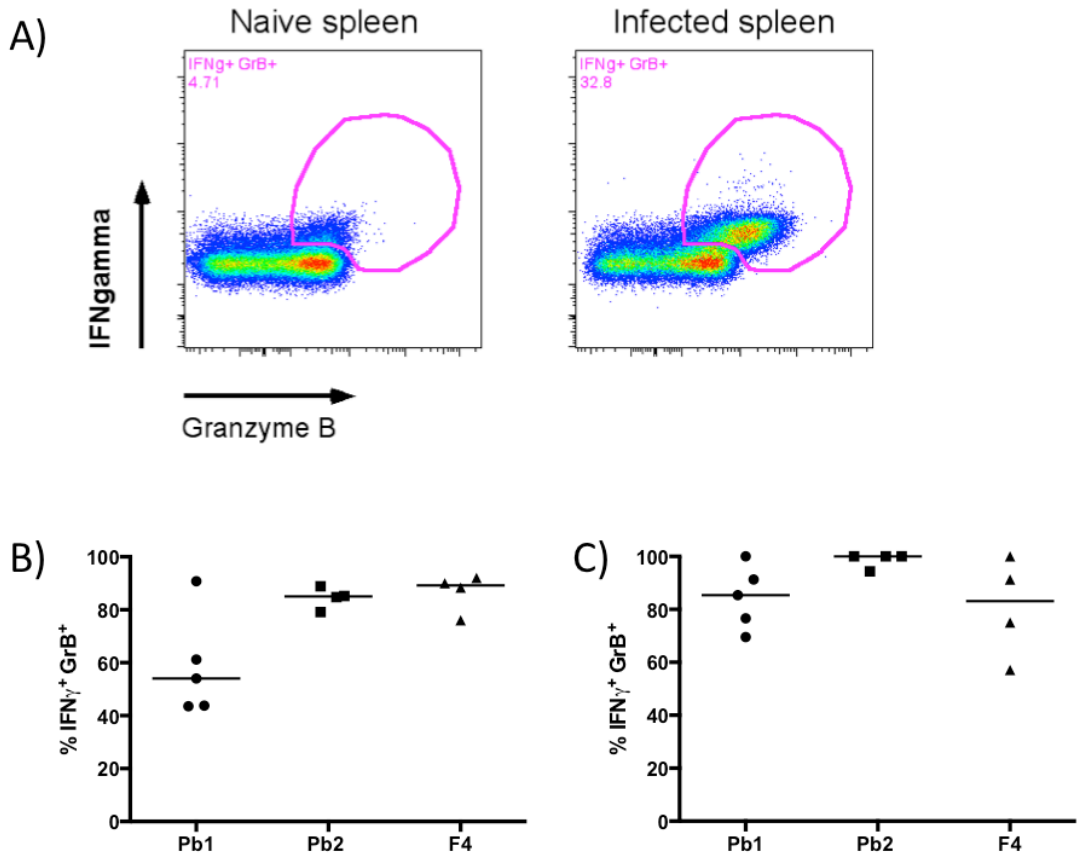

Figure 29. Expression of intracellular IFNγ and granzyme B in malaria-specific CD8$^+$ T cells during PbA infection. Total CD8$^+$ T cells in naïve and PbA-infected mice were compared to determine the IFNγ$^+$GrB$^+$ double-positive gate (A), which was then applied onto tetramer-positive CD8$^+$ T cells. The frequencies of malaria-specific CD8$^+$ T cells that are IFNγ$^+$GrB$^+$ in the (B) spleens and (C) brains of infected mice were shown. Bars represent medians.

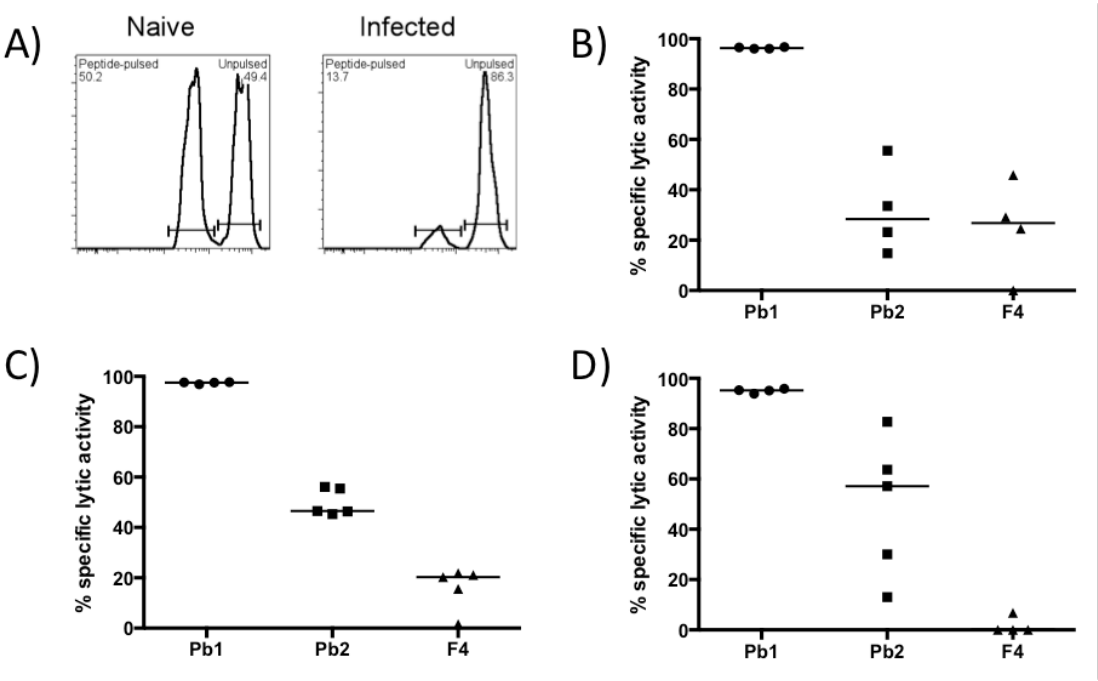

Figure 30. In vivo cytotoxicity of malaria-specific CD8$^+$ T cells in infected mice. Unpulsed, CFSE^{high} and peptide-pulsed, CFSE^{low} donor splenocytes were transferred in equal numbers into infected mice at day 6 post-infection. The next day, frequencies of donor splenocytes in recipient spleens were gated (A). The specific cytolytic activities of CD8$^+$ T cells of different specificities in (B) PbA-, (C) Py17X- and (D) PbNK65-infected mice were shown. Bars represent medians.

Activated CD8$^+$ T cells express pro-inflammatory cytokine IFNγ and cytolytic granule granzyme B (GrB), and these are found to be indispensable for ECM (91, 122). To confirm if malaria-specific CD8$^+$ T cells express these molecules, intracellular cytokine staining was performed together with tetramer staining. The IFNγ$^+$GrB$^+$ double-positive gate was drawn after comparison of total CD8$^+$ T cells between naïve and infected mice, and this was used to gate on tetramer-positive CD8$^+$ T cells (figure 29A). Indeed, a large population of these cells in the spleens (figure 29B) and brains (figure 29C) of infected mice expresses both markers, indicating that they are functional. To further demonstrate their cytolytic activity, an *in vivo* cytolysis assay was performed. Differentially CFSE-labeled donor splenocytes pulsed with or without the target peptides were adoptively transferred into infected mice one day before

ECM symptoms manifest. The mice were sacrificed the next day to analyze the relative numbers of pulsed and unpulsed donor cells. Figure 30 shows that Pb1-specific $CD8^+$ T cells were highly cytolytic in all infections. Pb2- and F4-specific $CD8^+$ T cells were moderately cytolytic in almost all infections, except for the latter, which had no activity in PbNK65-infected mice.

Malaria epitopes are cross-presented on cells in the brain microvessels only in mice infected with PbA

As there was no contrasting difference in terms of induction and cytolytic capability of malaria-specific $CD8^+$ T cells between ECM and non-ECM infections, the attention was then turned towards the potential target cells in the brain. It has been speculated that cells in the brain endothelium can phagocytose parasite materials and cross-present parasite antigens during inflammation (87, 123, 126, 155). If this is indeed the case, T reporter cells recognizing Pb1, Pb2 or F4 in the context of MHC class I molecules can interact with cells that are cross-presenting parasite antigens in the brain vasculature fragments *in vitro*, which then trigger LacZ expression in the former and turn blue upon X-gal staining. Wells with brain microvessel fragments from PbA-infected mice had hundreds of blue spots when incubated with LR-BSL8.4a (figure 31A), as compared to about 10-20 blue spots from that of naïve mice. Py17X- and PbNK65-infected brains gave spot counts that were not statistically different from naïve mice. This clearly indicates that cross-presentation of Pb1 epitope on cells in brain microvessels only occur in mice infected with PbA parasites, supporting

the hypothesis that such cross-presentation is necessary for mice to succumb to ECM. This observation is also applicable to cross-presentation of Pb2 (figure 31B).

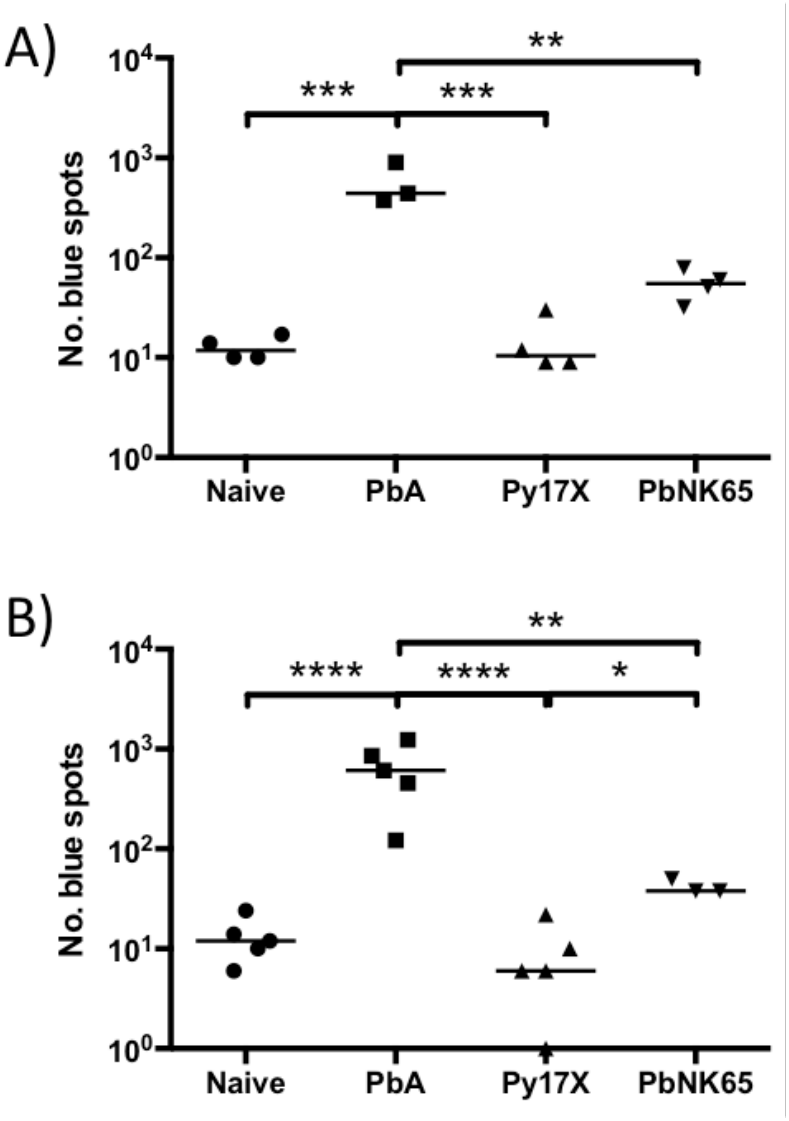

Figure 31. Cross-presentation of malaria epitopes on the cells lining the brain microvessels during infection. Brain microvessels from naïve or infected mice were isolated, processed and incubated with (A) LR-BSL8.4a (recognize H-2D^b-Pb1) and (B) LR-BSL13.6b (H-2K^b-Pb2) overnight in 96-well filter plates. X-gal staining was performed the next day, and the number of blue cells were counted. Bars represent medians. * $p < 0.05$, ** $p < 0.01$, *** $p < 0.001$, **** $p < 0.0001$, one-way ANOVA on log-transformed data with Bonferroni's multiple comparison.

Table 15: List of F4-specific TCRα and TCRβ sequences and identities from single cell clones, analyzed with IMGT/V-QUEST. The most likely TCRαβ pair that was over-represented was shaded in gray, and were cloned into lectivector to generate LR-WH3.4 T reporter cell line. Sequences for some clones could not be identified.

Clone	TRAV	TRAJ	TCRα Junction	TRBV	TRBD	TRBJ	TCRβ Junction
A17	3D-3*02 or 3N-3*01	6*01	CAV#TSGGNYKPTF				×
A18	13-4/DV7	52	CAMALGANTGKLTF	12-1	1	2-1	CASFTSNYAEQFS
A19	13-4/DV7	52	CAMALGANTGKLTF	12-1	1	2-1	CASFTSNYAEQFF
A20	13-4/DV7	52	CAMALGANTGKLTF	12-1	1	2-1	CASFTSNYAEQFF
A21				1	1	1-1	CTCSGTEVFF
A23	16N	6	CAMRAPGGNYKPTF	20	1	2-2	CGASRDRNTGQLYF
A24			×	20	1	2-2	CGASRDRNTGQLYF

- unproductive TCR sequence that arose due to frame-shifting.
× - failed sequencing result

In order to see if the F4 epitope is also cross-presented on the cells lining the brain microvessels, a T reporter cell line that recognizes F4 in the context of H-2K^{b} MHC class I needs to be created. Single cell TCR sequencing was performed on sorted F4-specific CD8^{+} T cells isolated from infected mice. Single cell PCR was required in order to pair up the TCRα and β variable regions. The desired PCR products of about 500 bp were purified and sequenced following gel electrophoresis (figure 32A). A list of the TCRαβ pairs obtained was tabulated in table 15. The TCRαβ pair that was found in more than one cell (highlighted in gray) was cloned into a lentiviral construct to transduce NFAT-LacZ reporter cells. The T reporter cell clone LR-WH3.4a was selected for high expression of TCR (figure 32B) and excellent LacZ activation upon stimulation with minimal background (figure 32C). These cells were then used to assay cross-presentation of F4 epitope on the brain

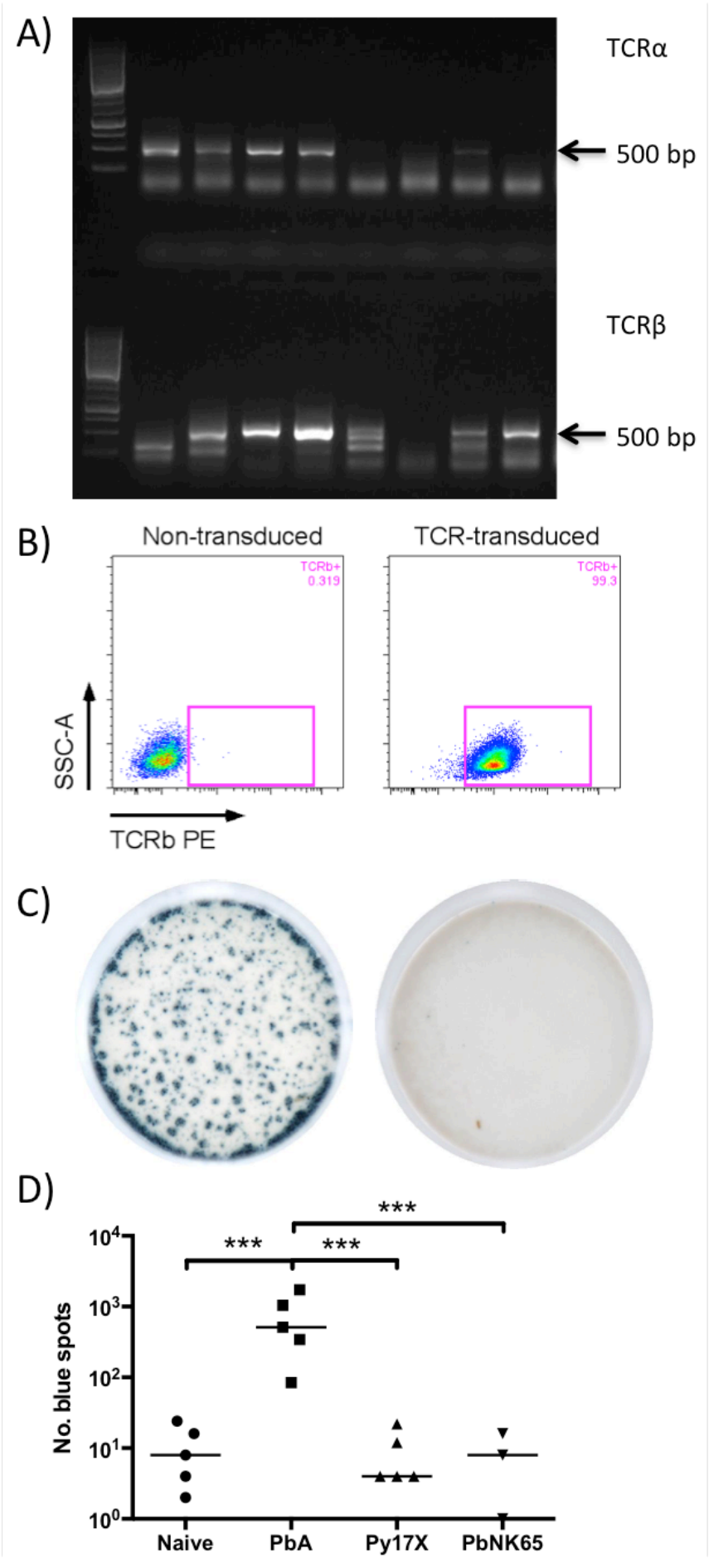
A)
TCRα
500 bp
TCRβ
500 bp
B)
Non-transduced
TCR-transduced
TCRb+
0.319
TCRb+
99.3
SSC-A
TCRb PE
C)
D)
***
***
***
No. blue spots
10^4
10^3
10^2
10^1
10^0
Naive
PbA
Py17X
PbNK65

Figure 32. Creation of T reporter cell line recognizing F4 epitope on H-2K^b MHC class I (LR-WH3.4a). (A) Representative results of single cell amplification of the variable regions of TCR α and β. Each lane corresponds to one CD8$^+$ T cell; desired bands are ~500 bp. were obtained in some cells. One TCRαβ pair from table 15 was transduced to create T reporter cells. (B) TCRβ expression and (C) LacZ activity upon stimulation with F4-pulsed EL4 cells (left) and unpulsed EL4 cells (right) of the selected reporter clone LR-WH3.4a. (D) LR-WH3.4a was used to assess cross-presentation of F4 epitope in the brain microvessels of mice infected with malaria parasites, as described in figure 31.

microvessels of mice infected with malaria parasites. In agreement with the Pb1 and Pb2 results, cross-presentation of F4 epitope only occurs efficiently when mice were infected with ECM-causing PbA parasites (figure 32D), showing that such a finding is likely to be generalized to all malaria CD8 epitopes.

Malaria-specific CD8$^+$ T cells induced during infection can damage BBB in vivo

We sought to further show that the epitope-specific CD8$^+$ T cells that were induced during PbA infection have the ability to exert cytolytic effects on cells in the BBB and thereby lead to hemorrhages and edema as seen in CM cases. An experimental setup was devised, where mice were infected, treated with anti-malarial drugs at day 6 post-infection, injected with Pb1, Pb2 or F4 peptide multiple times (figure 33A). The rationale is to rapidly stop cross-presentation by removing the source of antigen, then to artificially pulse the brain endothelial cells with a particular peptide epitope. Any subsequent damage to the BBB can be attributed to CD8$^+$ T cells recognizing only this particular epitope. The use of chloroquine and artesunate in combination decreased the parasite load in the body rapidly (figure 33B), while the numbers of Pb1-specific CD8$^+$ T cells in treated mice did not differ significantly than when left untreated (figure 33C), corroborating earlier findings (122, 202). Cross-

presentation of Pb1 in the brains of mice was abolished following treatment (figure 33D). After repeated injections of Pb1 peptide to pulse the endothelial cells *in vivo*, mice developed slight ECM signs (hunched back, ruffled fur and lethargy) without progressing further to paralysis, coma and death. We thus sought a clearer readout of BBB damage. From the literature, Hermsen *et al* reported that i.v. injection of folic

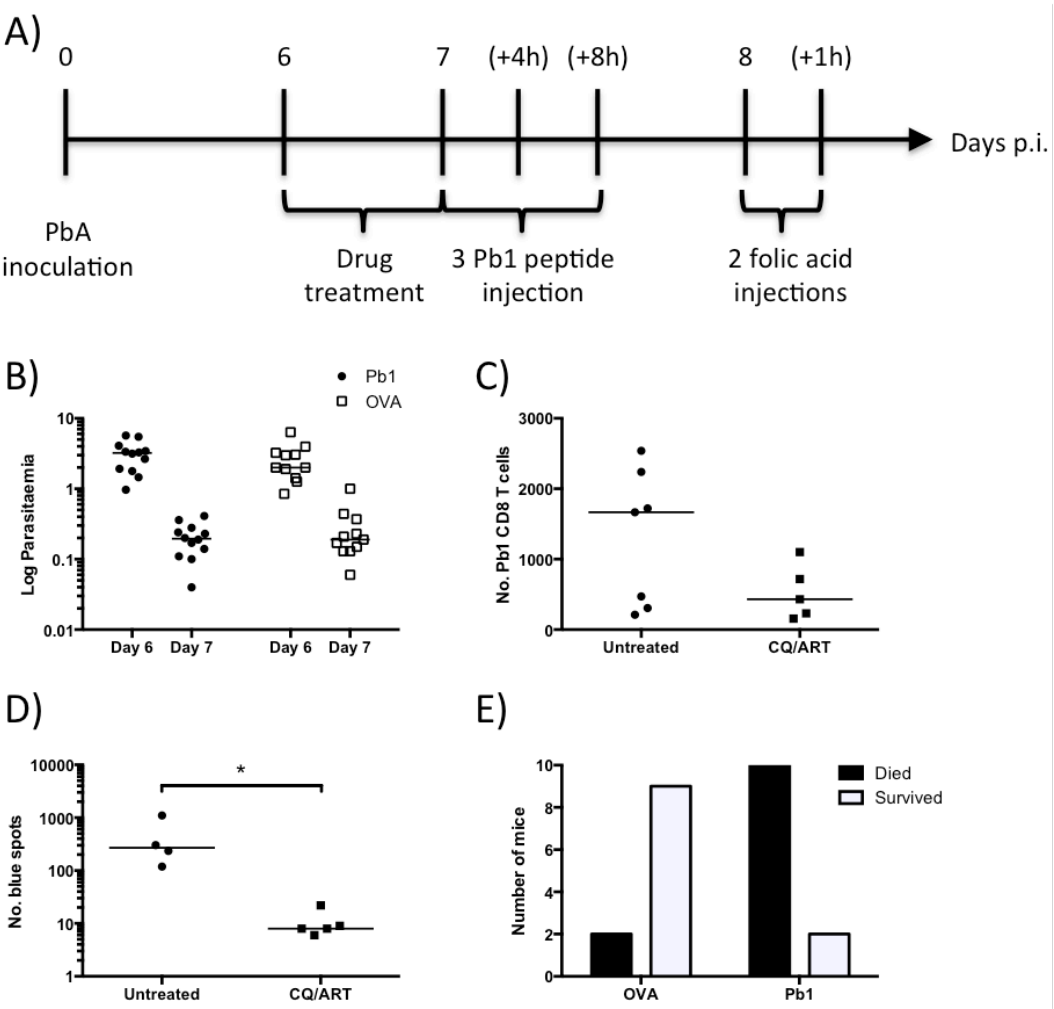

Figure 33. Pb1-specific CD8$^+$ T cells can damage BBB on their own, causing mice to be susceptible to folic acid challenge. The experimental setup is shown in (A), where mice treated with chloroquine and artesunate (CQ/ART) after PbA infection were injected with 100 µg peptide thrice, before challenged with folic acid. The parasitaemia of mice decreased drastically in both Pb1- and OVA-treated groups (B), but Pb1 CD8$^+$ T cells in the brains remain unchanged (C). This was accompanied with a drop in cross-presentation of Pb1 epitope (D). Results of the folic acid challenge in Pb1- and OVA-treated mice was shown in (E). Bars represent medians. * $p < 0.05$ in (C), Mann-Whitney U test. $p = 0.0033$ in (E), Fisher's exact test.

acid into C57BL/6J mice infected with ECM-causing *P. berghei* K173 parasites induced strong convulsions and death in mice, and this is due to increased BBB leakage (203). When folic acid administration was added to the experimental schedule (figure 33A), mice injected with Pb1 peptide developed convulsions and subsequently died during the observation window (figure 33E). In contrast, mice with irrelevant OVA peptide injections remain largely unaffected.

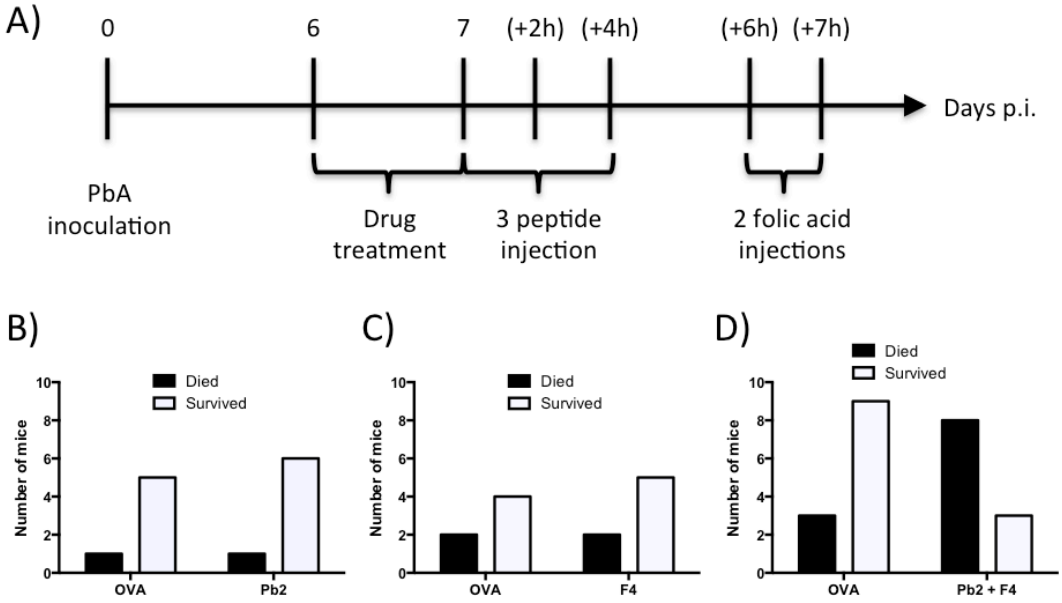

Figure 34. Pb2- and F4-specific CD8$^+$ T cells synergistically damage BBB and render mice susceptible to folic acid challenge. The schematics of the modified protocol is illustrated in (A), where the duration of peptide (100 µg for each peptide) and folic acid injections were shortened to detect cytolytic effects of these CD8$^+$ T cells. The survival graphs of mice after injected with (B) Pb2, (C) F4 or (D) both Pb2 and F4 were shown. In (D), control mice were given 200 µg OVA peptide per injection. p = 0.0391 for result in (D), Fisher's exact test.

When the same experiment was carried out to analyze Pb2- and F4-specific CD8$^+$ T cells, no damage to the BBB was observed. Given the lesser cytolytic capability of Pb2- and F4-specific CD8$^+$ T cells (compared to Pb1) *in vivo*, we sought to increase the sensitivity of the experiment. The protocol was modified (figure 34A) such that folic acid injections were done on the same day as the peptide injections,

so that the recovery window for BBB repair was reduced. In this modified setup, mice that were treated with Pb2 (figure 34B) and F4 (figure 34C) peptide separately were largely resistant to folic acid challenge. When both peptides were combined and injected into mice, the majority of mice convulsed and died after injection with folic acid, as opposed to mice treated with equal amounts of OVA peptide (figure 34D). Together, these experiments demonstrate that malaria-specific $CD8^+$ T cells have the ability to damage the BBB in an additive manner, and this presumably leads to the onset of ECM.

Suppressing the induction of Pb1-, Pb2- and F4-specific $CD8^+$ T cells is not sufficient to protect mice against ECM

In a study on control of *Trypanosoma cruzi* infections by specific $CD8^+$ T cells, Rosenberg and colleagues suppressed the induction of the latter by injecting large quantities of specific peptides and found them to be necessary for control of *T. cruzi* infection (196). The method of tolerizing mice against induction of specific $CD8^+$ T cells was applied into this study, in order to see if Pb1-, Pb2- and F4-specific $CD8^+$ T cells are largely responsible for ECM pathology. As depicted in figure 35A, mice were injected thrice with OVA or a combination of Pb1, Pb2 and F4 peptides prior to PbA infection. Mice given the 3 malaria peptides were not protected against ECM and all mice were dead by day 9 post-infection (figure 35B). In separate experiments, tetramer stainings were performed at day 7 post-infection to ascertain if the targeted $CD8^+$ T cells were indeed suppressed during infection. In the spleens, the numbers of $CD8^+$ T cells specific for Pb1 (figure 35C) and Pb2 (figure 35D), but not F4

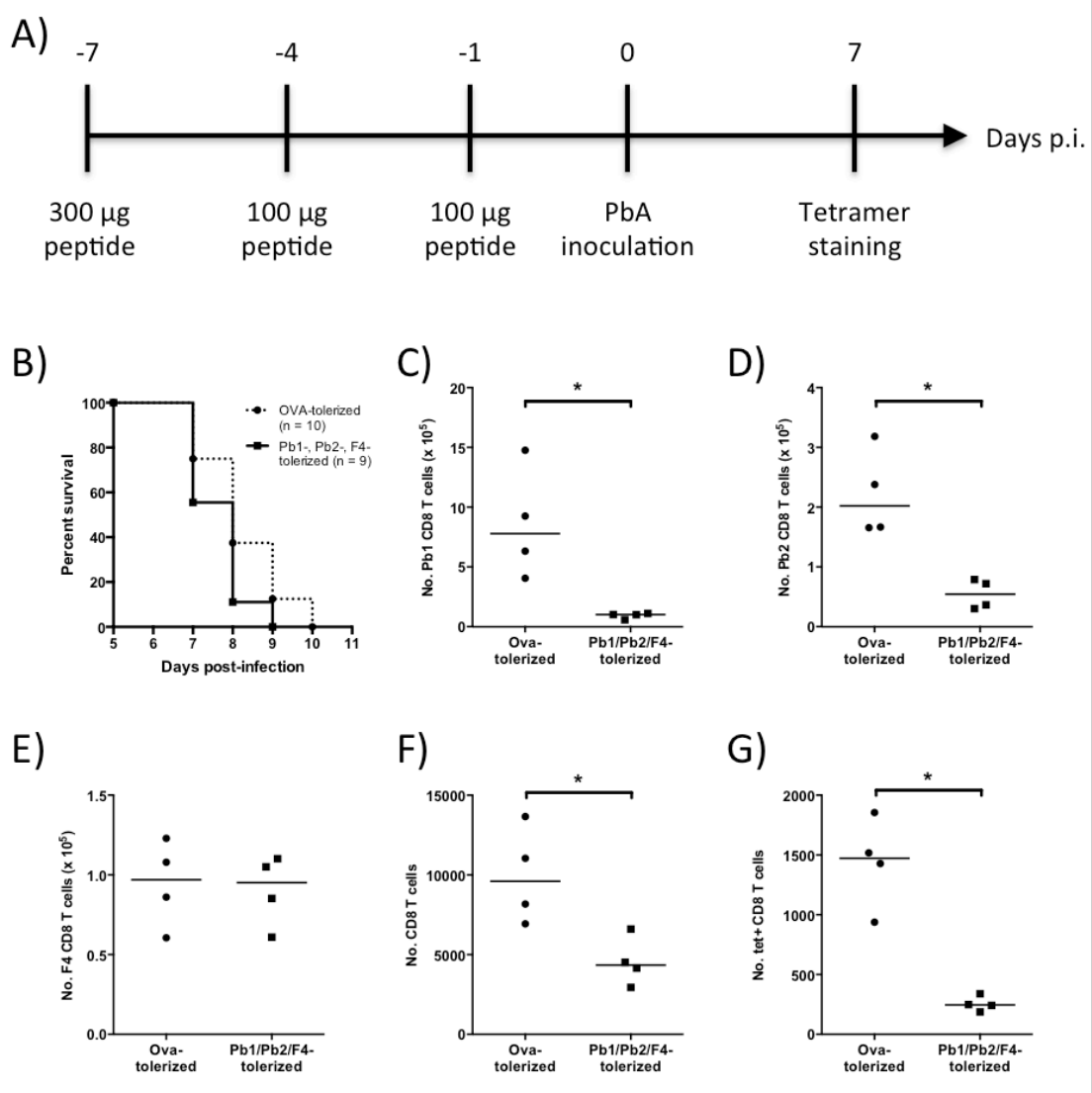

Figure 35. CD8$^+$ T cells of other malaria specificities contribute to ECM. The workflow for the tolerization experiment is illustrated in (A), with the amount of each peptide to be given i.v. to each mouse indicated before PbA infection. To equalize the amount of peptides given in both groups, the amount of OVA peptide given to the control mice was 3 times the amount stated. Survival of mice after tolerization with OVA or 3 malaria epitopes and infection were depicted in (B). Analysis of (C) Pb1-, (D) Pb2- and (E) F4-specific CD8$^+$ T cells in the spleens of mice were shown. (F) Total and (G) malaria-specific CD8$^+$ T cells in BSL from infected mice were also analyzed. Due to the small number of BSLs obtained in each brain, the analysis of tetramer-positive cells in the brains were incorporated together. Bars represent medians. * $p < 0.05$, Mann-Whitney U test.

(figure 35E), decreased following peptide tolerization regimen. Since F4-specific CD8$^+$ T cells were not highly cytolytic (figure 30B) and cannot cause enough damage to the BBB on their own to render mice susceptible to folic acid-induced convulsions (figure

34C), it is unlikely that they are the main reason for the failure to protect mice against ECM. In the brains, the total numbers of $CD8^+$ T cells (figure 35F), as well as those specific for the 3 malaria epitopes (figure 35G), were reduced after tolerization of the 3 malaria-specific $CD8^+$ T cells. It is likely that the remaining $CD8^+$ T cells, largely specific to other PbA epitopes, were sufficient to damage the BBB during PbA infection and cause mice to succumb to ECM.

Discussion

It is the first time that $CD8^+$ T cells specific for endogenous malaria epitopes can be targeted and analyzed during ECM pathogenesis. Before this, such studies were restricted to either total $CD8^+$ T cells (91, 122, 128) or $CD8^+$ T cells specific for a non-endogenous epitope, SIINFEKL from ovalbumin (94, 127). When Lau and colleagues reported the first malaria epitopes discovered, they were limited to detection of IFNγ secretion by peptide-stimulated spleen cells and *in vivo* cytolysis. They could not analyze epitope-specific $CD8^+$ T cells in the brain due to high background. In this study, we confirmed that $CD8^+$ T cells specifically recognizing the novel epitopes Pb1 and Pb2 and the recently reported F4 epitope (130) are induced during PbA infection and migrate to the brain. Pb1- and Pb2-specific $CD8^+$ T cells were present at similar numbers in the spleen during ECM induction, but in the brain, Pb1-specific $CD8^+$ T cells were much more numerous. $CD8^+$ T cells recognizing F4 epitope were induced at similar levels as those recognizing Pb1.

It was initially speculated that the inability of Py17X and PbNK65 to induce ECM in infected mice could be due to the failure to induce cytotoxic parasite-specific $CD8^+$ T cells. As the Pb1, Pb2 and F4 epitopes are conserved between *P. berghei* and *P. yoelii*, we were able to compare the specific $CD8^+$ T cell responses to these epitopes in PbA versus non-ECM strains. Unexpectedly, mice infected with non-ECM-causing parasites Py17X and PbNK65 did induce $CD8^+$ T cells recognizing these 3 epitopes. Indeed, induction of Pb1-specific $CD8^+$ T cells was especially strong in Py17X infection as compared to mice infected with PbA or PbNK65, clearly indicating

that there was no shortage of antigen-specific $CD8^+$ T cells in this non-ECM mouse model.

Changes in chemokine levels during steady state and inflammatory conditions play an important role in immune regulation [reviewed by (204)]. In the context of ECM, increased production of chemokines RANTES (Regulated on activation, normal T-cell expressed and secreted), CXCL9 and CXCL10 were observed in the brains of infected mice (135, 139). This is concomitant with the essential role of CXCR3 receptor in ECM, as mice deficient in CXCR3 expression were protected when infected with PbA (136, 142). In this study, activated malaria-specific $CD8^+$ T cells in the spleen were positive for CCR5 and CXCR3, but these populations down-regulated the latter receptor upon reaching the brain. Binding of CXCR3 receptors to its ligands was shown to result in internalization of the whole complex (205). We postulate that in the context of ECM, the concentration levels of CXCL9 and CXCL10 are highest in the brain and lowest in the vicinity of the lymphoid organs. CXCR3 internalization in response to ligand binding may be important for continued migration up the concentration gradient, as increasing levels of chemokines are needed to maintain the chemotactic response. It remains to be seen if other chemokine receptor-ligand interactions operate in a similar fashion in ECM.

The absence of ECM in mice infected with non-ECM-causing parasites could not be attributed to the lack of cytolytic activity in malaria-specific $CD8^+$ T cells. Rather, we demonstrated in this study that the cross-presentation of Pb1, Pb2 and F4 epitopes in the brain microvasculature was found to occur only during PbA

infection, leading us to propose that this is the crucial difference between ECM and non-ECM infections. This finding strengthens the proposed mechanism that malaria-specific $CD8^+$ T cells migrate to the brain and exert their cytolytic effects on the cross-presenting cells lining the BBB, leading to BBB leakage and the manifestations of ECM. A possible explanation for the differences in cross-presentation is that PbA iRBCs sequester efficiently in the brain as compared to Py17X or PbNK65 iRBC (132, 202), which may promote uptake of parasite material by the activated brain endothelial cells. In addition, PbA parasites may form unique receptor-ligand interactions with host cells in the brain, which the non-ECM parasites may not. Identification of such molecular interactions, if any, could suggest alternative options for intervening with ECM.

In the *in vivo* cytolysis assays, Pb1-specific $CD8^+$ T cells exerted very strong cytotoxic activity against target cells whereas cells recognizing Pb2 and F4 had only modest activity. On a similar note, injection of Pb1 peptide alone could trigger death in convalescent mice during folic acid challenge assay. Pb2 and F4 had to be combined to render mice susceptible to folic acid-induced convulsions. These findings suggest that Pb2 and F4 epitopes are less immunodominant than Pb1. In a study conducted by Lin and colleagues, the expression of the model epitope SIINFEKL from chicken ovalbumin at different compartments within the parasite influences the magnitude of specific $CD8^+$ T cell response, with localization at the PVM inducing a stronger response than expression in the cytosol (206). Correlating to this finding, GAP50 is localized near to the PVM, bergheilysin in the food vacuole deep within the parasite, and replication factor A being in the nucleus (which harbours F4 epitope).

Thus, the localizations of the corresponding antigens may be one reason for their contrasting immunodominance.

The folic acid challenge assays demonstrated that $CD8^+$ T cells of the three specificities tested were capable of damaging the BBB in convalescent mice, following the introduction of corresponding exogenous peptides. However, the extent of BBB damage was limited; severe neurological symptoms and death occurred only after injection of neurotoxic folic acid. This implies that there are likely additional unknown specificities of $CD8^+$ T cells that can inflict BBB damage, and the synergistic effects of these known and unknown $CD8^+$ T cells are required to initiate full-blown ECM. The tolerization experiment results also point towards the presence of additional CD8 epitopes, as successful suppression of the $CD8^+$ T cell response against Pb1 and Pb2 had no effect on ECM onset or incidence. Another possibility suggested by the tolerization experiment is that multiple specificities may have redundant, mutually compensating roles in destroying BBB integrity during PbA infection. With Pb1-, Pb2- and F4-specific $CD8^+$ T cells representing only a fraction of total $CD8^+$ T cells in the brains during ECM, it is highly likely that there are more players than the 3 specificities that were characterized here. The recent report on the discovery of yet another $CD8^+$ T cell epitope, PbT-I, by Lau *et al* (207) is a good example. It will be interesting to investigate if the $CD8^+$ T cell response induced by the PbT-I epitope and brain microvessel cross-presentation of PbT-I share similar characteristics with what has been reported here.

Perspectives

The discoveries of two novel malaria $CD8^+$ T cell epitopes, Pb1 and Pb2, together with the application of MHC tetramers that can label these specific $CD8^+$ T cells, represent considerable progress in understanding the $CD8^+$ T cell-mediated pathogenesis of ECM. Analysis of these $CD8^+$ T cells induced during infection, together with those recognizing the contemporaneously reported F4 epitope, showed that they are cytolytic in nature and are able to participate in damaging the BBB, leading to ECM development. The quest to demonstrate the latter proved difficult. Unlike Lau and colleagues, who demonstrated through adoptive transfer that PbT-I $CD8^+$ T cells from transgenic mice could cause ECM (207), we are still in the process of generating transgenic mice for two years thus far. Instead, we indirectly demonstrated this by removing the parasite load in infected mice and loading exogenous peptides onto MHC class I molecules in their brains and using folic acid to detect BBB damage.

From this study, we conclude that ECM pathogenesis is likely caused by the concerted actions of $CD8^+$ T cells recognizing multiple specificities. This was inferred from two observations. One, $CD8^+$ T cells of one specificity alone were unable to replicate ECM-like symptoms in convalescent mice when the corresponding peptide was introduced into the circulation. Instead, the damage to the BBB could only be reliably detected when challenged with foilc acid injection. Two, mice that were tolerized against Pb1, Pb2 and F4 epitopes still developed ECM, despite a decrease in accumulation of total and epitope-specific $CD8^+$ T cells in their brains. However, this

is not surprising given that *Plasmodium* parasites possess over 5,000 genes. The CD8 epitope repertoire that is presented by the host immune system can be much greater than that from viruses or bacteria. One can imagine that the combined effect of all the parasite-specific $CD8^+$ T cells recognizing their cognate epitopes cross-presented on the cells constituting the BBB is massive enough to lead to edema and hemorrhages, the characteristics of ECM. In our tolerization system, there could be other, yet to be discovered epitope-specific $CD8^+$ T cells that can cause BBB breakdown. This brings up the notion that when a certain threshold of damage has been inflicted onto the brain microvessels, that is beyond the ability of the body to repair, fatal ECM will occur. Multiple specificities must be targeted at the same time in order to bring down the damage below this speculated threshold, which is a challenging and impractical approach.

Despite being recognized by pathogenic $CD8^+$ T cells during blood-stage malaria infection, the epitopes discovered in this study may have potential in conferring protection against liver-stage malaria. Experiments with liver-stage infections showed that parasite-specific $CD8^+$ T cells are essential in mediating sterile immunity in humans (39, 42, 208) and mouse models (209, 210). If the epitopes in this study are also presented by infected hepatocytes (211), then vaccines to mount $CD8^+$ T cell immune responses against them may be able to prevent blood-stage infection by killing the liver-stage parasites before they release merozoites into the circulation. Malaria-specific $CD8^+$ T cells are pathogenic in blood-stage infections, where almost all of them must be suppressed in order to combat ECM pathogenesis. Conversely, in asymptomatic liver-stage infection, $CD8^+$ T cells of one or a few

specificities could be enough to recognize infected hepatocytes and eliminate them before they mature and release merozoites into the circulation. Finally, the epitope discovery strategy that was outlined in this study could be useful to search for additional protective epitopes in both mice and humans.

In areas where malaria infections are endemic, victims suffering from severe malaria, including HCM, are most often admitted into hospitals when life-threatening symptoms have already manifested. Even with medical attention and prompt anti-malarial treatment, mortality is unacceptably high at about 20% (212). Many trials have been conducted on combining anti-malaria drugs with adjunctive therapies, ranging from anti-inflammatory drugs (213-218), monoclonal antibodies against tumor necrosis factor α (219, 220), injections of immunoglobulin from semi-immune individuals (221), anti-sequestration drugs (222, 223), anti-seizures (224-226), osmotherapy to reduce oedema (227-229), iron chelation (230, 231), correcting metabolic acidosis (232-235), and managing circulatory shock (236, 237). All these trials failed to provide substantial benefits to HCM patients. Based on post-mortem HCM observations and experimental results from ECM studies, the underlying cause of HCM is speculated to be the cytoadhesion of infected erythrocytes to the brain endothelium. Whether this subsequently leads to cross-presentation of parasite antigens in the brains of infected patients remains to be validated. The mechanisms of HCM may turn out to be vastly different from that in ECM. Epitopes and tools to examine this in the human context are lacking, but the strategy described in this study may be applicable for such a purpose.

Preventing the interactions between T cells and antigen presenting cells has been a major approach in treating T cell-mediated autoimmune diseases and in preventing transplant rejections. Some of these treatments may be relevant to HCM as we have shown here that ECM is a disease mediated by antigen-specific $CD8^+$ T cells. The main targets are usually the TCR itself (238), the accompanying adhesion molecules such as CD11a (239), or the co-stimulatory molecules such as CD80 (240). Blocking these interactions may prevent T cell activation and/or recognition to the target cells, thereby averting further T cell-mediated damage and disease remission. In particular, we demonstrated that epitope-specific $CD8^+$ T cells in ECM express elevated levels of LFA-1, a heterodimer of CD11a and CD18. Injection of antibodies against CD11a into PbA-infected mice one day before ECM symptoms develop completely abrogated the neurocomplication (145, 192). Despite this discovery, it was never translated into use in humans. Efalizumab, the humanized recombinant antibody that binds to CD11a, was introduced into the market as a long-term psoriasis treatment in 2003. After 6 years, this drug was withdrawn from the market after some patients developed fatal brain infections, due to the reactivation of latent viral infections (241-243). This has essentially halted further development of CD11a blockers, which is a pity as these drugs could prove to be efficacious as short-term treatments for CM. There is little incentive for for-profit drug companies to reinitialize the development and marketing of CD11a blockers for treating HCM, even with the approval from health regulatory authorities, as almost all the patients cannot afford them.

Therapies directed towards the brain endothelial cells may also prove useful in HCM, either by inhibiting uptake or cross-presentation of parasite protein, or by encouraging the repair of the damaged BBB. One example of the former approach could come in the form of proteasome inhibitors. Proteasomes play a role in breaking down proteins within the cell into short peptides that can be loaded onto MHC molecules [reviewed in (244)]. It is likely that they are also involved in cross-presentation of malaria epitopes in endothelial cells lining along the brain vasculature, since these cells can acquire characteristics of APCs in a pro-inflammatory milieu (156). If this process can be interrupted, cross-presentation of parasite epitopes would be reduced, making the endothelial cells poorer targets for $CD8^+$ T cell-mediated cytolysis. Current proteasome inhibitors in the market, such as bortezomib and carfilzomib, could be assessed for such potential. On the other hand, repairing the destruction in the BBB could take the form of growth factors and hormones that induce wound repair and angiogenesis. Erythropoietin (EPO) is a potential candidate for this purpose. PbA-infected mice treated early in infection with EPO were protected from ECM, with reduced inflammation, decreased T cell trafficking and decreased leakage in the brain (245). When combined with artesunate one day before ECM develops, the majority of infected mice survived and ECM was abolished (246). The exact mechanism behind the protective effects of EPO is not completely defined, but it is thought to generate anti-apoptotic signals in endothelial cells in a protein kinase B-dependent manner (247). In addition to its effects on endothelial cells, EPO has also been shown to inhibit death-related signaling pathways in neurons (248). Another neuroprotective molecule, neuregulin-1, was shown to confer protection against ECM to PbA-infected mice, with

concomitant decreases in pro-inflammatory markers in the brain (249). The immunomodulatory, neuroprotective effects of EPO and neuregulin-1 in ECM suggest that neuroprotective therapies may be effective in ameliorating HCM in patients when used in combination with anti-malarial drugs.

In conclusion, the discovery of novel malaria $CD8^+$ T cell epitopes and characterization of cognate $CD8^+$ T cells in ECM mouse models demonstrate that the destruction of BBB integrity during ECM is caused by $CD8^+$ T cells of multiple malaria specificities. The observation that cross-presentation of malaria epitopes by cells lining the BBB is restricted to PbA-infected mice suggests that this is the crucial difference that defines susceptibility to ECM. Further research into the requirements and mechanisms of such cross-presentation may open up new avenues for adjunct therapy that can rapidly halt ECM progression, and hopefully HCM in humans.

Reference

1. Mu J, Duan J, Makova KD, et al. 2002. Chromosome-wide SNPs reveal an ancient origin for Plasmodium falciparum. *Nature*. 418(6895):323–26
2. Wilson RJ, Williamson DH. 1997. Extrachromosomal DNA in the Apicomplexa. *Microbiol. Mol. Biol. Rev.* 61(1):1–16
3. Barker G. 2006. *The Agricultural Revolution in Prehistory : Why did Foragers become Farmers?: Why did Foragers become Farmers?* OUP Oxford
4. Livingstone FB. 1958. Anthropological Implications of Sickle Cell Gene Distribution in West Africa1. *American Anthropologist*. 60(3):533–62
5. Carter R, Mendis KN. 2002. Evolutionary and historical aspects of the burden of malaria. *Clin. Microbiol. Rev.* 15(4):564–94
6. Nerlich AG, Schraut B, Dittrich S, et al. 2008. Plasmodium falciparum in ancient Egypt. *Emerging Infect. Dis.* 14(8):1317–19
7. Neghina R, Neghina AM, Marincu I, et al. 2010. Malaria, a journey in time: in search of the lost myths and forgotten stories. *Am. J. Med. Sci.* 340(6):492–98
8. Reiter P. 2000. From Shakespeare to Defoe: malaria in England in the Little Ice Age. *Emerging Infect. Dis.* 6(1):1–11
9. World Health Organization. 2015. Report 2014., pp. 1–242
10. Pasvol G. 2010. Protective hemoglobinopathies and Plasmodium falciparum transmission. *Nat. Genet.* 42(4):284–85
11. Gueirard P, Tavares J, Thiberge S, et al. 2010. Development of the malaria parasite in the skin of the mammalian host. *Proc. Natl. Acad. Sci. U.S.A.*

107(43):18640–45

12. Mota MM, Pradel G, Vanderberg JP, et al. 2001. Migration of Plasmodium sporozoites through cells before infection. *Science*. 291(5501):141–44

13. Mota MM, Hafalla JCR, Rodriguez A. 2002. Migration through host cells activates Plasmodium sporozoites for infection. *Nat Med*. 8(11):1318–22

14. Sturm A, Amino R, van de Sand C, et al. 2006. Manipulation of host hepatocytes by the malaria parasite for delivery into liver sinusoids. *Science*. 313(5791):1287–90

15. Baer K, Klotz C, Kappe SHI, et al. 2007. Release of hepatic Plasmodium yoelii merozoites into the pulmonary microvasculature. *PLoS Pathog*. 3(11):e171

16. Dvorak J, Miller L, Whitehouse W, et al. 1975. Invasion of erythrocytes by malaria merozoites. *Science*. 187(4178):748–50

17. Hanssen E, Dekiwadia C, Riglar DT, et al. 2013. Electron tomography of Plasmodium falciparum merozoites reveals core cellular events that underpin erythrocyte invasion. *Cellular Microbiology*. 15(9):1457–72

18. Riglar DT, Richard D, Wilson DW, et al. 2011. Super-resolution dissection of coordinated events during malaria parasite invasion of the human erythrocyte. *Cell Host and Microbe*. 9(1):9–20

19. Singh S, Alam MM, Pal-Bhowmick I, et al. 2010. Distinct external signals trigger sequential release of apical organelles during erythrocyte invasion by malaria parasites. *PLoS Pathog*. 6(2):e1000746

20. Baum J, Richard D, Healer J, et al. 2006. A conserved molecular motor drives cell invasion and gliding motility across malaria life cycle stages and other apicomplexan parasites. *J. Biol. Chem.* 281(8):5197–5208

21. Jones ML, Kitson EL, Rayner JC. 2006. Plasmodium falciparum erythrocyte invasion: a conserved myosin associated complex. *Mol. Biochem. Parasitol.* 147(1):74–84

22. Glushakova S, Yin D, Li T, et al. 2005. Membrane transformation during malaria parasite release from human red blood cells. *Curr. Biol.* 15(18):1645–50

23. Gilson PR, Crabb BS. 2009. Morphology and kinetics of the three distinct phases of red blood cell invasion by Plasmodium falciparum merozoites. *Int J Parasitol*. 39(1):91–96

24. Whitten MMA, Shiao SH, Levashina EA. 2006. Mosquito midguts and malaria: cell biology, compartmentalization and immunology. *Parasite Immunology*. 28(4):121–30

25. Meshnick SR, Dobson MJ. 2001. The history of antimalarial drugs., pp. 15–25

26. Schlitzer M. 2008. Antimalarial drugs - what is in use and what is in the pipeline. *Arch. Pharm. (Weinheim)*. 341(3):149–63

27. Packard RM. 2014. The origins of antimalarial-drug resistance. *N Engl J Med*. 371(5):397–99

28. Wongsrichanalai C, Pickard AL, Wernsdorfer WH, et al. 2002. Epidemiology of drug-resistant malaria. *Lancet Infect Dis*. 2(4):209–18

29. Wernsdorfer WH, Payne D. 1991. The dynamics of drug resistance in Plasmodium falciparum. *Pharmacol. Ther.* 50(1):95–121

30. Baird JK, Schwartz E, Hoffman SL. 2007. Prevention and treatment of vivax malaria. *Curr Infect Dis Rep*. 9(1):39–46

31. White NJ. 1997. Assessment of the pharmacodynamic properties of

antimalarial drugs in vivo. *Antimicrob. Agents Chemother.* 41(7):1413–22

32. Woodrow CJ, Haynes RK, Krishna S. 2005. Artemisinins. *Postgrad Med J*. 81(952):71–78

33. Posner GH, O'Neill PM. 2004. Knowledge of the proposed chemical mechanism of action and cytochrome p450 metabolism of antimalarial trioxanes like artemisinin allows rational design of new antimalarial peroxides. *Acc. Chem. Res.* 37(6):397–404

34. Dondorp AM, Nosten F, Yi P, et al. 2009. Artemisinin resistance in Plasmodium falciparum malaria. *N Engl J Med*. 361(5):455–67

35. Ashley EA, Dhorda M, Fairhurst RM, et al. 2014. Spread of artemisinin resistance in Plasmodium falciparum malaria. *N Engl J Med*. 371(5):411–23

36. Miotto O, Almagro-Garcia J, Manske M, et al. 2013. Multiple populations of artemisinin-resistant Plasmodium falciparum in Cambodia. *Nat. Genet.* 45(6):648–55

37. Marsh K, Kinyanjui S. 2006. Immune effector mechanisms in malaria. *Parasite Immunology*. 28(1-2):51–60

38. Hoffman SL, Goh LML, Luke TC, et al. 2002. Protection of humans against malaria by immunization with radiation-attenuated Plasmodium falciparum sporozoites. *J. Infect. Dis.* 185(8):1155–64

39. Hoffman SL, Billingsley PF, James E, et al. 2010. Development of a metabolically active, non-replicating sporozoite vaccine to prevent Plasmodium falciparum malaria. *Hum Vaccin*. 6(1):97–106

40. Vaughan AM, Wang R, Kappe SHI. 2010. Genetically engineered, attenuated whole-cell vaccine approaches for malaria. *Hum Vaccin*. 6(1):107–13

41. Mueller A-K, Labaied M, Kappe SHI, et al. 2005. Genetically modified Plasmodium parasites as a protective experimental malaria vaccine. *Nature*. 433(7022):164–67

42. Roestenberg M, McCall M, Hopman J, et al. 2009. Protection against a malaria challenge by sporozoite inoculation. *N Engl J Med*. 361(5):468–77

43. Kumar KA, Baxter P, Tarun AS, et al. 2009. Conserved Protective Mechanisms in Radiation and Genetically Attenuated uis3(-) and uis4(-) Plasmodium Sporozoites. *PLoS ONE*. 4(2):e4480

44. Casares S, Brumeanu T-D, Richie TL. 2010. The RTS,S malaria vaccine. *Vaccine*. 28(31):4880–94

45. Crompton PD, Pierce SK, Miller LH. 2010. Advances and challenges in malaria vaccine development. *J. Clin. Invest.* 120(12):4168–78

46. The RTS,S Clinical Trials Partnership. 2011. First Results of Phase 3 Trial of RTS,S/AS01 Malaria Vaccine in African Children. *N Engl J Med*. 365(20):1863–75

47. Bojang KA, Milligan PJ, Pinder M, et al. 2001. Efficacy of RTS,S/AS02 malaria vaccine against Plasmodium falciparum infection in semi-immune adult men in The Gambia: a randomised trial. *Lancet*. 358(9297):1927–34

48. Alonso PL, Sacarlal J, Aponte JJ, et al. 2004. Efficacy of the RTS, S/AS02A vaccine against Plasmodium falciparum infection and disease in young African children: randomised controlled trial. *Lancet*. 364(9443):1411–20

49. Guinovart C, Aponte JJ, Sacarlal J, et al. 2009. Insights into Long-Lasting Protection Induced by RTS,S/AS02A Malaria Vaccine: Further Results from a Phase IIb Trial in Mozambican Children. *PLoS ONE*. 4(4):e5165

50. Bejon P, Lusingu J, Olotu A, et al. 2008. Efficacy of RTS,S/AS01E Vaccine against Malaria in Children 5 to 17 Months of Age. *N Engl J Med*. 359(24):2521–32

51. Kester KE, Cummings JF, Ofori-Anyinam O, et al. 2009. Randomized, double-blind, phase 2a trial of falciparum malaria vaccines RTS,S/AS01B and RTS,S/AS02A in malaria-naive adults: safety, efficacy, and immunologic associates of protection. *J. Infect. Dis.* 200(3):337–46

52. Stoute JA, Slaoui M, Heppner DG, et al. 1997. A preliminary evaluation of a recombinant circumsporozoite protein vaccine against Plasmodium falciparum malaria. RTS,S Malaria Vaccine Evaluation Group. *N Engl J Med*. 336(2):86–91

53. Stoute JA, Kester KE, Krzych U, et al. 1998. Long-term efficacy and immune responses following immunization with the RTS,S malaria vaccine. *J. Infect. Dis.* 178(4):1139–44

54. Bartoloni A, Zammarchi L. 2012. Clinical aspects of uncomplicated and severe malaria. *Mediterr J Hematol Infect Dis*. 4(1):e2012026

55. Warrell DA, Molyneux ME, Beales PF. 1990. Severe and complicated malaria. World Health Organization Division of Control of Tropical Diseases. *Trans. R. Soc. Trop. Med. Hyg.* 84(Supplement 2):

56. Brewster DR, Kwiatkowski D, White NJ. 1990. Neurological sequelae of cerebral malaria in children. *Lancet*. 336(8722):1039–43

57. Holding PA, Stevenson J, Peshu N, et al. 1999. Cognitive sequelae of severe malaria with impaired consciousness. *Trans. R. Soc. Trop. Med. Hyg.* 93(5):529–34

58. Holding PA, Snow RW. 2001. Impact of Plasmodium falciparum malaria on performance and learning: review of the evidence. *Am. J. Trop. Med. Hyg.* 64(1-2 Suppl):68–75

59. Idro R, Carter JA, Fegan G, et al. 2006. Risk factors for persisting neurological and cognitive impairments following cerebral malaria. *Arch. Dis. Child.* 91(2):142–48

60. Carter JA, Neville BGR, White S, et al. 2004. Increased prevalence of epilepsy associated with severe falciparum malaria in children. *Epilepsia*. 45(8):978–81

61. Carter JA, Lees JA, Gona JK, et al. 2006. Severe falciparum malaria and acquired childhood language disorder. *Dev Med Child Neurol*. 48(1):51–57

62. Idro R, Kakooza-Mwesige A, Balyejjussa S, et al. 2010. Severe neurological sequelae and behaviour problems after cerebral malaria in Ugandan children. *BMC Res Notes*. 3:104

63. MacPherson GG, Warrell MJ, White NJ, et al. 1985. Human cerebral malaria. A quantitative ultrastructural analysis of parasitized erythrocyte sequestration. *Am J Pathol*. 119(3):385–401

64. Pongponratn E, Riganti M, Punpoowong B, et al. 1991. Microvascular sequestration of parasitized erythrocytes in human falciparum malaria: a pathological study. *Am. J. Trop. Med. Hyg.* 44(2):168–75

65. Taylor TE, Fu WJ, Carr RA, et al. 2004. Differentiating the pathologies of cerebral malaria by postmortem parasite counts. *Nat Med*. 10(2):143–45

66. Berendt AR, Tumer GD, Newbold CI. 1994. Cerebral malaria: the sequestration hypothesis. *Parasitol. Today (Regul. Ed.)*. 10(10):412–14

67. Phillips RE, Warrell DA. 1986. The pathophysiology of severe falciparum malaria. *Parasitol. Today (Regul. Ed.)*. 2(10):271–82

68. Patnaik JK, Das BS, Mishra SK, et al. 1994. Vascular clogging, mononuclear cell margination, and enhanced vascular permeability in the pathogenesis of human cerebral malaria. *Am. J. Trop. Med. Hyg.* 51(5):642–47

69. Silamut K, Phu NH, Whitty C, et al. 1999. A quantitative analysis of the microvascular sequestration of malaria parasites in the human brain. *AJPA*. 155(2):395–410

70. Grau GE, Mackenzie CD, Carr RA, et al. 2003. Platelet accumulation in brain microvessels in fatal pediatric cerebral malaria. *J. Infect. Dis.* 187(3):461–66

71. Engwerda C, Belnoue E, Grüner AC, et al. 2005. Experimental models of cerebral malaria. *Curr. Top. Microbiol. Immunol.* 297:103–43

72. Hearn J, Rayment N, Landon DN, et al. 2000. Immunopathology of Cerebral Malaria: Morphological Evidence of Parasite Sequestration in Murine Brain Microvasculature. *Infect. Immun.* 68(9):5364–76

73. White NJ, Turner GDH, Medana IM, et al. 2010. The murine cerebral malaria phenomenon. *Trends Parasitol*. 26(1):11–15

74. Hunt NH, Grau GE, Engwerda C, et al. 2010. Murine cerebral malaria: the whole story. *Trends Parasitol*. 26(6):272–74

75. Carvalho LJM. 2010. Murine cerebral malaria: how far from human cerebral malaria? *Trends Parasitol*. 26(6):271–72

76. de Souza JB, Hafalla JCR, Riley EM, et al. 2010. Cerebral malaria: why experimental murine models are required to understand the pathogenesis of disease. *Parasitology*. 137(5):755–72

77. Van den Steen PE, Geurts N, Deroost K, et al. 2010. Immunopathology and dexamethasone therapy in a new model for malaria-associated acute respiratory distress syndrome. *Am. J. Respir. Crit. Care Med.* 181(9):957–68

78. de Souza JB, Williamson KH, Otani T, et al. 1997. Early gamma interferon responses in lethal and nonlethal murine blood-stage malaria. *Infect. Immun.* 65(5):1593–98

79. Abbott NJ, Patabendige AAK, Dolman DEM, et al. 2010. Structure and function of the blood-brain barrier. *Neurobiol. Dis.* 37(1):13–25

80. Kuhnline Sloan CD, Nandi P, Linz TH, et al. 2012. Analytical and biological methods for probing the blood-brain barrier. *Annu Rev Anal Chem (Palo Alto Calif)*. 5:505–31

81. Hansen AJ. 1985. Effect of anoxia on ion distribution in the brain. *Physiol. Rev.* 65(1):101–48

82. Bernacki J, Dobrowolska A, Nierwińska K, et al. 2008. Physiology and pharmacological role of the blood-brain barrier. *Pharmacol Rep*. 60(5):600–622

83. Gingrich MB, Junge CE, Lyuboslavsky P, et al. 2000. Potentiation of NMDA receptor function by the serine protease thrombin. *J. Neurosci.* 20(12):4582–95

84. Gingrich MB, Traynelis SF. 2000. Serine proteases and brain damage - is there a link? *Trends Neurosci.* 23(9):399–407

85. Nadal A, Fuentes E, Pastor J, et al. 1995. Plasma albumin is a potent trigger of calcium signals and DNA synthesis in astrocytes. *Proc. Natl. Acad. Sci. U.S.A.* 92(5):1426–30

86. Neill AL, Hunt NH. 1992. Pathology of fatal and resolving Plasmodium berghei cerebral malaria in mice. *Parasitology*. 105(02):165

87. Belnoue E, Kayibanda M, Vigário AM, et al. 2002. On the pathogenic role of brain-sequestered alphabeta CD8+ T cells in experimental cerebral malaria. *J. Immunol.* 169(11):6369–75

88. Curfs JHAJ, Meer JWMVD, Sauerwein RW, et al. 1990. *IL-1 treatment inhibits parasitemia and protects against development of cerebral hemorrhages in P. berghei infected mice.* Wiley-Liss Inc. 7 p.

89. Chen L, Zhang Z, Sendo F. 2000. Neutrophils play a critical role in the pathogenesis of experimental cerebral malaria. *Clin. Exp. Immunol.* 120(1):125–33

90. Hansen DS, Bernard NJ, Nie CQ, et al. 2007. NK cells stimulate recruitment of CXCR3+ T cells to the brain during Plasmodium berghei-mediated cerebral malaria. *J. Immunol.* 178(9):5779–88

91. Yañez DM, Manning DD, Cooley AJ, et al. 1996. Participation of lymphocyte subpopulations in the pathogenesis of experimental murine cerebral malaria. *J. Immunol.* 157(4):1620–24

92. Hermsen C, Van De Wiel T, Mommers E, et al. 1997. Depletion of CD4+ or CD8+ T-cells prevents Plasmodium berghei induced cerebral malaria in end-stage disease. *Parasitology*. 114 (Pt 1):7–12

93. deWalick S, Amante FH, McSweeney KA, et al. 2007. Cutting edge: conventional dendritic cells are the critical APC required for the induction of experimental cerebral malaria. *J. Immunol.* 178(10):6033–37

94. Lundie RJ, de Koning-Ward TF, Davey GM, et al. 2008. Blood-stage

Plasmodium infection induces CD8+ T lymphocytes to parasite-expressed antigens, largely regulated by CD8alpha+ dendritic cells. *Proc. Natl. Acad. Sci. U.S.A.* 105(38):14509–14

95. Lundie RJ, Young LJ, Davey GM, et al. 2010. Blood-stage Plasmodium berghei infection leads to short-lived parasite-associated antigen presentation by dendritic cells. *Eur. J. Immunol.* 40(6):1674–81

96. Piva L, Tetlak P, Claser C, et al. 2012. Cutting Edge: Clec9A+ Dendritic Cells Mediate the Development of Experimental Cerebral Malaria. *J. Immunol.* 189(3):1128–32

97. Guermonprez P, Helft J, Claser C, et al. 2013. Inflammatory Flt3l is essential to mobilize dendritic cells and for T cell responses during Plasmodium infection. *Nat Med*. 19(6):730–38

98. Schwartz RH. 2003. T cell anergy. *Annu. Rev. Immunol.* 21:305–34

99. Kershaw MH, Westwood JA, Darcy PK. 2013. Gene-engineered T cells for cancer therapy. *Nature Publishing Group*. 13(8):525–41

100. Berke G. 1995. The CTL's kiss of death. *Cell*. 81(1):9–12

101. Heusel JW, Wesselschmidt RL, Shresta S, et al. 1994. Cytotoxic lymphocytes require granzyme B for the rapid induction of DNA fragmentation and apoptosis in allogeneic target cells. *Cell*. 76(6):977–87

102. Shresta S, Pham CT, Thomas DA, et al. 1998. How do cytotoxic lymphocytes kill their targets? *Curr. Opin. Immunol.* 10(5):581–87

103. Cresswell P. 2000. Intracellular surveillance: controlling the assembly of MHC class I-peptide complexes. *Traffic*. 1(4):301–5

104. Dick TP. 2004. Assembly of MHC class I peptide complexes from the

perspective of disulfide bond formation. *Cellular and Molecular Life Sciences (CMLS)*. 61(5):547–56

105. Lin M-L, Zhan Y, Villadangos JA, et al. 2008. The cell biology of cross-presentation and the role of dendritic cell subsets. *Immunol. Cell Biol.* 86(4):353–62

106. Heath WR, Carbone FR. 2001. Cross-presentation in viral immunity and self-tolerance. *Nature Reviews Immunology*. 1(2):126–34

107. Guermonprez P, Saveanu L, Kleijmeer M, et al. 2003. ER-phagosome fusion defines an MHC class I cross-presentation compartment in dendritic cells. *Nature*. 425(6956):397–402

108. Cresswell P, Bangia N, Dick T, et al. 1999. The nature of the MHC class I peptide loading complex. *Immunol. Rev.* 172:21–28

109. Ackerman AL, Kyritsis C, Tampé R, et al. 2005. Access of soluble antigens to the endoplasmic reticulum can explain cross-presentation by dendritic cells. *Nat Immunol*. 6(1):107–13

110. Houde M, Bertholet S, Gagnon E, et al. 2003. Phagosomes are competent organelles for antigen cross-presentation. *Nature*. 425(6956):402–6

111. Touret N, Paroutis P, Terebiznik M, et al. 2005. Quantitative and dynamic assessment of the contribution of the ER to phagosome formation. *Cell*. 123(1):157–70

112. Russell DG. 2003. Phagosomes, fatty acids and tuberculosis. *Nat. Cell Biol.* 5(9):776–78

113. Cossart P, Sansonetti PJ. 2004. Bacterial invasion: the paradigms of enteroinvasive pathogens. *Science*. 304(5668):242–48

114. Groothuis TAM, Neefjes J. 2005. The many roads to cross-presentation. *J. Exp. Med.* 202(10):1313–18

115. Harshyne LA, Watkins SC, Gambotto A, et al. 2001. Dendritic cells acquire antigens from live cells for cross-presentation to CTL. *J. Immunol.* 166(6):3717–23

116. Davis MM, Altman JD, Newell EW. 2011. PERSPECTIVES. *Nature Reviews Immunology*. 11(8):551–58

117. Altman JD, Moss PA, Goulder PJ, et al. 1996. Phenotypic analysis of antigen-specific T lymphocytes. *Science*. 274(5284):94–96

118. Bakker AH, Schumacher TNM. 2005. MHC multimer technology: current status and future prospects. *Curr. Opin. Immunol.* 17(4):428–33

119. Rodenko B, Toebes M, Hadrup SR, et al. 2006. Generation of peptide–MHC class I complexes through UV-mediated ligand exchange. *Nat Protoc*. 1(3):1120–32

120. Toebes M, Coccoris M, Bins A, et al. 2006. Design and use of conditional MHC class I ligands. *Nat Med*. 12(2):246–51

121. Grotenbreg GM, Roan NR, Guillen E, et al. 2008. Discovery of CD8+ T cell epitopes in Chlamydia trachomatis infection through use of caged class I MHC tetramers. *Proc. Natl. Acad. Sci. U.S.A.* 105(10):3831–36

122. Haque A, Best SE, Unosson K, et al. 2011. Granzyme B Expression by CD8+ T Cells Is Required for the Development of Experimental Cerebral Malaria. *J. Immunol.* 186(11):6148–56

123. Nitcheu J, Bonduelle O, Combadiere C, et al. 2003. Perforin-dependent brain-infiltrating cytotoxic CD8+ T lymphocytes mediate experimental

cerebral malaria pathogenesis. *J. Immunol.* 170(4):2221–28

124. Claser C, Malleret B, Gun SY, et al. 2011. CD8+ T Cells and IFN-γ Mediate the Time-Dependent Accumulation of Infected Red Blood Cells in Deep Organs during Experimental Cerebral Malaria. *PLoS ONE*. 6(4):e18720

125. McQuillan JA, Mitchell AJ, Ho YF, et al. 2010. International Journal for Parasitology. *Int J Parasitol*, pp. 1–9

126. Rénia L, Potter SM, Mauduit M, et al. 2006. Pathogenic T cells in cerebral malaria. *Int J Parasitol*. 36(5):547–54

127. Miyakoda M, Kimura D, Yuda M, et al. 2008. Malaria-specific and nonspecific activation of CD8+ T cells during blood stage of Plasmodium berghei infection. *J. Immunol.* 181(2):1420–28

128. Bagot S, Nogueira F, Collette A, et al. 2004. Comparative Study of Brain CD8+ T Cells Induced by Sporozoites and Those Induced by Blood-Stage Plasmodium berghei ANKA Involved in the Development of Cerebral Malaria. *Infect. Immun.* 72(5):2817–26

129. Howland SW, Claser C, Poh CM, et al. 2015. Pathogenic CD8(+) T cells in experimental cerebral malaria. *Semin Immunopathol*

130. Lau LS, Fernandez Ruiz D, Davey GM, et al. 2011. Blood-Stage Plasmodium berghei Infection Generates a Potent, Specific CD8+ T-Cell Response Despite Residence Largely in Cells Lacking MHC I Processing Machinery. *J. Infect. Dis.* 204(12):1989–96

131. Poh CM, Howland SW, Grotenbreg GM, et al. 2014. Damage to the blood-brain barrier during experimental cerebral malaria results from the synergistic effects of CD8+ T cells with different specificities. *Infect. Immun.*

132. Howland SW, Poh CM, Gun SY, et al. 2013. Brain microvessel cross-presentation is a hallmark of experimental cerebral malaria. *EMBO Mol Med*. 5(7):984–99

133. Belnoue E, Costa FTM, Vigário AM, et al. 2003. Chemokine receptor CCR2 is not essential for the development of experimental cerebral malaria. *Infect. Immun.* 71(6):3648–51

134. Belnoue E, Kayibanda M, Deschemin J-C, et al. 2003. CCR5 deficiency decreases susceptibility to experimental cerebral malaria. *Blood*. 101(11):4253–59

135. Miu J, Mitchell AJ, Müller M, et al. 2008. Chemokine gene expression during fatal murine cerebral malaria and protection due to CXCR3 deficiency. *J. Immunol.* 180(2):1217–30

136. Campanella GSV, Tager AM, Khoury El JK, et al. 2008. Chemokine receptor CXCR3 and its ligands CXCL9 and CXCL10 are required for the development of murine cerebral malaria. *Proc. Natl. Acad. Sci. U.S.A.* 105(12):4814–19

137. Nie CQ, Bernard NJ, Norman MU, et al. 2009. IP-10-mediated T cell homing promotes cerebral inflammation over splenic immunity to malaria infection. *PLoS Pathog*. 5(4):e1000369

138. Srivastava K, Cockburn IA, Swaim A, et al. 2008. Platelet factor 4 mediates inflammation in experimental cerebral malaria. *Cell Host and Microbe*. 4(2):179–87

139. Hanum PS, Hayano M, Kojima S. 2003. Cytokine and chemokine responses in a cerebral malaria-susceptible or -resistant strain of mice to Plasmodium berghei ANKA infection: early chemokine expression in the brain. *Int.*

Immunol. 15(5):633–40

140. Miu J, Hunt NH, Ball HJ. 2008. Predominance of interferon-related responses in the brain during murine malaria, as identified by microarray analysis. *Infect. Immun.* 76(5):1812–24

141. Oakley MS, McCutchan TF, Anantharaman V, et al. 2008. Host biomarkers and biological pathways that are associated with the expression of experimental cerebral malaria in mice. *Infect. Immun.* 76(10):4518–29

142. Van den Steen PE, Deroost K, Aelst IV, et al. 2008. CXCR3 determines strain susceptibility to murine cerebral malaria by mediating T lymphocyte migration toward IFN-γ-induced chemokines. *Eur. J. Immunol.* 38(4):1082–95

143. El-Assaad F, Wheway J, Mitchell AJ, et al. 2013. Cytoadherence of Plasmodium berghei-Infected Red Blood Cells to Murine Brain and Lung Microvascular Endothelial Cells In Vitro. *Infect. Immun.* 81(11):3984–91

144. Amante FH, Haque A, Stanley AC, et al. 2010. Immune-Mediated Mechanisms of Parasite Tissue Sequestration during Experimental Cerebral Malaria. *J. Immunol.* 185(6):3632–42

145. Grau GE, Pointaire P, Piguet PF, et al. 1991. Late administration of monoclonal antibody to leukocyte function-antigen 1 abrogates incipient murine cerebral malaria. *Eur. J. Immunol.* 21(9):2265–67

146. De Kossodo S, Grau GE. 1993. Role of cytokines and adhesion molecules in malaria immunopathology. *Stem Cells*. 11(1):41–48

147. Medana IM, Hunt NH, Chaudhri G. 1997. Tumor necrosis factor-alpha expression in the brain during fatal murine cerebral malaria: evidence for production by microglia and astrocytes. *AJPA*. 150(4):1473–86

148. Engwerda CR. 2002. Locally Up-regulated Lymphotoxin alpha, Not Systemic Tumor Necrosis Factor alpha, Is the Principle Mediator of Murine Cerebral Malaria. *Journal of Experimental Medicine*. 195(10):1371–77

149. Lucas R, Juillard P, Decoster E, et al. 1997. Crucial role of tumor necrosis factor (TNF) receptor 2 and membrane-bound TNF in experimental cerebral malaria. *Eur. J. Immunol.* 27(7):1719–25

150. Amani V, Vigário AM, Belnoue E, et al. 2000. Involvement of IFN-γ receptor-mediated signaling in pathology and anti-malarial immunity induced by Plasmodium berghei infection. *Eur. J. Immunol.* 30(6):1646–55

151. Belnoue E, POTTER SM, ROSA DS, et al. 2008. Control of pathogenic CD8 +T cell migration to the brain by IFN-γ during experimental cerebral malaria. *Parasite Immunology*. 30(10):544–53

152. Hunt NH, Ball HJ, Hansen AM, et al. 2014. Cerebral malaria: gamma-interferon redux. *Front Cell Infect Microbiol*. 4:113

153. Villegas-Mendez A, Greig R, Shaw TN, et al. 2012. IFN-γ-producing CD4+ T cells promote experimental cerebral malaria by modulating CD8+ T cell accumulation within the brain. *J. Immunol.* 189(2):968–79

154. Rénia L, Howland SW, Claser C, et al. 2012. Cerebral malaria: mysteries at the blood-brain barrier. *Virulence*. 3(2):193–201

155. Pino P, Taoufiq Z, Nitcheu J, et al. 2005. Blood-brain barrier breakdown during cerebral malaria: suicide or murder? *Thromb Haemost*. 94(2):336–40

156. Pober JS, Cotran RS. 1991. Immunologic interactions of T lymphocytes with vascular endothelium. *Adv. Immunol.* 50:261–302

157. Mai J, Virtue A, Shen J, et al. 2013. An evolving new paradigm: endothelial

cells--conditional innate immune cells. *J Hematol Oncol*. 6:61

158. Lovegrove FE, Gharib SA, Patel SN, et al. 2007. Expression microarray analysis implicates apoptosis and interferon-responsive mechanisms in susceptibility to experimental cerebral malaria. *AJPA*. 171(6):1894–1903

159. Falk K, Rötzschke O, Deres K, et al. 1991. Identification of naturally processed viral nonapeptides allows their quantification in infected cells and suggests an allele-specific T cell epitope forecast. *J. Exp. Med.* 174(2):425–34

160. Griem P, Wallny HJ, Falk K, et al. 1991. Uneven tissue distribution of minor histocompatibility proteins versus peptides is caused by MHC expression. *Cell*. 65(4):633–40

161. Sanderson S, Shastri N. 1994. LacZ inducible, antigen/MHC-specific T cell hybrids. *Int. Immunol.* 6(3):369–76

162. Davis CA, Benzer S. 1997. Generation of cDNA expression libraries enriched for in-frame sequences. *Proc. Natl. Acad. Sci. U.S.A.* 94(6):2128–32

163. Moreno-Palanques RF, Fuldner RA. 1994. CHAPTER FIFTEEN - Construction of cDNA Libraries. In *Automated DNA Sequencing and Analysis*, eds MD Adams, F C, C Venter, pp. 102–9. San Diego: Academic Press. 8 p.

164. Davis C, Barvish Z, Gitelman I. 2007. A method for the construction of equalized directional cDNA libraries from hydrolyzed total RNA. *BMC Genomics*. 8(1):363

165. Malleret B, Claser C, Ong ASM, et al. 2011. A rapid and robust tri-color flow cytometry assay for monitoring malaria parasite development. *Sci Rep*. 1:118

166. Lund AH, Duch M, Pedersen FS. 1996. Increased cloning efficiency by

temperature-cycle ligation. *Nucleic Acids Res.* 24(4):800–801

167. Ohashi-Kunihiro S, Yohda M, Masaki H, et al. 2007. A novel vector for positive selection of inserts harboring an open reading frame by translational coupling. *Biotech.* 43(6):751–54

168. Skerra A. 1992. Phosphorothioate primers improve the amplification of DNA sequences by DNA polymerases with proofreading activity. *Nucleic Acids Res.* 20(14):3551–54

169. de Noronha CM, Mullins JI. 1992. Amplimers with 3'-terminal phosphorothioate linkages resist degradation by vent polymerase and reduce Taq polymerase mispriming. *PCR Methods Appl.* 2(2):131–36

170. Kanaori K, Tamura Y, Wada T, et al. 1999. Structure and Stability of the Consecutive Stereoregulated Chiral Phosphorothioate DNA Duplex †. *Biochemistry*. 38(49):16058–66

171. Howland SW, Poh CM, Rénia L. 2011. Directional, seamless, and restriction enzyme-free construction of random-primed complementary DNA libraries using phosphorothioate-modified primers. *Anal. Biochem.* 416(1):141–43

172. Hall N, Karras M, Raine JD, et al. 2005. A comprehensive survey of the Plasmodium life cycle by genomic, transcriptomic, and proteomic analyses. *Science*. 307(5706):82–86

173. Grassi G, Maccaroni P, Meyer R, et al. 2003. Inhibitors of DNA methylation and histone deacetylation activate cytomegalovirus promoter-controlled reporter gene expression in human glioblastoma cell line U87. *Carcinogenesis*. 24(10):1625–35

174. Brooks AR, Harkins RN, Wang P, et al. 2004. Transcriptional silencing is

associated with extensive methylation of the CMV promoter following adenoviral gene delivery to muscle. *J Gene Med*. 6(4):395–404

175. Kreiss P, Cameron B, Rangara R, et al. 1999. Plasmid DNA size does not affect the physicochemical properties of lipoplexes but modulates gene transfer efficiency. *Nucleic Acids Res.* 27(19):3792–98

176. Patanjali SR, Parimoo S, Weissman SM. 1991. Construction of a uniform-abundance (normalized) cDNA library. *Proc. Natl. Acad. Sci. U.S.A.* 88(5):1943–47

177. Komiya T, Tanigawa Y, Hirohashi S. 1997. A large-scale in situ hybridization system using an equalized cDNA library. *Anal. Biochem.* 254(1):23–30

178. Chew SL, Or MY, Chang CXL, et al. 2011. Stability screening of arrays of major histocompatibility complexes on combinatorially encoded flow cytometry beads. *J. Biol. Chem.* 286(32):28466–75

179. Hadrup SR, Bakker AH, Shu CJ, et al. 2009. Parallel detection of antigen-specific T-cell responses by multidimensional encoding of MHC multimers. *Nature Methods*. 6(7):520–26

180. Schatz PJ. 1993. Use of peptide libraries to map the substrate specificity of a peptide-modifying enzyme: a 13 residue consensus peptide specifies biotinylation in Escherichia coli. *Biotechnology (N.Y.)*. 11(10):1138–43

181. Stahl G, McCarty GP, Farabaugh PJ. 2002. Ribosome structure: revisiting the connection between translational accuracy and unconventional decoding. *Trends Biochem. Sci.* 27(4):178–83

182. Harger JW, Meskauskas A, Dinman JD. 2002. An “integrated model” of programmed ribosomal frameshifting. *Trends Biochem. Sci.* 27(9):448–54

183. Moutaftsi M, Peters B, Pasquetto V, et al. 2006. A consensus epitope prediction approach identifies the breadth of murine TCD8+-cell responses to vaccinia virus. *Nat Biotechnol*. 24(7):817–19

184. Mishto M, Liepe J, Textoris-Taube K, et al. 2014. Proteasome isoforms exhibit only quantitative differences in cleavage and epitope generation. *Eur. J. Immunol.* 44(12):3508–21

185. Shin E-C, Seifert U, Kato T, et al. 2006. Virus-induced type I IFN stimulates generation of immunoproteasomes at the site of infection. *J. Clin. Invest.* 116(11):3006–14

186. Yeoman JA, Hanssen E, Maier AG, et al. 2011. Tracking Glideosome-associated protein 50 reveals the development and organization of the inner membrane complex of Plasmodium falciparum. *Eukaryotic Cell*. 10(4):556–64

187. Bosch J, Paige MH, Vaidya AB, et al. 2012. Crystal structure of GAP50, the anchor of the invasion machinery in the inner membrane complex of Plasmodium falciparum. *J. Struct. Biol.* 178(1):61–73

188. Murata CE, Goldberg DE. 2003. Plasmodium falciparum falcilysin: an unprocessed food vacuole enzyme. *Mol. Biochem. Parasitol.* 129(1):123–26

189. Murata CE, Goldberg DE. 2003. Plasmodium falciparum falcilysin: a metalloprotease with dual specificity. *J. Biol. Chem.* 278(39):38022–28

190. Eggleson KK, Duffin KL, Goldberg DE. 1999. Identification and characterization of falcilysin, a metallopeptidase involved in hemoglobin catabolism within the malaria parasite Plasmodium falciparum. *J. Biol. Chem.* 274(45):32411–17

191. Cheesman S, Raza A, Carter R. 2006. Mixed strain infections and strain-specific protective immunity in the rodent malaria parasite Plasmodium chabaudi chabaudi in mice. *Infect. Immun.* 74(5):2996–3001

192. Falanga PB, Butcher EC. 1991. Late treatment with anti-LFA-1 (CD11a) antibody prevents cerebral malaria in a mouse model. *Eur. J. Immunol.* 21(9):2259–63

193. Aichele P, Kyburz D, Ohashi PS, et al. 1994. Peptide-induced T-cell tolerance to prevent autoimmune diabetes in a transgenic mouse model. *Proc. Natl. Acad. Sci. U.S.A.* 91(2):444–48

194. Aichele P, Brduscha-Riem K, Oehen S, et al. 1997. Peptide antigen treatment of naive and virus-immune mice: antigen-specific tolerance versus immunopathology. *Immunity*. 6(5):519–29

195. Wlodarczyk MF, Kraft AR, Chen HD, et al. 2013. Anti-IFN-γ and peptide-tolerization therapies inhibit acute lung injury induced by cross-reactive influenza A-specific memory T cells. *J. Immunol.* 190(6):2736–46

196. Rosenberg CS, Martin DL, Tarleton RL. 2010. CD8+ T Cells Specific for Immunodominant Trans-Sialidase Epitopes Contribute to Control of Trypanosoma cruzi Infection but Are Not Required for Resistance. *J. Immunol.* 185(1):560–68

197. Weiss WR, Good MF, Hollingdale MR, et al. 1989. Genetic control of immunity to Plasmodium yoelii sporozoites. *J. Immunol.* 143(12):4263–66

198. Yoeli M, Most H. 1965. Studies on Sporozoite-Induced Infections of Rodent Malaria: I. The Pre-Erythrocytic Tissue Stage of Plasmodium berghei. *Am. J. Trop. Med. Hyg.* 14(5):700–714

199. Mack M, Cihak J, Simonis C, et al. 2001. Expression and characterization of the chemokine receptors CCR2 and CCR5 in mice. *J. Immunol.* 166(7):4697–4704

200. Song L, Pachter JS. 2003. Culture of murine brain microvascular endothelial cells that maintain expression and cytoskeletal association of tight junction-associated proteins. *In Vitro Cell. Dev. Biol. Anim.* 39(7):313–20

201. Wu Z, Hofman FM, Zlokovic BV. 2003. A simple method for isolation and characterization of mouse brain microvascular endothelial cells. *J. Neurosci. Methods*. 130(1):53–63

202. Baptista FG, Pamplona A, Pena AC, et al. 2010. Accumulation of Plasmodium berghei-Infected Red Blood Cells in the Brain Is Crucial for the Development of Cerebral Malaria in Mice. *Infect. Immun.* 78(9):4033–39

203. Hermsen CC, Mommers E, Van De Wiel T, et al. 1998. Convulsions Due to Increased Permeability of the Blood-Brain Barrier in Experimental Cerebral Malaria Can Be Prevented by Splenectomy or Anti-T Cell Treatment. *J. Infect. Dis.* 178(4):1225–27

204. Mortier A, Van Damme J, Proost P. 2012. Overview of the mechanisms regulating chemokine activity and availability. *Immunol. Lett.* 145(1-2):2–9

205. Meiser A, Mueller A, Wise EL, et al. 2008. The chemokine receptor CXCR3 is degraded following internalization and is replenished at the cell surface by de novo synthesis of receptor. *J. Immunol.* 180(10):6713–24

206. Lin J-W, Shaw TN, Annoura T, et al. 2014. The Subcellular Location of Ovalbumin in Plasmodium berghei Blood Stages Influences the Magnitude of T-Cell Responses. *Infect. Immun.* 82(11):4654–65

207. Lau LS, Fernandez-Ruiz D, Mollard V, et al. 2014. CD8+ T Cells from a Novel T Cell Receptor Transgenic Mouse Induce Liver-Stage Immunity That Can Be Boosted by Blood-Stage Infection in Rodent Malaria. *PLoS Pathog*. 10(5):e1004135

208. Epstein JE, Tewari K, Lyke KE, et al. 2011. Live Attenuated Malaria Vaccine Designed to Protect Through Hepatic CD8+ T Cell Immunity. *Science*. 334(6055):475–80

209. Belnoue E, Voza T, Costa FTM, et al. 2008. Vaccination with live Plasmodium yoelii blood stage parasites under chloroquine cover induces cross-stage immunity against malaria liver stage. *J. Immunol.* 181(12):8552–58

210. Butler NS, Schmidt NW, Vaughan AM, et al. 2011. Superior Antimalarial Immunity after Vaccination with Late Liver Stage-ArrestingGenetically Attenuated Parasites. *Cell Host and Microbe*. 9(6):451–62

211. Tarun AS, Peng X, Dumpit RF, et al. 2008. A combined transcriptome and proteome survey of malaria parasite liver stages. *Proc. Natl. Acad. Sci. U.S.A.* 105(1):305–10

212. Dondorp AM, Fanello CI, Hendriksen ICE, et al. 2010. Artesunate versus quinine in the treatment of severe falciparum malaria in African children (AQUAMAT): an open-label, randomised trial. *Lancet*. 376(9753):1647–57

213. Warrell DA, Looareesuwan S, Warrell MJ, et al. 1982. Dexamethasone Proves Deleterious in Cerebral Malaria. *N Engl J Med*. 306(6):313–19

214. Hoffman SL, Rustama D, Punjabi NH, et al. 1988. High-dose dexamethasone in quinine-treated patients with cerebral malaria: a double-blind, placebo-controlled trial. *J. Infect. Dis.* 158(2):325–31

215. Di Perri G, Di Perri IG, Monteiro GB, et al. 1995. Pentoxifylline as a supportive agent in the treatment of cerebral malaria in children. *J. Infect. Dis.* 171(5):1317–22

216. Looareesuwan S, Wilairatana P, Vannaphan S, et al. 1998. Pentoxifylline as an ancillary treatment for severe falciparum malaria in Thailand. *Am. J. Trop. Med. Hyg.* 58(3):348–53

217. Das BK, Mishra S, Padhi PK, et al. 2003. Pentoxifylline adjunct improves prognosis of human cerebral malaria in adults. *Trop. Med. Int. Health*. 8(8):680–84

218. Lell B, Köhler C, Wamola B, et al. 2010. Pentoxifylline as an adjunct therapy in children with cerebral malaria. *Malaria Journal*. 9:368

219. van Hensbroek MB, Palmer A, Onyiorah E, et al. 1996. The effect of a monoclonal antibody to tumor necrosis factor on survival from childhood cerebral malaria. *J. Infect. Dis.* 174(5):1091–97

220. Looareesuwan S, Sjostrom L, Krudsood S, et al. 1999. Polyclonal anti-tumor necrosis factor-alpha Fab used as an ancillary treatment for severe malaria. *Am. J. Trop. Med. Hyg.* 61(1):26–33

221. Taylor TE, Molyneux ME, Wirima JJ, et al. 1992. Intravenous immunoglobulin in the treatment of paediatric cerebral malaria. *Clin. Exp. Immunol.* 90(3):357–62

222. Dondorp AM, Silamut K, Charunwatthana P, et al. 2007. Levamisole inhibits sequestration of infected red blood cells in patients with falciparum malaria. *J. Infect. Dis.* 196(3):460–66

223. Maude RJ, Silamut K, Plewes K, et al. 2014. Randomized controlled trial of

levamisole hydrochloride as adjunctive therapy in severe falciparum malaria with high parasitemia. *J. Infect. Dis.* 209(1):120–29

224. White NJ, Looareesuwan S, Phillips RE, et al. 1988. Single dose phenobarbitone prevents convulsions in cerebral malaria. *Lancet*. 2(8602):64–66

225. Crawley J, Waruiru C, Mithwani S, et al. 2000. Effect of phenobarbital on seizure frequency and mortality in childhood cerebral malaria: a randomised, controlled intervention study. *Lancet*. 355(9205):701–6

226. Gwer SA, Idro RI, Fegan G, et al. 2013. Fosphenytoin for seizure prevention in childhood coma in Africa: a randomized clinical trial. *J Crit Care*. 28(6):1086–92

227. Newton CR, Crawley J, Sowumni A, et al. 1997. Intracranial hypertension in Africans with cerebral malaria. *Arch. Dis. Child.* 76(3):219–26

228. Namutangula B, Ndeezi G, Byarugaba JS, et al. 2007. Mannitol as adjunct therapy for childhood cerebral malaria in Uganda: a randomized clinical trial. *Malaria Journal*. 6:138

229. Mohanty S, Mishra SK, Patnaik R, et al. 2011. Brain swelling and mannitol therapy in adult cerebral malaria: a randomized trial. *Clin. Infect. Dis.* 53(4):349–55

230. Gordeuk V, Thuma P, Brittenham G, et al. 1992. Effect of iron chelation therapy on recovery from deep coma in children with cerebral malaria. *N Engl J Med*. 327(21):1473–77

231. Thuma PE, Mabeza GF, Biemba G, et al. 1998. Effect of iron chelation therapy on mortality in Zambian children with cerebral malaria. *Trans. R.*

Soc. Trop. Med. Hyg. 92(2):214–18

232. Watt G, Jongsakul K, Ruangvirayuth R. 2002. A pilot study of N-acetylcysteine as adjunctive therapy for severe malaria. *QJM*. 95(5):285–90

233. Treeprasertsuk S, Krudsood S, Tosukhowong T, et al. 2003. N-acetylcysteine in severe falciparum malaria in Thailand. *Southeast Asian J. Trop. Med. Public Health*. 34(1):37–42

234. Charunwatthana P, Abul Faiz M, Ruangveerayut R, et al. 2009. N-acetylcysteine as adjunctive treatment in severe malaria: a randomized, double-blinded placebo-controlled clinical trial. *Crit. Care Med.* 37(2):516–22

235. Yeo TW, Lampah DA, Rooslamiati I, et al. 2013. A randomized pilot study of L-arginine infusion in severe falciparum malaria: preliminary safety, efficacy and pharmacokinetics. *PLoS ONE*. 8(7):e69587

236. Maitland K, Pamba A, English M, et al. 2005. Randomized trial of volume expansion with albumin or saline in children with severe malaria: preliminary evidence of albumin benefit. *Clin. Infect. Dis.* 40(4):538–45

237. Planche T. 2005. Malaria and fluids--balancing acts. *Trends Parasitol*. 21(12):562–67

238. Midtvedt K, Fauchald P, Lien B, et al. 2003. Individualized T cell monitored administration of ATG versus OKT3 in steroid-resistant kidney graft rejection. *Clin Transplant*. 17(1):69–74

239. Lebwohl M, Tyring SK, Hamilton TK, et al. 2003. A novel targeted T-cell modulator, efalizumab, for plaque psoriasis. *N Engl J Med*. 349(21):2004–13

240. Gottlieb AB, Lebwohl M, Totoritis MC, et al. 2002. Clinical and histologic response to single-dose treatment of moderate to severe psoriasis with an

anti-CD80 monoclonal antibody. *J. Am. Acad. Dermatol.* 47(5):692–700

241. DeFrancesco L. 2009. RIP Raptiva? *Nature Publishing Group*, April, p. 303

242. Kothary N, Diak I-L, Brinker A, et al. 2011. Progressive multifocal leukoencephalopathy associated with efalizumab use in psoriasis patients. *J. Am. Acad. Dermatol.* 65(3):546–51

243. Berger JR, Houff SA, Major EO. 2009. Monoclonal antibodies and progressive multifocal leukoencephalopathy. *MAbs*. 1(6):583–89

244. Kloetzel P-M. 2004. The proteasome and MHC class I antigen processing. *Biochim. Biophys. Acta*. 1695(1-3):225–33

245. Wei X, Li Y, Sun X, et al. 2013. Erythropoietin Protects against Murine Cerebral Malaria through Actions on Host Cellular Immunity. *Infect. Immun.*

246. Bienvenu A-L, Ferrandiz J, Kaiser K, et al. 2008. Artesunate-erythropoietin combination for murine cerebral malaria treatment. *Acta Tropica*. 106(2):104–8

247. Peterson TE, Katusic ZS. 2007. EPO tecting the endothelium. *Br. J. Pharmacol.* 150(7):823–25

248. Chong ZZ, Lin S-H, Kang J-Q, et al. 2003. Erythropoietin prevents early and late neuronal demise through modulation of Akt1 and induction of caspase 1, 3, and 8. *J. Neurosci. Res.* 71(5):659–69

249. Solomon W, Wilson NO, Anderson L, et al. 2014. Neuregulin-1 attenuates mortality associated with experimental cerebral malaria. *J Neuroinflammation*. 11(1):9